REPORT NO. FR82-72-614
HAC REF. NO. E5542

ELECTRO-OPTICAL AND
DARPA SYSTEMS GROUP
HUGHES
HUGHES AIRCRAFT COMPANY

OPTICAL RESONANCE TRANSFER LASER (ORTL) DEVELOPMENT

HUGHES AIRCRAFT COMPANY
EL SEGUNDO, CALIFORNIA 90245

JULY 1982

Final Technical Report for Period
27 May 1980 – 27 May 1982

The views and conclusions contained in this document are those of the authors and should not be interpreted as necessarily representing the official policies, either expressed or implied of the Defense Advanced Research Projects Agency or the U.S. Government

SPONSORED BY
Defense Advanced Research Projects Agency
DARPA Order No. 3932

MONITORED BY
Mr. Wayne Whitney, NRL Code 6540, under
Contract No. N00173-80-C-0132

CONTRACT EFFECTIVE DATE: 27 May 1980
CONTRACT EXPIRATION DATE: 27 July 1982

UNCLASSIFIED

SECURITY CLASSIFICATION OF THIS PAGE (When Data Entered)

REPORT DOCUMENTATION PAGE		READ INSTRUCTIONS BEFORE COMPLETING FORM
1 REPORT NUMBER	2. GOVT ACCESSION NO.	3 RECIPIENT'S CATALOG NUMBER
4 TITLE (and Subtitle) OPTICAL RESONANCE TRANSFER LASER (ORTL) DEVELOPMENT		5 TYPE OF REPORT & PERIOD COVERED Final Report - 27 May 1980 to 27 May 1982 6. PERFORMING ORG. REPORT NUMBER FR82-72-814
7 AUTHOR(s) P.K. Baily, J.H.S. Wang, J. Finzi, R.C. Smith, J. Paranto, and D. Bruns		8 CONTRACT OR GRANT NUMBER(s) N00173-80-C-0132
9 PERFORMING ORGANIZATION NAME AND ADDRESS Hughes Aircraft Company P.O. Box 902 El Segundo, CA 90245		10. PROGRAM ELEMENT, PROJECT, TASK AREA & WORK UNIT NUMBERS DARPA Order No. 3932
11 CONTROLLING OFFICE NAME AND ADDRESS Advanced Research Projects Agency 1400 Wilson Blvd. Arlington, Virginia		12. REPORT DATE July 1982 13. NUMBER OF PAGES 121
14 MONITORING AGENCY NAME & ADDRESS(if different from Controlling Office) Naval Research Laboratory 4555 Overlook Ave. S.W. Washington, D.C.		15. SECURITY CLASS. (of this report) Unclassified 15a. DECLASSIFICATION DOWNGRADING SCHEDULE

16 DISTRIBUTION STATEMENT (of this Report)

Approved for Public Release:
distribution unlimited

17 DISTRIBUTION STATEMENT (of the abstract entered in Block 20, if different from Report)

None

18 SUPPLEMENTARY NOTES

None

19 KEY WORDS (Continue on reverse side if necessary and identify by block number)

Hydrogen Fluoride Laser
Chemical Laser
Optical Pumping
Transfer Lasers
Mode Control

20 ABSTRACT (Continue on reverse side if necessary and identify by block number)

Temporally stable spectrally controlled intracavity HF ORTL operation has been demonstrated with ORTL powers up to 152 watts and overall HF radiation conversion efficiencies up to 38 percent. Experiments with both helium and SF_6 as the ORTL diluent were performed. Spectral control of the HF chemical laser was achieved by means of specially designed resonator optics. The effect of ORTL medium inlet temperature, composition, and pressure was investigated. Energy division between the optical elements, the ORTL medium, and outcoupled

DD FORM 1 JAN 73 1473 EDITION OF 1 NOV 65 IS OBSOLETE

UNCLASSIFIED

SECURITY CLASSIFICATION OF THIS PAGE (When Data Entered)

20. ABSTRACT (Continued)

radiation was measured, as was the ORTL small signal gain. An intracavity ORTL model was developed and used to model the experiments. Agreement is such that projections for larger systems can be made with confidence.

SUMMARY

This report describes an experimental program aimed at assessing the feasibility of using an intracavity ORTL system for HF laser mode control. The initial experiments utilized existing extracavity ORTL hardware to continue the investigation of ORTL kinetics. The most significant result of these initial experiments was the identification of SF_6 as an alternative diluent to helium. The major part of the program was devoted to the fabrication and use of new intracavity ORTL hardware. Temporally stable spectrally controlled intracavity ORTL operation was demonstrated for the first time. The combined use of spectral control coatings in the chemical laser resonator and inlet temperature control of the ORTL medium resulted in ORTL outputs up to 152 watts and overall efficiencies of conversion of HF chemical laser radiation to HF ORTL output up to 38 ~~percent~~.

Detailed measurements of energy deposition in mirrors and in the ORTL medium, of temperature profiles, and of small signal gain utilizing helium and SF_6 as ORTL diluents were made over a wide range of operational ORTL parameters. The simultaneous development of an intracavity ORTL model, including an HF chemical laser simulation, allowed comparison of theory and experiment. This resulted in the achievement of a good understanding of the physical processes which are important for efficient intracavity ORTL operation. The model code can now be used for the design of larger systems. Efficiencies of 85 to 90 ~~percent~~ should be attainable in large systems.

PREFACE

This report was authored by P.K. Baily, J.H.S. Wang, J. Finzi, R.C. Smith, J. Paranto, and D. Bruns. The authors would like to acknowledge the assistance of D. Anders, L. Williams, J. Jacobson, and C. Lovejoy in designing apparatus and performing the experiments and the efforts of K.K. Hui in computer model development. We are also grateful for the insight gained in numerous technical discussions with W. Whitney, E.R. Peressini, M.M. Mann, W. Watt, and R. Sepucha.

CONTENTS

LIST OF ILLUSTRATIONS

LIST OF ILLUSTRATIONS (Continued)

LIST OF ILLUSTRATIONS (Continued)

LIST OF TABLES

1.0 INTRODUCTION

Optical Resonance Transfer Laser* (ORTL) technology has at least two potential applications for high energy chemical lasers. The first is to extend the scaling limit by providing a medium for combining two or more laser beams into a single higher power beam. The second is to provide a means of achieving diffraction limited operation that does not involve complex expensive optical components. The primary objective of the work reported here was to achieve good physical understanding of ORTL operation by means of a laboratory demonstration of HF ORTL operation in the potentially most efficient physical configuration.

Because of problems associated with maintaining the chemical laser medium homogeneity and with the complexity of the resonator design of the cylindrical chemical laser configuration, it is difficult to achieve near diffraction limited beams directly. Utilizing the ORTL technique, the high energy chemical laser acts as an optical pump exciting a second laser, the ORTL. With this technology, the original stringent mode and medium requirements on the high energy chemical laser are significantly relaxed and the cylindrical chemical laser resonator arrangement simplified. Because the role of the chemical laser is reduced to that of a source of optical power only, multi-mode characteristics of the chemical laser are no longer detrimental. The output beam control function of the total laser system is transferred in this new approach to the ORTL. The two functions of the laser system, to generate power and to concentrate that power into a highly confined beam, are separated. Of course, the premise that is fundamental to the ORTL approach to high energy laser system optimization is that each of the two functions can be solved separately in a more optimum way, and that the efficiency of conversion of chemical laser to ORTL radiation is high enough that better far field target irradiance can be achieved by the chemical laser/ORTL system than by directly focusing the same primary chemical laser power onto the target.

---

*J.S. Wang, J. Finzi, and F.N. Mastrup, Appl. Phys. Lett. 31, 35(1977).

The intermolecular ORTL technique as originally demonstrated made use of two molecules, a donor and an acceptor, as the active ORTL medium, flowing in a helium diluent. The chemical laser (DF) served as the optical pump exciting the donor (DF) molecules in the ORTL cell. This donor then collisionally transferred its energy to an acceptor (CO_2) molecule which then became the active laser molecule for the ORTL. Subsequent to the original DF/CO_2 (10.6 μ) demonstration, this technique was extended to DF/HBr (4.1 μ) and DF/N_2O (10.8 μ) systems.* In addition, a similar process in which only one molecule (DF) was present in the ORTL cell was demonstrated.** In this intramolecular DF ORTL system, the DF molecule served as both donor and acceptor. The DF molecules absorbed on the transition of the chemical pumping laser and excitation from one vibrational band to a higher band was achieved. Then, the energy was redistributed among the rotational levels of each vibrational band as the system approached rotational equilibrium. As this occurred, population inversions on non-pumped vibration-rotational transitions were achieved and laser oscillation occurred. There was, of course, a slight wavelength shift.

The issues that must be addressed before either ORTL approach can become a practicable and preferred solution to the high energy cylindrical laser beam control problem are whether very high conversion efficiency from multi-line HF or DF chemical laser power to ORTL power is achievable, and whether adequate medium homogeneity to permit the extraction of near diffraction limited beams at realistically scaled output power levels is possible. In order to gain the detailed technical understanding with which to address these issues, the High Energy ORTL Study† and the ORTL Development Program were performed. Because the primary interest for DARPA applications is in HF lasers, these programs concentrated on HF laser pumped systems. Prior work had dealt exclusively with DF laser pumped systems.

---

*Hughes IR&D, 1978

**4.3 Micrometer Laser Demonstration Experiment, Contract No. N00173-77-C-0174, Final Report, December 1977.

†High Energy Optical Resonance Transfer Laser Study, Contract No. N00173-78-C-0470, Final Report, August 1979.

The High Energy ORTL Study concentrated on the extracavity configuration and primarily addressed intramolecular HF ORTL kinetics and efficiency optimization. The ORTL Development Program reported on in this report concentrated on intracavity operation where the ORTL and chemical laser media were both inside the chemical laser optical resonator.

This program consisted of three tasks. The first task utilized the extracavity apparatus from the previous program to continue to investigate the ORTL physics, and to assess potential diluents other than helium. Experiments with helium, SF_6, and CF_4 as diluents were performed. Helium and SF_6 both performed well. The second task involved the largest effort and consisted of the design, fabrication, and experimental usage of a new intracavity ORTL apparatus. This involved specially designed spectral control coatings for the chemical laser resonator, a new chemical laser nozzle, and a temperature controlled ORTL medium. Temporally stable spectrally controlled intracavity operation with an overall conversion efficiency of 38 percent was demonstrated. The third task consisted of intracavity model development, analysis of the experiments, and use of the model to predict performance parameters at high energy.

2.0 EXTRACAVITY EXPERIMENTS

The objective of this task was to experimentally evaluate the ORTL efficiency as a function of the pump laser irradiance and spectral distribution, and as a function of the ORTL operating parameters, e.g., HF mole fraction, gas inlet temperature, and diluent. Tests of various diluents were designed to investigate potential bottlenecks in the r-r transfer process that would limit the ORTL efficiency under high flux conditions and to identify which diluent would enhance the r-r transfer process to minimize such bottleneck effects. These experiments were designed to obtain data for anchoring the ORTL model, and not to demonstrate optimum ORTL efficiency.

Existing experimental apparatus was utilized. This apparatus will be briefly described in Section 2.1 with the emphasis on the improvements implemented in this program. A detailed description has been reported previously.* The experimental results will be discussed in Section 2.2.

2.1 EXPERIMENTAL APPARATUS

The experiments reported here utilized the multiple pass cell developed during the High Energy ORTL Study, with the addition of a heat exchanger to preheat the ORTL medium, and other improvements, including improved reflectivity of the side mirrors, control of the pump irradiance level, and provision for the use of alternate diluents.

A diagram of the overall experimental configuration is shown in Figure 1. The chemical laser was a combustion driven, supersonic flow device. A stable resonator consisting of a 3 meter radius total reflector facing a flat outcoupler at a separation of 58 cm was used for all experiments; the outcoupling fraction was varied as described below. Following the chemical laser outcoupling mirror, an angled CaF_2 window sampled the beam to permit monitoring of the output power and spectral distribution of the pump laser. The powermeter at I_o (Laser Precision model RK-3240) was calibrated against the

*High Energy ORTL Study, Contract No. N00173-78-C-0470, Final Report, August 1979.

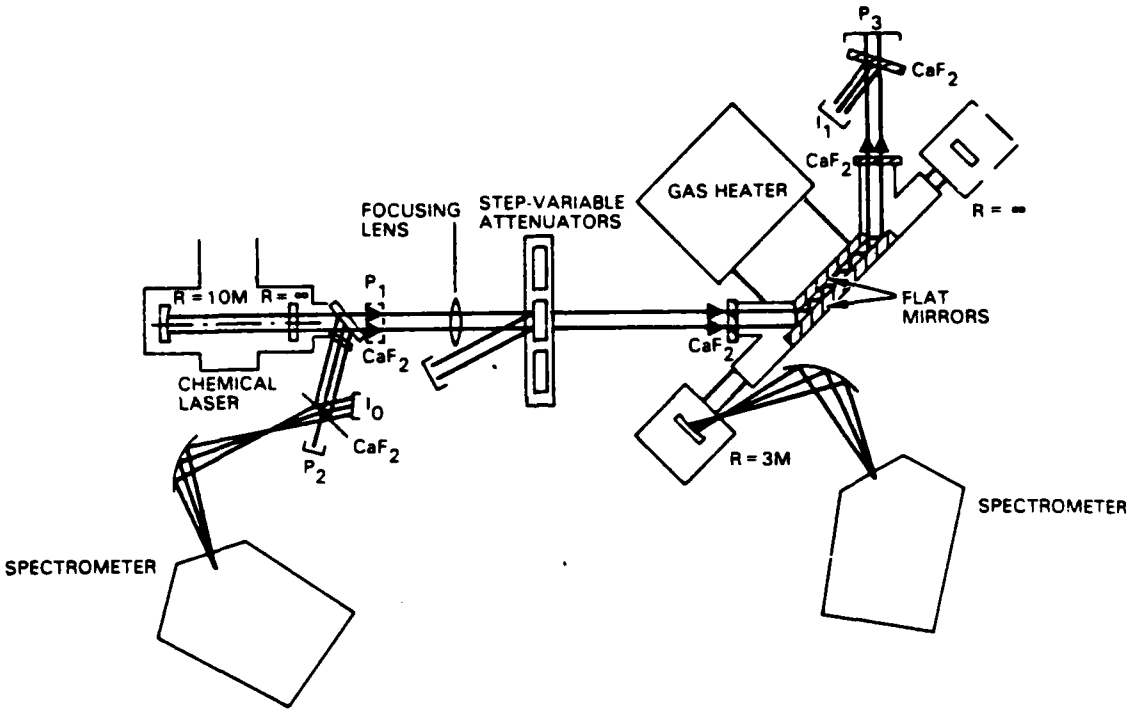

Figure 1. Extracavity configuration.

powermeter at P_1 (Coherent Radiation model 213), and provided continuous monitoring of the pump laser power, without interrupting the beam. The spectrometer (McPherson model 218 with an InSb detector) monitored the spectral distribution of the pump laser from light scattered from the CaF_2 window.

A cylindrical CaF_2 lens, focal length 51 cm, focused the pump beam (in the vertical direction) to a height of 0.55 cm in the center of the ORTL cell. Following the lens, step-variable attenuation of the pump laser was provided by inserting partially transmitting mirrors. These were silicon substrate, multilayer dielectric coated, chemical laser outcoupling mirrors, aligned at a small angle to the incident beam. This permitted collection of the reflected power and avoided returning it to the chemical laser. The small angle of tilt (approximately 2 degrees) minimized the change in beam position as it passed through the attenuator.

The pump beam entered the multiple pass cell through a CaF_2 entrance window and underwent eleven reflections between the flat, parallel side mirrors before exiting through a second CaF_2 window. The side mirrors were water cooled, aluminum substrate, gold coated total reflectors, which were attached directly to the cell body. The cell sides and mirror mounting surfaces were machined so that the mirror surfaces were parallel to within 500 microradians. The ORTL gain length was 8.8 cm. The side mirrors extended beyond this to accommodate a 1.1 cm region of "curtain" gas in order to confine the flow at each end and prevent the formation of a static absorbing region at each end. A nozzle extended from the heat exchanger, mounted below the cell, to the mirror edges. The bottom surface of the ORTL cell then sealed against the top surface of the heat exchanger.

The design of the coatings on the side mirrors was controlled by several effects. Too high a reflectivity would have lowered the threshold gain in the direction between the side mirrors and could have caused parasitic losses, while too low a reflectivity would have resulted in unacceptable losses of pump laser power. The choice was further influenced by the corrosive nature of the ORTL medium. Hot, gaseous HF might be expected to react with many materials. Even noncorrosive materials may present problems. For example, ThF_4, widely used as an overcoat for silver, is prone to water absorption, which lowers its reflectivity in the HF region. For these reasons, bare gold, despite its softness, was chosen as the material for coating the side mirrors. The substrates were coated with an electroless nickel layer to permit a high polish and stored under dry nitrogen except during ORTL runs. The reflectivity of the final surfaces was measured to be 98.7 percent and retained that level throughout the extracavity ORTL experiments. The reflectivity measurement utilized the 11-bounce configuration, measuring the sum of absorbed and scattered light via transmittance and the power absorbed by the mirror surfaces via calorimetry. The sum of transmitted and absorbed power was within 2 percent of the incident power, with an uncertainty of approximately 4 percent.

At the exit of the multiple pass cell, a second powermeter (Coherent Radiation model 213) was located at I_1 so the ratio of the incident and throughput powers (I_o and I_1) could be used to calculate the power absorbed

by the ORTL gas. Alternatively, the pump beam could be returned to the cell with a cylindrical total reflector, thereby increasing the effective irradiance.

The side mirror separation, 1.1 cm, and the angle of incidence of the pump beam, 45 degrees, dictated the chemical laser beam width, 1.56 cm. The ORTL optical axis was co-planar with that of the pump beam, and perpendicular to the direction of ORTL flow. The ORTL resonator consisted of a flat total reflector facing a 3 meter radius, spherical total reflector. ORTL power was measured in this "closed cavity" configuration by monitoring the temperature rise of the resonator mirrors, and applying a small correction for cooling. This correction was inferred from the cooling rate between experiments. The spectral distribution of the ORTL was monitored by sampling the light scattered from the concave mirror surface, with a second spectrometer (McPherson model 218, InSb detector). A shutter was installed between the resonator mirrors to allow pumping without lasing.

The ORTL medium and curtain gases entered the interaction zone and flowed upward at velocities variable from 3 to 30 meters/second. The pump beam height of 0.55 cm gave an interaction time of 0.02 to 0.2 msec. Boundary layer control was provided by a Laval-type, two-dimensional nozzle. A straight nozzle was also used in some experiments to duplicate the results of the previous program. The temperature of the ORTL medium was monitored both before and after the interaction zone by means of thermocouples traversing the gas flow. The power absorbed by the ORTL medium was then calculated from the observed temperature rise in the flowing gas, as monitored by the series of 8 thermocouples which were placed across the flow 3 cm downstream of the interaction zone where the deactivation of excited states would be complete. Tests conducted with inlet gas temperatures greater than ambient demonstrated that the centerline temperature was only slightly affected by heat transfer to the cooled walls.

Power lost to the side mirrors (both by optical absorption during the repeated reflections and by heat transfer from the ORTL medium) was measured by monitoring the flow rate and temperature rise of the side mirror coolant.

The use of single pass cooling water for all measurements enhanced baseline stability.

The ORTL diluent and curtain gas consisted of either helium, sulfur hexafluoride, or tetrafluoromethane. Since water is a major HF deactivator, it was important to note the concentration of water in the diluents. The SF_6 and CF_4 were purchased from Air Products, and had 8 and 9 molar ppm of water, respectively. The helium, which was obtained from Airco, contained less than 12 ppm water.

HF was purified by a distillation technique and stored over CoF_3. The HF flow rate was controlled by a Matheson mass flow controller, which was calibrated at the beginning and end of each day. The flow rate was calibrated by monitoring the increase in pressure with time in a known volume. The temperature of the gas was monitored; to avoid nonlinearities due to the non-ideal gas nature of HF, the pressure was limited to less than 100 torr as measured by an MKS Baratron capacitance manometer. Sonic metering orifices controlling the flow rate of diluent were calibrated by the same procedure, without the limitation on operating pressure. The relative error in concentration was thus very small. The drift in HF flow rate was less than 4 percent.

Inlet temperature of the ORTL medium was controlled by flowing the gas through a fixed bed heat exchanger, Figure 2. At the inlet of the heat exchanger, a nickel screen distributed the flow evenly. The gas then traveled through a 10 cm depth of 0.2 cm diameter aluminum pellets. A second screen distributed the flow evenly into the approach nozzle and the ORTL cell. The packed bed was contained within a nickel-plated box, that was enclosed within an airtight outer box for thermal isolation. Unheated curtain flow was brought through the top of the box, and exited alongside the ORTL medium flow through nickel screens.

The heat exchanger was charged by passing hot nitrogen through it at atmospheric pressure. This gas was heated by two commercial heaters (HottWatt model PF-010). The temperature of the gas exiting the bed through the nozzle was monitored, and when the temperature was constant, the bed was considered to be fully charged. The thermal capacity of the bed (2 kG

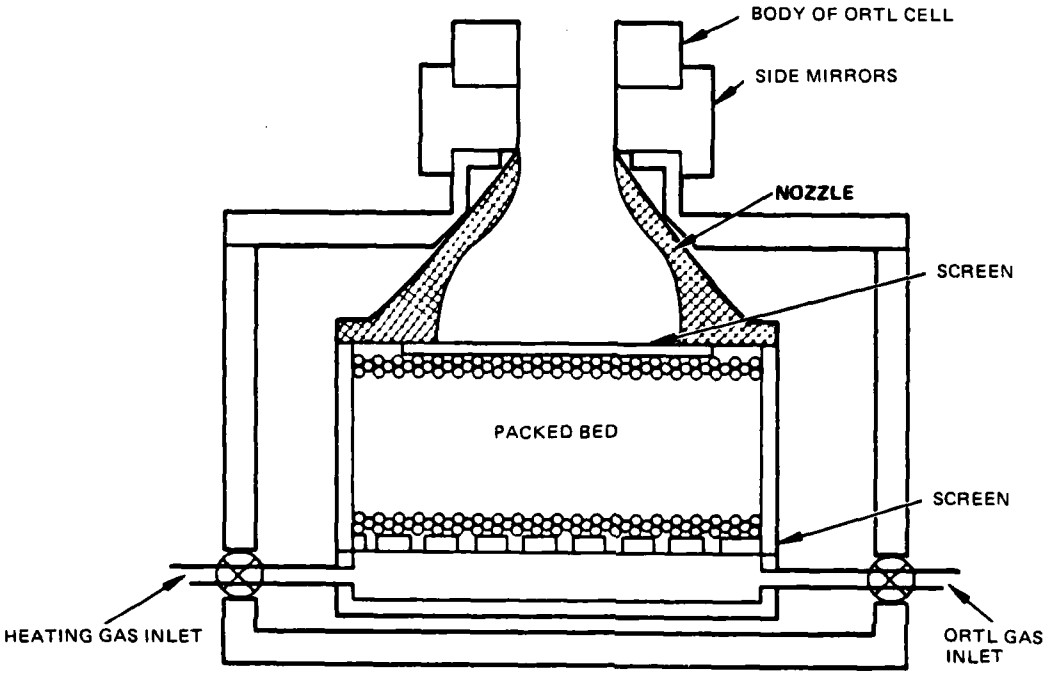

Figure 2. ORTL heater.

of aluminum) was several times that required to heat the ORTL diluent for a typical run time.

The large surface area and high thermal mass of the pellets allowed heating of the ORTL gas to the bed temperature in a short distance. The remainder of the bed was little affected by the gas temperature and served mainly to smooth out small temperature variations. The top layer of pellets did not change temperature until the bed charge was nearly exhausted. Because the high efficiency of the heat exchanger did not require extremely high metal temperatures and because the aluminum fluoride formed in the packed bed during passivation was stable at these temperatures, the reaction of HF with the bed was not expected to be a problem once the bed had been exposed to HF at elevated temperatures. An early experiment showed that the ORTL power and temperature rise were unaffected by passing the HF/helium mixture through the heat exchanger, rather than bypassing the bed. Prior to use, the bed was

dried by going through several heated gas cycles. It was then stored under ultra-pure grade dry nitrogen.

The entire ORTL apparatus was leak checked at various stages of assembly. The leak rate of the assembled system was approximately 10^{-8} moles/second, sufficiently low to ensure that no negative effects could be caused by an increase in the deactivation rates.

To prevent attenuation of the pump beam by atmospheric water vapor, the entire optical path was purged with nitrogen drawn from a liquid nitrogen supply, as were the spectrometers, preventing the calibration from changing with time.

In the High Energy ORTL study, the ORTL mirror absorption was measured to obtain the ORTL power. The sum of the scattered and the diffracted power was measured by spillover calorimetry, using collar tubes with high absorption surfaces that were placed between each ORTL resonator mirror and the side mirrors. The temperature rises of these tubes were monitored as functions of time. The sum of the scattered and diffractive losses was derived from the temperature rise and the specific heat of each tube. The ratio of the power absorbed in each ORTL mirror to that absorbed by its spill-over tube was found to be 1:0.15. Therefore, a correction factor of 1.15 should be applied to the ORTL power as measured by mirror absorption. This correction factor was used throughout this program and should be applied to the data from the previous program.

2.2 EXTRACAVITY EXPERIMENTS

This task had as its primary aim the determination of the dependence of ORTL efficiency upon various operating parameters such as pump laser spectral distribution, pump laser irradiance, ORTL gas inlet temperature, ORTL gas inlet velocity, and partial pressure of HF in the ORTL cell. The effect of various diluent gases in the ORTL cell was also investigated. Understanding of the changes in ORTL performance as these parameters are varied would provide the basis for re-evaluation of the kinetic rates used in the computer model so that the code could be made a reliable forecaster of experimental results to be expected in different (e.g., larger) ORTL systems.

2.2.1 Preliminary Measurements

Before the parametric variation study was initiated, a preliminary series of experiments was performed to standardize run procedures and to define the region of parameter space that was both available and of interest. During this series, the effects of side mirror reflectivity, pump beam focusing, ORTL gas flow velocity, and return of throughput pump flux to the ORTL for a second pass was investigated. The pump chemical laser was operated as nearly as possible at the same set of operating conditions each time. About 700 watts of power distributed over the J=4, 5 and 6 lines of the V=1→0 and V=2→1 bands were outcoupled in a beam which, when focused with a cylindrical mirror, had a cross section of 1.7 cm x 0.55 cm at the ORTL cell. Unfocused, the beam was 1.7 cm x 1.65 cm.

The data in Table 1 are representative of the best obtained in this preliminary investigation (runs 4-10) and in the earlier High Energy ORTL Study program (runs 1-3). In Table 1, P_{IN} corresponds to the chemical laser power incident on the multiple pass cell aperture, and P_M corresponds to the power absorbed in the side mirrors. In the High Energy ORTL Study, it was assumed that, had the side mirrors had lower reflectivities, the extra power would have been absorbed by the gas and utilized in ORTL operation. Accordingly, this power was subtracted from P_{IN} in computing the overall efficiency. Analysis of data from the current program, with the higher reflectivity side mirrors, leads to the conclusion that this assumption was not fully correct. The last column in Table 1, represents the overall efficiency computed relative to P_{IN}, with nothing subtracted, and is defined as absolute efficiency. The true efficiency, of course, lies somewhere in between the tabulated η_o and η_{AB}. η_{AB} as presented in the table is an absolute lower bound to true ORTL efficiency. Runs #9 and 10 tend to confirm the notion that the multiple pass ORTL cell is long enough to absorb substantially all pump power capable of being absorbed by this gas mixture on a single pass, even when side wall reflection losses have been substantially reduced. A higher HF mixture might have produced more output power. Whatever ambiguities remain in our calculation of ORTL efficiency, one indisputable observation is that the absolute efficiency (η_{AB}) achieved using focused flux in the present program significantly surpassed all earlier results.

TABLE 1. MULTIPLE PASS CELL EFFICIENCY MEASUREMENTS

Run	Date	Side Mirror Reflectivity	Pump Flux	Gas Velocity (10^3cm/sec)	# of Flux Passes	P_{IN} (Watts)	P_{ORTL} (Watts)	P_M (Watts)	$\dot{Q}_{GAS}$ (Watts)	ΔT (^oK)	η_o	η_{AB}
1	4/12/79	0.975	ϕ	0.65	2	702	155	232				0.221
2	4/12/79	0.975	ϕ	1.30	2	718	147	239	147	136	0.307	0.205
3	4/12/79	0.975	ϕ	3.80	2	751	142	262	207	64	0.290	0.189
4	9/05/80	0.963	ϕ	3.0	2	766	188	322	182	713	0.421	0.245
5	9/14/80	0.963	3ϕ	0.3	2	677	176	376				0.260
6	9/14/80	0.963	3ϕ	1.0	2	677	191	340	102	123	0.567	0.282
7	9/14/80	0.963	3ϕ	3.0	2	677	154	350	159	64	0.471	0.227
8	9/14/80	0.963	3ϕ	3.0	1	677	161	240	147	59	0.368	0.238
9	9/24/80	0.986	3ϕ	1.0	2	735	185.6	171	90.6	109	0.328	0.252
10	9/24/80	0.986	3ϕ	1.0	1	735	172	111	68	82	0.275	0.233

Notes: 1) HF mole fraction = 0.004, inlet temp = 300^oK

2) Closed cavity ORTL resonator, reflectivity of each mirror ≈ 0.988

3) Pump flux: $\phi \approx 500$ watts/cm^2
$3\phi \approx 1500$ watts/cm^2

4) $\eta_o = \frac{P_{ORTL}}{P_{IN}-P_M}$; $\eta_{AB} = \frac{P_{ORTL}}{P_{IN}}$

2.2.2 Parameter Selection

Utilizing the results of the preliminary measurements, experimental conditions for the parametric performance characterization were selected as follows:

1. A single pass of the pump flux through the ORTL cell was selected for all runs. With the focused flux, the second pass did not greatly improve ORTL output and, in the apparatus used, the throughput beam provided a convenient method of alignment.
2. An ORTL inlet gas flow velocity of 3×10^3 cm/sec was chosen for use throughout this investigation. The rather small reduction in ORTL output from that obtainable at lower velocity was a small price to pay for the experimental convenience of lower temperature operation. (This apparatus did not permit as accurate measurement of large temperature increases as of small ones so comparison with model results would have been more difficult in that situation.)
3. Side mirrors with R = 0.986 were used to minimize the power coupled into them.
4. The ORTL resonator configuration with each mirror having a reflectivity of 0.986 was retained.
5. Two pump laser operating conditions were chosen. One resulted in a spectrum ("low J") with a lower average value of J and a lower output power than the other (the "high J" spectrum). These spectra are shown in Tables 2 and 3.
6. SF_6 and CF_4 were chosen as alternative diluents to helium. A literature search for gases that have both small cross sections for HF deactivation and large cross sections for assisting rotational-rotational (R-R) excitation transfer in HF produced these two as leading candidates. To make temperature rises about the same for different diluents, pressures of diluents were made inversely proportional to their specific heat.
7. For the runs with helium diluent, a total ORTL gas pressure of 76 torr with HF partial pressures of 0.076 torr, 0.152 torr, 0.304 torr, 0.532 torr, and 0.760 torr (i.e., 0.1, 0.2, 0.4, 0.7, and 1.0 percent) were selected because of the expectation that, for the pump spectra used, maximum ORTL output would occur in this range.
8. Pump irradiances of 1504, 892, and 405 watts/cm^2 were used for the low J laser condition because the spectrum typically contained about 700 watts and the available focusing lens and attenuators provided these values.

TABLE 2. LOW J-DISTRIBUTION CHEMICAL LASER OPERATING CONDITIONS (EXTRACAVITY EXPERIMENTS)

Output Power: 720 watts Beam Shape: 1.70 cm x 0.55 cm (0.935 cm^2)			
Spectral Distribution			
V = 1 → V = 0		V = 2 → V = 1	
Transition	Power (%)	Transition	Power (%)
P(4)	9.0	P(4)	14.7
P(5)	22.7	P(5)	26.0
P(6)	15.3	P(6)	10.0
P(7)	0.6	P(7)	1.7
	47.6		52.4

TABLE 3. HIGH J-DISTRIBUTION CHEMICAL LASER OPERATING CONDITIONS (EXTRACAVITY EXPERIMENTS)

Output Power: 1075 watts Beam Shape: 1.70 cm x 0.55 cm (0.935 cm^2)			
Spectral Distribution			
V = 1 → V = 0		V = 2 → V = 1	
Transition	Power (%)	Transition	Power (%)
P(4)	2.0	P(4)	7.0
P(5)	16.0	P(5)	23.0
P(6)	21.0	P(6)	14.0
P(7)	11.0	P(7)	4.0
P(8)	1.0	P(8)	1.0
	51.0		49.0

9. Heat losses from the fixed bed heat exchanger limited the maximum ORTL gas inlet temperature to 450°K. Therefore, 300°K, 375°K, and 450°K were chosen as ORTL gas inlet temperatures.

These choices were made both for experimental convenience in utilizing the existing hardware and with the aim of providing information to be used in modeling other systems. They were not made with the aim of demonstrating high ORTL efficiency. Therefore, choices of some parameters are not those that would provide highest ORTL output. Nevertheless, data were taken sufficiently close to optimal conditions to induce confidence that the correct parameter dependences have been obtained. As an example, Figure 3 shows single flux pass focused data taken during this program and double flux pass, unfocused data from an earlier one. The conclusion that higher flux density shifts the peak ORTL power point to higher HF pressure is considered valid even though the ORTL output could probably have been increased at all of the pressures used by slowing the ORTL gas flow.

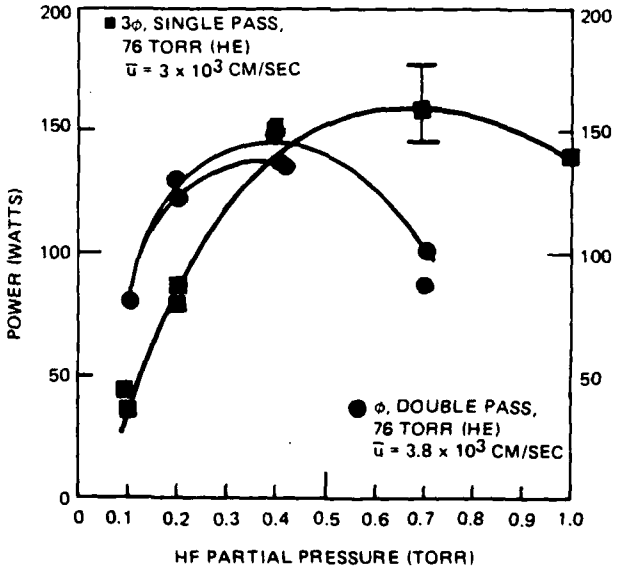

Figure 3. ORTL performance at two different values of pump flux.

2.2.3 Parametric Performance Characterization

After analysis of preliminary data had been completed and the matrix of parameter combinations selected for the main body of the laboratory investigation, it was found, upon reactivating the system, that ORTL output power levels had decreased by about 20 percent from those obtained for apparently identical preliminary runs. Considerable effort did not reveal the reason for this.

Whatever the source of the difficulty, the newer results were seen to be internally consistent. There was not significant day-to-day variation nor were there longer term trends. It was therefore concluded that the aims of the program, namely, to ascertain dependence of ORTL performance on the above mentioned parameters, could as well be met at this reduced operating level. Indeed, the stability of the ORTL system (at the lower output levels) persisted throughout the remainder of the program, permitting rerunning of experiments on different days with the same results.

2.2.3.1 Diluent Screening Tests

To achieve equal temperature increases, SF_6 experiments were run at 16 torr, CF_4 at 23 torr, and helium at 76 torr. Based on the results presented in Figures 4, 5 and 6, CF_4 was eliminated from further consideration. Evidently, for the conditions studied, SF_6 and helium were equally favorable for ORTL efficiency. However, the possibility of operating with SF_6 at lower gas pressure has an important advantage for the intracavity configuration, namely, that the flow rate of the aerodynamic window used therein will be lower than with helium, with which higher ORTL pressure is required to achieve comparable results.

2.2.3.2 Variation of Pump Intensity

Of particular interest in this part of the investigation was the flux level, if any, at which R-R rates so limit ORTL output that efficiency begins to decrease. The overall efficiency, η_o, is the ORTL output power divided by the available chemical laser power and may be expressed as the product of input efficiency η_{IN} and conversion efficiency η_c, where η_{IN} is the total power absorbed by the ORTL medium divided by the available chemical laser power and

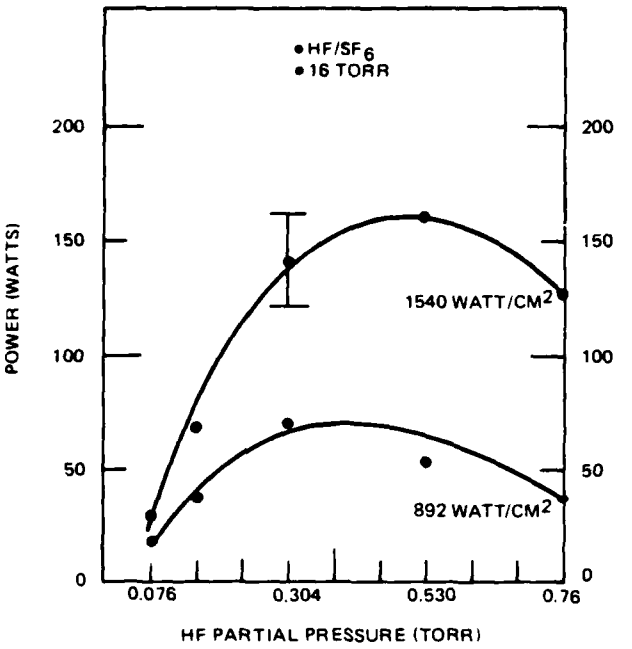

Figure 4. Extracavity ORTL performance with SF_6 diluent.

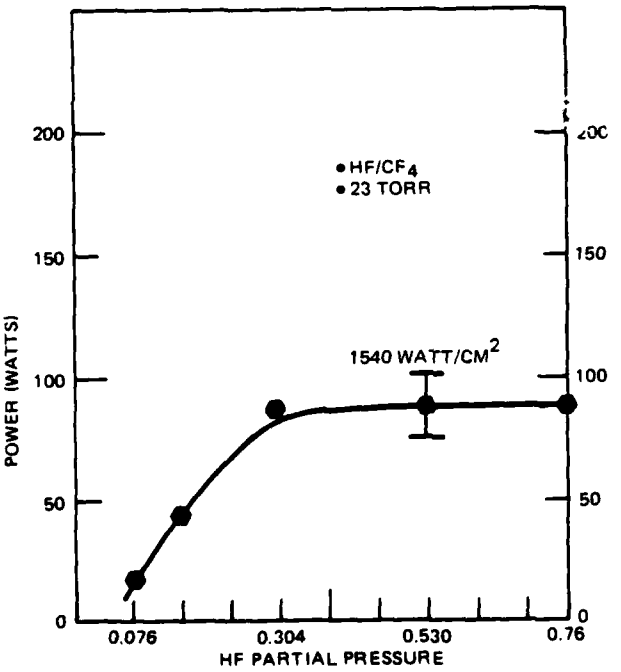

Figure 5. Extracavity ORTL performance with CF_4 diluent.

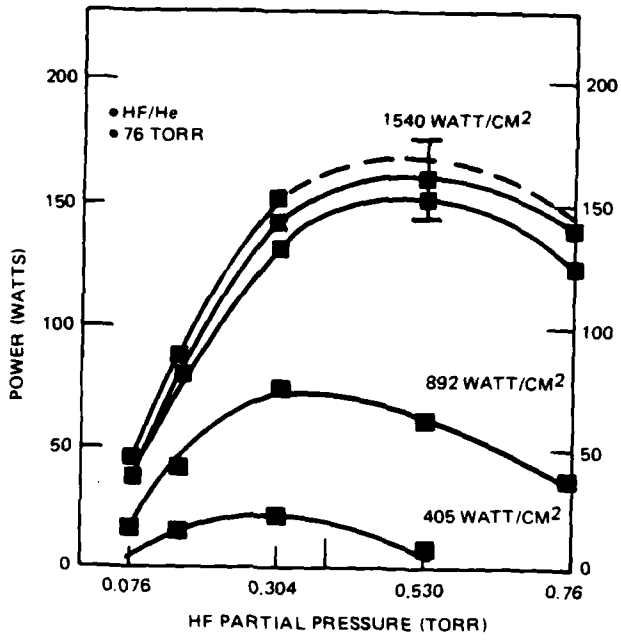

Figure 6. Extracavity ORTL performance with helium diluent.

η_c is the ORTL output power divided by the power absorbed by the medium. Figures 7 and 8 show that the overall efficiency and the partial pressure of HF at which the peak efficiency was attained both increased with increasing pump irradiance for both helium and SF_6 diluents. Figure 9 presents the helium data differently to show that ORTL efficiency increased with pump flux for all HF pressures used. The highest available irradiance evidently was sufficient to approach maximum efficiency in the low HF fraction cases (0.001, 0.002) but the more HF in the ORTL gas, the more rapidly the efficiencies climbed. In no case did efficiency decline with increasing irradiance. As indicated in Figure 9, it is not difficult to make the extrapolation that 40-50 percent efficiency would be achieved at 3 KW/cm^2.

2.2.3.3 Variation of ORTL Gas Inlet Temperature

At room temperature, most of the HF molecules in the V=0 level are at J values lower than those needed for resonance absorption of radiation concentrated in the J = 4, 5, 6 lines. Preheating the ORTL gas should alleviate this mismatch and would be expected, therefore, to improve input efficiency.

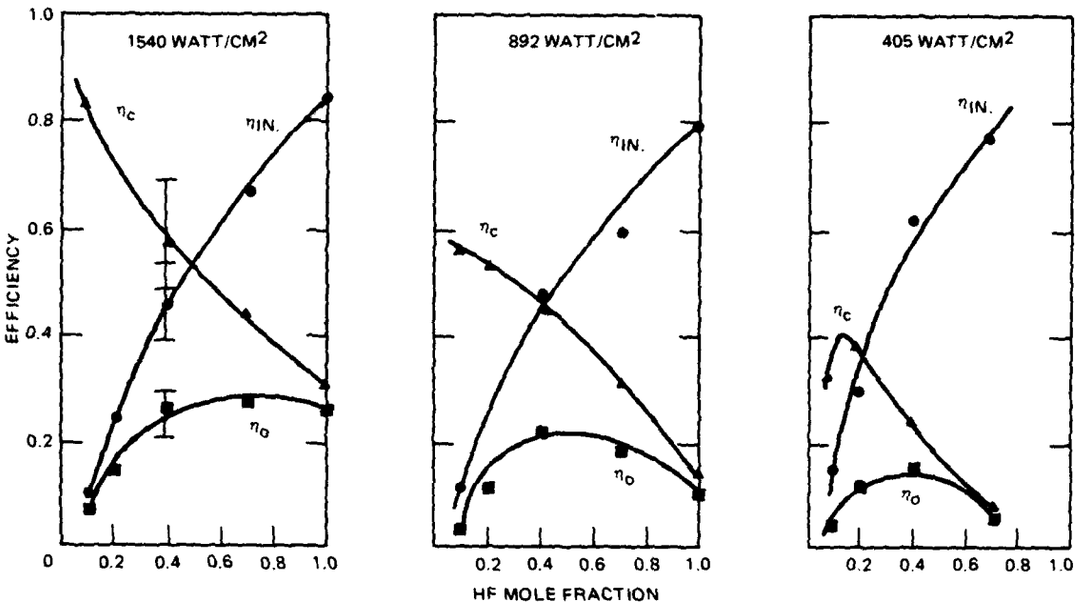

Figure 7. HF/He extracavity ORTL efficiencies.

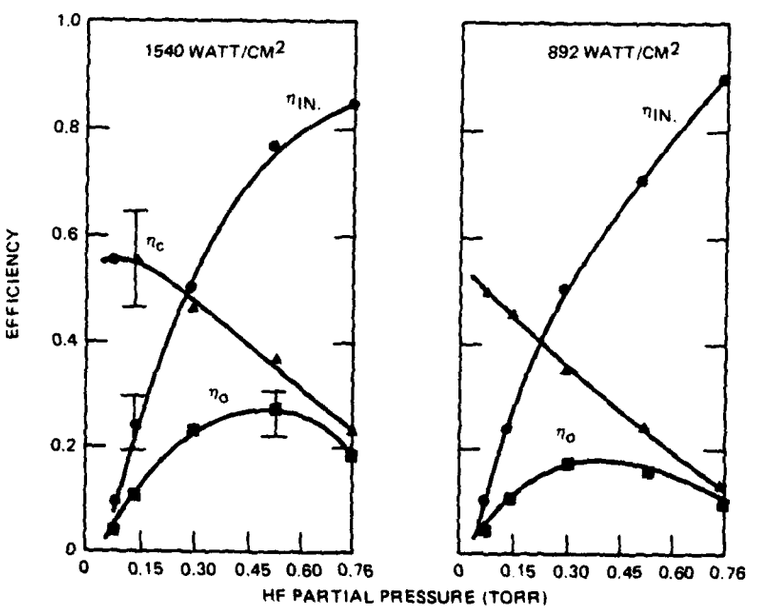

Figure 8. HF/SF_6 extracavity ORTL efficiencies.

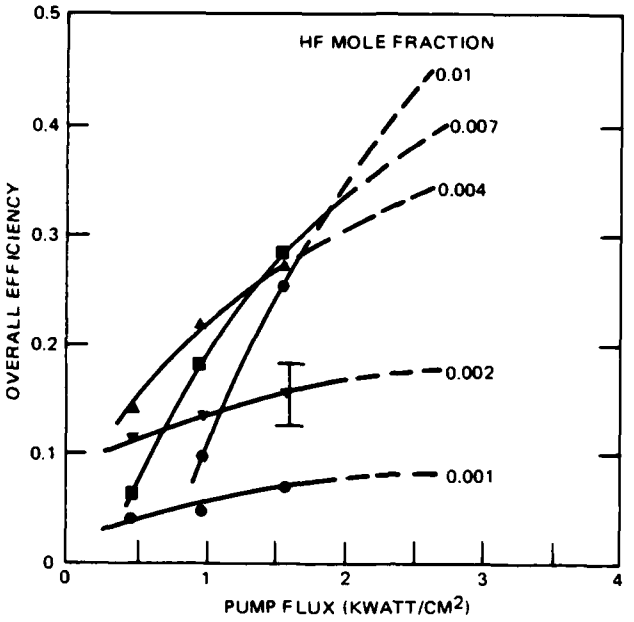

Figure 9. Extracavity ORTL efficiency versus pump flux (helium diluent – 76 torr).

The effect on overall efficiency would depend upon the outcome of competition between this enhancing effect and the deleterious effect of increased deactivation at higher temperature. Figure 10 shows that, as inlet temperature increased, peak ORTL output increased and shifted toward lower HF partial pressure, reflecting the more efficient pumping available at high temperature. Figure 11 underscores this effect. Greater improvement was obtained with the high J spectrum than with the low J spectrum since the mismatch between pump laser spectrum and 300°K ORTL population distribution was greater with the former.

2.2.4 Summary of Results and Observations

SF_6 performed about as well as helium and, because of its high specific heat, it offers the advantage of lower pressure operation. The first panels of Figures 7 and 8 suggest that, at low HF fraction, the conversion efficiency with SF_6 as the diluent drops significantly below that obtained when helium is used. This region may require reinvestigation, especially if such low HF partial pressure is to be used. However, efficient systems would probably be designed to operate nearer the peak overall efficiency region.

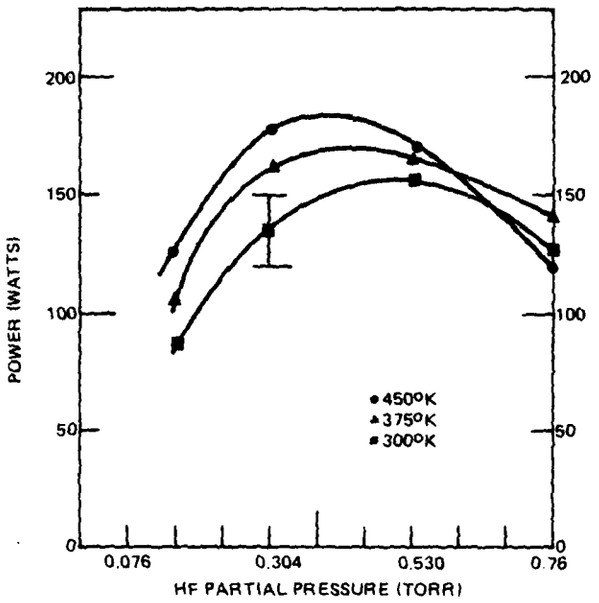

Figure 10. Dependence of HF/He ORTL performance on inlet temperature (low J pumping).

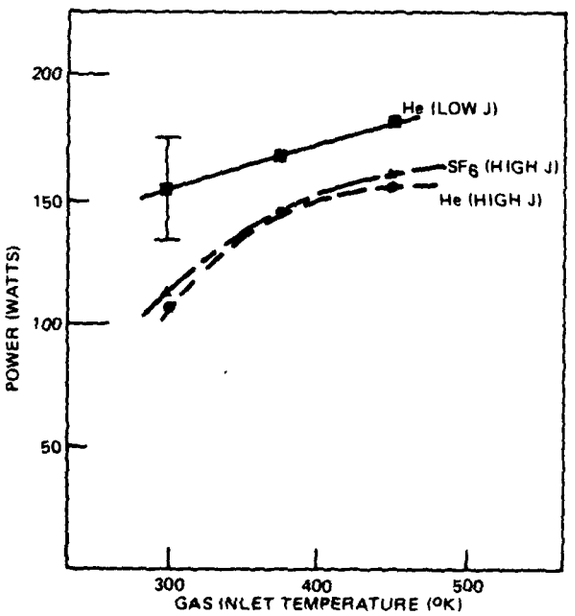

Figure 11. Peak ORTL performance at various inlet temperatures.

No rotational bottleneck was observed, even at 1.5 Kwatt/cm^2, the highest irradiance available in this investigation. (This lends confidence to the model predictions from the High Energy ORTL Study that indicate that overall efficiencies of 50 percent or higher in the extracavity configuration and 85 percent or greater in the intracavity configuration should be attainable at very high irradiance levels.)

Preheating the ORTL gas improved efficiency. This suggests that the resulting higher average ORTL gas temperature is the source of the efficiency increase often seen as gas velocity is lowered.

Although such numbers were not the primary consideration of this program, a summary of the highest obtained efficiencies seems appropriate here:

- An overall efficiency of 0.37 was achieved in a single pass configuration. (In the previous program, 0.33 was achieved.)
- An absolute efficiency of 0.28 was achieved. (0.22 was achieved previously.)
- Extrapolation of the experimental data leads to a projected single pass efficiency of 0.50 at irradiance levels two to three times higher than those used here.

3.0 INTRACAVITY EXPERIMENTS

The intracavity experiments required an apparatus different from that used for extracavity experiments. Therefore, chemical laser and ORTL hardware designed for the intracavity task were constructed. For effective intracavity ORTL operation, chemical laser oscillation must be confined to short wavelength and the ORTL medium must be regulated so that absorption is present at these wavelengths and gain is present at longer wavelengths. This was accomplished in these experiments by the use of step filter coatings on the chemical laser resonator optics and regulation of the ORTL gas inlet temperature. The chemical laser gain length was increased for these experiments to 50 cm in order to provide an adequate test of the spectral control filters and to allow a relatively high absorption coefficient to be used in the ORTL cell without suppressing chemical laser oscillation. An overall description of the fabricated apparatus is presented in Section 3.1. Critical design issues are specifically addressed in Section 3.1.4, and chemical laser characterization data are described in Section 3.1.5. The intracavity experiments are discussed in Section 3.2.

3.1 EXPERIMENTAL APPARATUS

Figure 12 is a photograph of the intracavity apparatus. The chemical laser with its 50 cm long nozzle is in the left center region of the photograph. Adjacent to the nozzle (approximately in the center of the photo) is the aerodynamic window which provides a controlled interface between the low pressure chemical laser gain region and the higher pressure ORTL environment. The ORTL and the chemical laser resonator optics reside in the two large boxes on either side of the chemical laser.

The HF combustion driven laser was typically operated at flow conditions that produced approximately 500 watts output with a 35 percent transmitting outcoupling mirror. The specific conditions and spectra will be discussed in Section 3.1.5. The beam as measured by plexiglass burns taken 20 cm from the outcoupling mirror, was approximately 3.5 mm by 22.5 mm (0.8 cm^2). Lasing was on J = 6-9 transitions of the 2 → 1 and 1 → 0 vibrational bands.

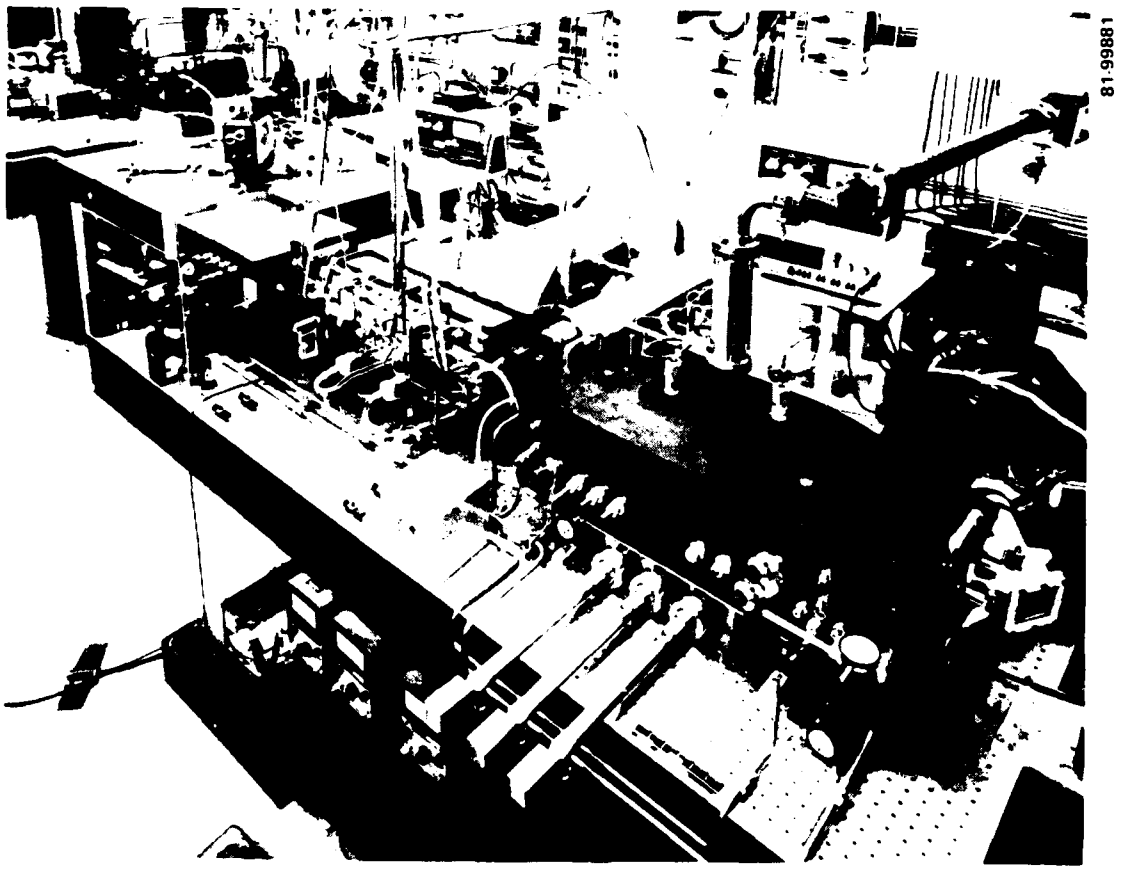

Figure 12. Intracavity ORTL apparatus.

3.1.1 Chemical Laser Resonator

Figure 13 shows two of the chemical laser resonator mirrors. In this photo the chemical laser beam enters and exits the mirror box at the upper left. Note that one, two, or three mirrors could be used at this end of the laser, allowing investigation of the effects of varying spectral control filter strengths. The water cooled chemical laser resonator mirrors were used as power meters by recording the cooling water temperature rise and flow rate. The spectral control filters consisted of coatings whose reflectivity varied with wavelength to limit lasing to specific J-transitions. The reflectivity curve furnished by the manufacturer, OCLI, are shown in Figure 14. The other end of the resonator was in the ORTL box at the mirror on the far right of Figure 15. Figure 15 also shows the ORTL cell and resonator optics which were

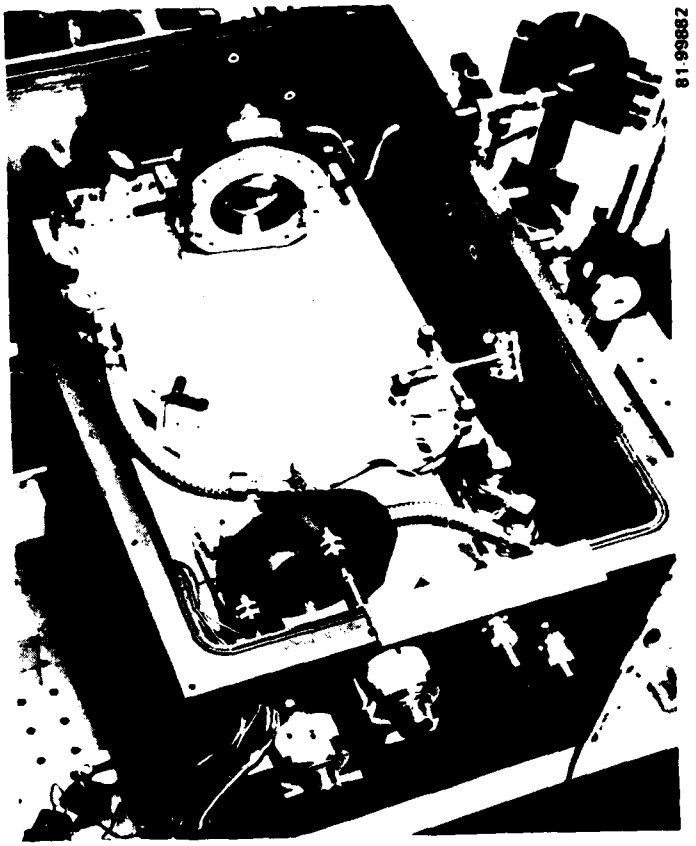

Figure 13. Chemical laser mirror box.

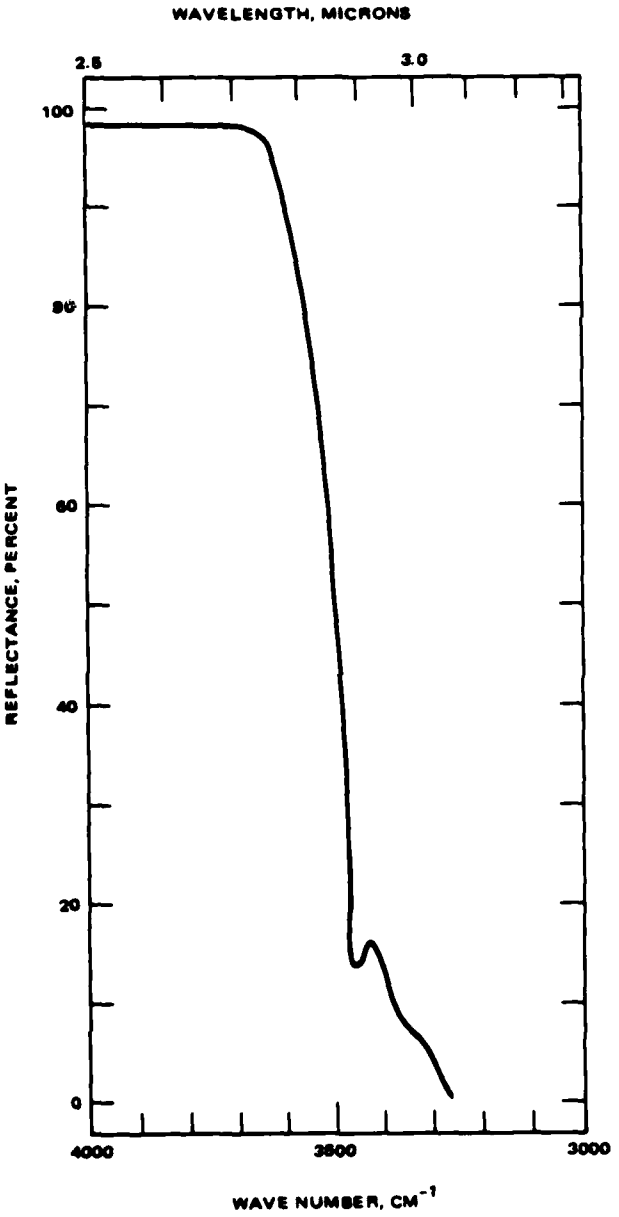

Figure 14. Spectral control mirror reflectance.

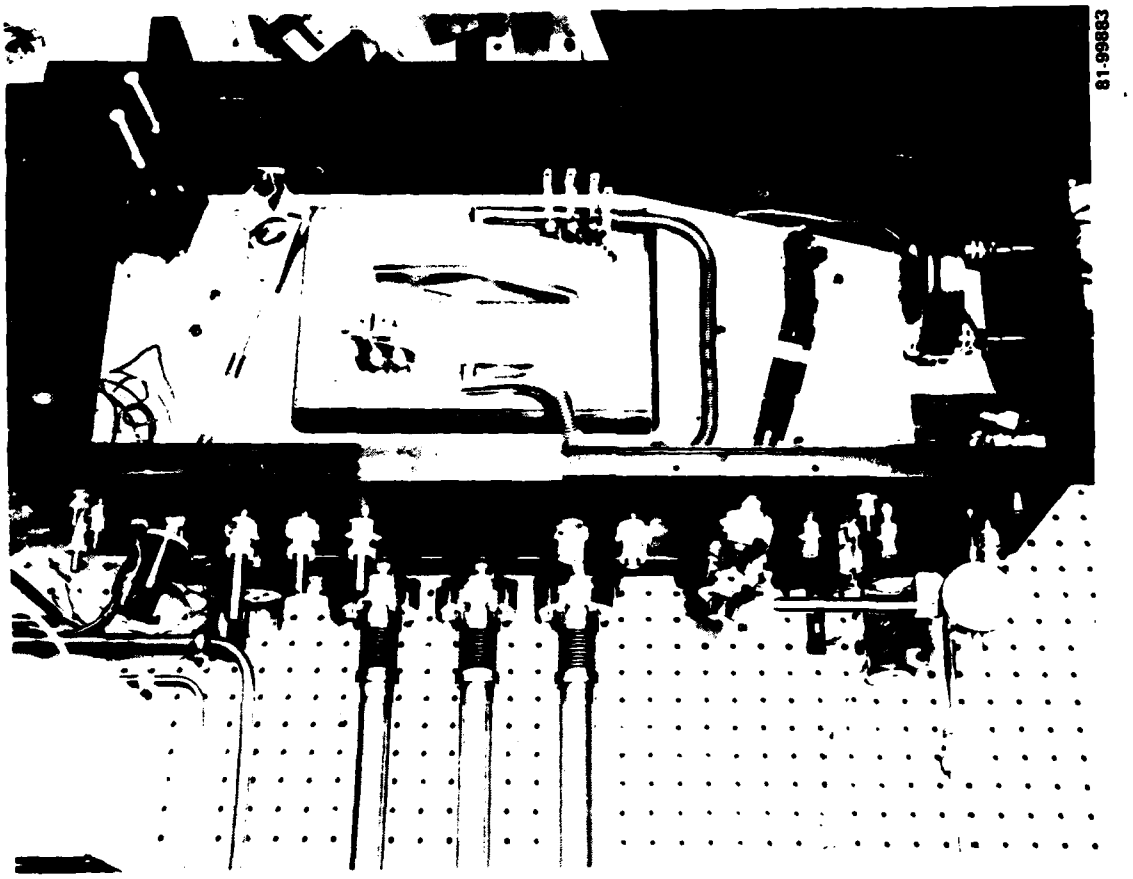

Figure 15. ORTL mirror box.

positioned to produce an ORTL optical axis skewed at 15 degrees to the chemical laser optical axis.

The chemical laser resonator axis was set 1.25 cm from the nozzle edge. The aerowindow aperture and apertures in front of each mirror served to suppress parasitic oscillations. The three apertures were thermally insulated, and their temperatures monitored. Thus the absorbed power could be obtained from temperature increases during experiments. Figure 16 shows the aperture dimensions and locations. Table 4 provides an estimate of the expected pump beam cross section at each optical component.

3.1.2 ORTL Configuration

The pump beam entered the box that housed the ORTL cell through an aerowindow. The aerowindow was an orifice of 7 x 34 mm cross section through

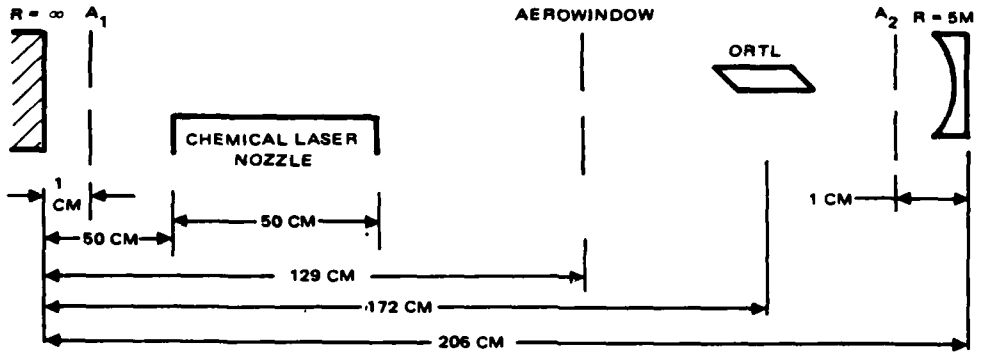

Figure 16. Chemical laser resonator layout.

TABLE 4. INTRACAVITY APERTURE SIZES AND CALCULATED BEAM SHAPE

Aperture	A_1	Aerowindow	A_2
Aperture Size (cm)	2.9 x 0.9	3.4 x 0.7	3.8 x 0.7
Calculated Beam Size (cm)	2.2 x 0.29	2.5 x 0.33	2.9 x 0.38
Note: Sizes calculated according to the method proposed by W.B. Bridges, *Appl. Opt.* 14, 2346 (1975).			

which sonic flow was maintained. In the center of the ORTL box were the ORTL nozzle and curtain manifold (see Figure 15). Below it was the particle bed gas heater. At the bottom of Figure 15 are three 1.8 kW gas heaters that preheated the bed heater. The ORTL nozzle and curtain manifold defined a 1 cm thick duct that symmetrically surrounded the ORTL nozzle. The flow leaving the ORTL nozzle formed a free standing jet that had to be confined by the curtain field until it exited the box. The distance from nozzle to exit was 1.25 cm. Midway, the flow crossed the pump beam and thereby defined the intracavity ORTL interaction volume.

Three ORTL nozzles were fabricated. They were parallelograms in cross section because the ORTL axis was skewed 15 degrees with respect to the pump beam. The oblique axis resulted in a 10 cm long gain length when projected on the ORTL axis. Figure 17 summarizes the interaction volumes, absorption lengths, and gain lengths. Nozzle N-2 was used for the majority of the experiments. Taking into account the rounded corners, the area of the fabricated

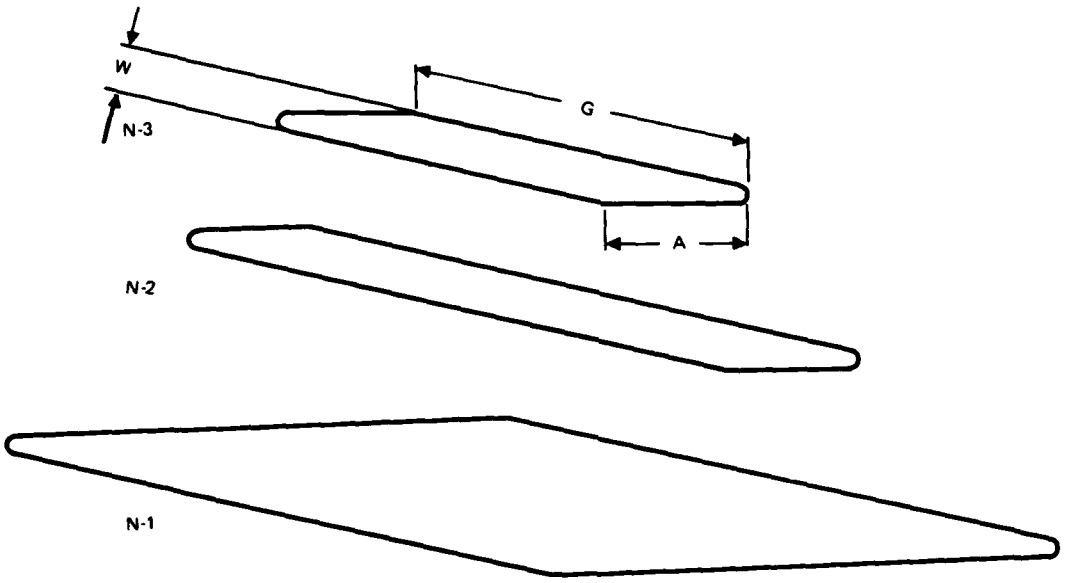

NOZZLE	ABSORPTION LENGTH, A (CM)	GAIN LENGTH, G (CM)	WIDTH, W (CM)	AREA (CM^2)	VOLUME (CM^3)
N-1	9	10	2.25	25.2	8.82
N-2	3	10	0.75	7.3	2.56
N-3	3	7	0.75	5.3	1.84

Figure 17. Dimensions of intracavity ORTL nozzles.

nozzle was 7.31 cm^2. Therefore, a 0.35 cm beam height defined a 2.6 cm^3 interaction volume.

The power absorbed from the pump radiation by the ORTL gas was determined by gas temperature measurements. Ten fine (0.020 inch diameter) thermocouples spaced 1 cm apart spanned the ORTL flow field. (Because nozzle N-3 is smaller than the other two nozzles, eight thermocouples spanned the ORTL flow field in that case). They were located at the exhaust duct, 6.5 mm up from

the ORTL interaction zone centerline, and were parallel to the ORTL optic axis. These measured exit temperature. Inlet temperature was determined from the same thermocouples but with the chemical laser radiation blocked.

3.1.3 ORTL Resonator

The ORTL resonator was a half symmetric optical cavity with a mirror separation of 48 cm. Both closed cavity and outcoupled cavity configurations were utilized. The outcoupling configuration utilized a three meter radius concave total reflector, and a flat silicon partial reflector. The output beam exited through a CaF_2 window and was monitored by a power meter (Coherent Radiation model 213). In addition, the temperature rise of each mirror substrate was measured by a thermocouple which was indium soldered to the surface. For closed cavity operation, flat and 5 meter concave radius water cooled molybdenum substrates were used. The power deposited in each mirror was determined by recording the water flow rate and temperature rise. ORTL spectra were obtained by imaging the laser radiation scattered off the flat mirror onto a scanning monochrometer (McPherson model 218).

In order to maximize the ORTL resonator extraction efficiency in the laboratory device, low outcoupling was used for the entire test series. Individual mirror reflectivities were determined by either laser calorimetry, or dual beam HF laser reflectance measurements. The latter uncertainty was ± 1 percent. Table 5 summarizes the reflectance values of individual mirror components used in different series of experiments. The difference between initial and final reflectivities was probably due to mirror degradation incurred during the experiments.

The ORTL power was measured as the sum of the power absorbed by the total reflector and that transmitted and absorbed by the outcoupling mirror. Typically, the sum of the ORTL power absorbed by the total reflector and that absorbed by the outcoupling substrate were 10 percent of the outcoupled power. The outcoupled power measured in the powermeter was adjusted to account for transmission through the 94 percent transmittance CaF_2 window.

TABLE 5. ORTL RESONATOR MIRROR REFLECTIVITIES

Test Series	Curved Mirror			Flat Mirror		
	Optic	Reflectivity		Optic	Reflectivity	
		Initial	Final		Initial	Final
I	M1	99.86	96.50	O1	96	88.0
II	M2	99.86	99.80	O2	96.5	93.6
III	M3	97.4	92*	M4	97.4	92*
IV	M2	99.80	99.80	O2	93.6	88*

Notes: M_1, M_2 - Molybdenum total reflector, 3m radius, enhanced silver coating

M_3, M_4 - Water cooled molybdenum substrate, gold coated, 5 meter radius and flat mirrors

O_1 - Silicon outcoupling flat, 96 percent nominal reflectance

O_2 - Same as O but different coating runs

* - Indicates estimated values

3.1.4 Critical Design Issues

The design criteria for the intracavity apparatus were formulated at the outset of the program. Major criteria were:

1. The pump laser, the ORTL, and their respective optical cavities must be evacuable and there must be no material windows in the beam path.
2. To maintain the chemical laser and ORTL gain media at different pressures, an aerowindow is required between them.
3. The optical components must be vibrationally and thermally isolated from the chemical laser nozzle.
4. In order to confine the ORTL flow a surrounding gas curtain is required.
5. A heater is required to preheat the ORTL flow.

The design and performance of the aerowindow, ORTL curtain, and heater will be described here.

3.1.4.1 Aerowindow

A longitudinal flow aerowindow utilizing a sonic orifice, rather than the familiar transverse flow aerodynamic window, was used. Figure 18 is a drawing of the aerowindow. The aerowindow was defined by the sharp edge of an aluminum orifice with a central slot, 7 x 34 mm. The two additional baffles shown in Figure 18 reduced the pressure gradient both upstream and downstream of the aerowindow aperture and the ORTL box pressurized the aerowindow to a pressure equal to the desired ORTL operating pressure. A radial injector inside the plenum injected nitrogen gas through forty 0.040 inch holes to achieve uniform pressure. The nitrogen was exhausted prior to entry into the chemical laser cavity through a 4 inch I.D. duct.

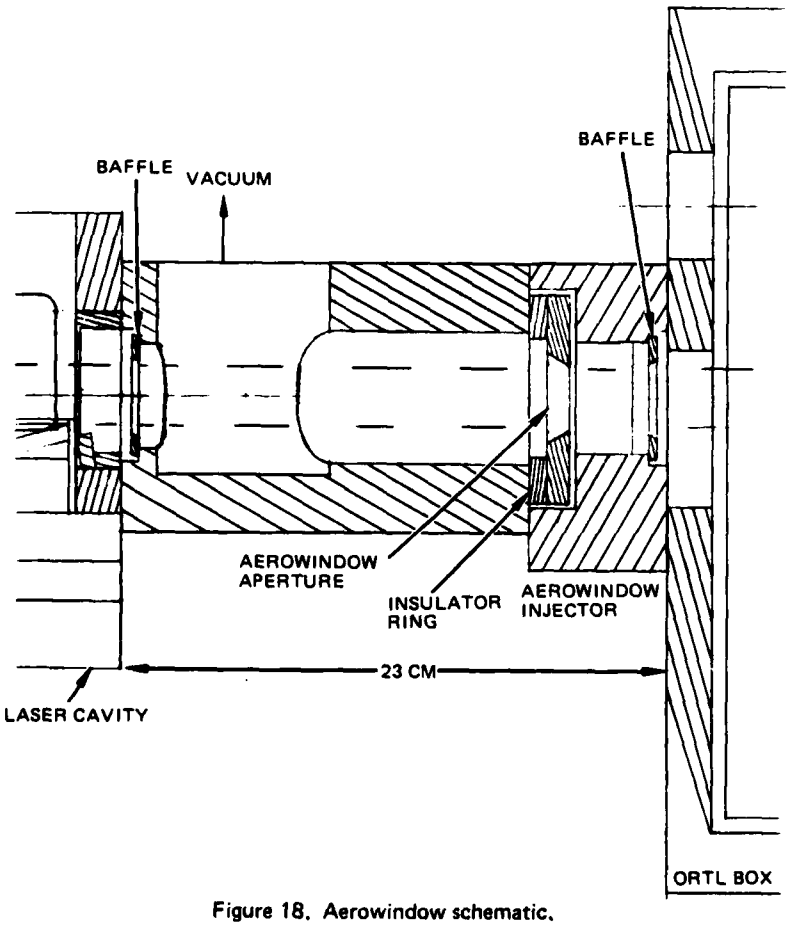

Figure 18. Aerowindow schematic.

The fluid dynamic considerations in this design were relatively simple. The aerowindow was designed to stand off a relatively small pressure differential. Given an aperture size and pressure differential, one can calculate the required aerowindow flow rate and the portion of that flow that will enter the chemical laser cavity. The analysis will be described briefly.

The flow rate through a sharp edge sonic orifice is given by the expression

$$\dot{Z} = CA^*P$$

where $\dot{Z}$ is the flow rate, C is a constant that depends on the molecular properties of the working fluid, A* is the area of the orifice, and P is the driving pressure. For the 7 x 34 mm aperture using nitrogen flow, the equation reduces to

$$\dot{Z} = 2.61 \times 10^{-3}P$$

where $\dot{Z}$ is in moles/sec and P is expressed in torr. The fraction of the flow that enters the laser cavity, $\dot{Z}_L$, depends on the pressure upstream and downstream of the aerowindow, the aerowindow cross section and the distance from the aerowindow aperture to the exhaust port. The approach used in calculating $\dot{Z}_L$ was to threat the flow $\dot{Z}$ leaving the aerowindow aperture as a two dimensional turbulent jet pointed toward the laser cavity. The fraction of the jet that is intercepted by the downstream aerowindow aperture is defined as $\dot{Z}_L$. The difference $\dot{Z}$-$\dot{Z}_L$ is exhausted through the aerowindow duct.

In order to ascertain the effects of the aerowindow flow on the chemical laser spectral distribution, a series of laser spectra were obtained at various ORTL pressures. For optical pumping, the lowest J-transitions are most effective. Therefore, the effective pump power for a room temperature ORTL was defined as the sum of the power of $P_1(6)$, $P_1(7)$, $P_2(5)$ and $P_2(6)$ lasing lines, and this sum was used as a figure of merit. The results are shown in Figure 19. The effective pump power decreased from 190 watts at 16 torr to 106 watts at 45 torr, a 44 percent decrease, although the total power decreased from 240 watts to 212 watts, a 12 percent decrease. Pressures below about 32 torr constitute the useful operating region for ORTL experiments with N_2 used to supply the

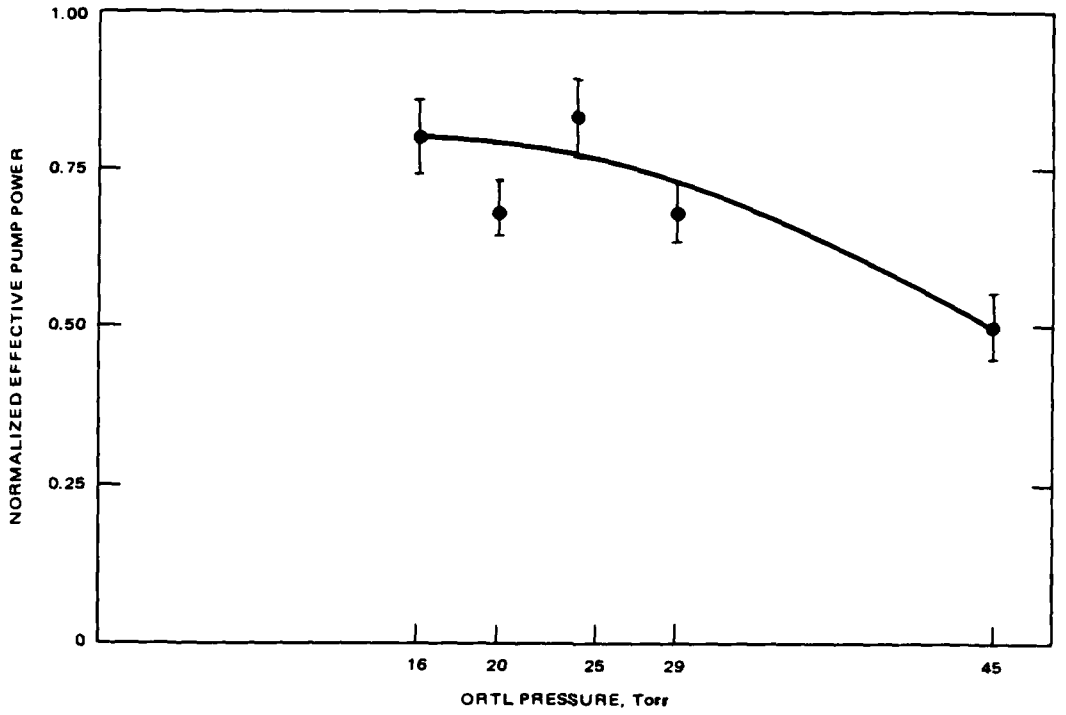

Figure 19. Effect of aerowindow flow on effective chemical laser power.

aerowindow. This experimentally determined upper pressure limit is defined by the maximum N_2 flow rate that can be injested by the chemical laser, without significantly affecting the lasing spectrum. In order to operate at higher pressure and not disturb the laser spectrum, a different gas would have to be considered. Polyatomic gases such as Freon, CF_4, or SF_6 have C values twice as small as N_2 and thus are potential candidates.

3.1.4.2 ORTL Flow Curtain

The design objectives for the ORTL nozzle and curtain were to deliver a uniform flow free of density fluctuations into the interaction zone, and to confine that flow well into the exhaust duct. In addition, duplication of extracavity flow conditions was desirable so that comparison would be possible. The choice of an extracavity comparison case resulted in the following requirements: HF/He operation at 76 torr, HF/SF_6 operation at 16 torr, an interaction time of 500 μsec. Coupled with an intracavity pump beam of 0.35 cm height this

resulted in a flow velocity of 700 cm/sec. The corresponding flow rate was specified for each specific nozzle cross section. The capacity to vary conditions about this operating point was also required.

A scale drawing of the nozzle/curtain assembly is shown in Figure 20. The ORTL flow prior to reaching the ORTL nozzle passed through two screens and the particle bed heater. The lower screen (not shown) served to damp out velocity gradients as the gas entered the heater plenum. The second screen (just below the nozzle) pressurized the top of the heater bed to ensure that the entire heater bed cross section (14 cm x 24 cm) contributed to heating the gas. Upon exiting the nozzle, the ORTL gas flowed alongside the curtain flow. The resultant flow fields extended 1.25 cm to the exhaust duct.

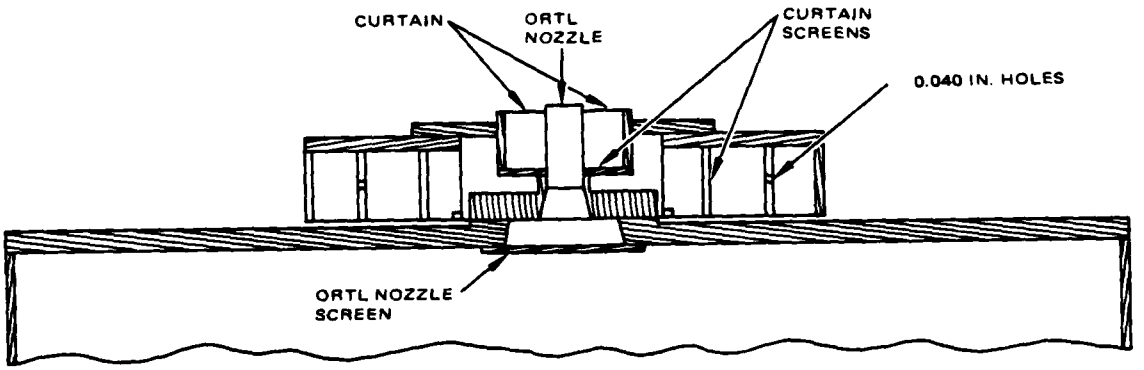

Figure 20. ORTL nozzle/curtain assembly.

The curtain manifold sat on top of the heater box but, as shown in Figure 20, made thermal contact only at the nozzle. The manifold had three chambers on either side and each was fed by a 1 cm diameter tube. The first chamber redistributed the incoming flow across the 25 cm long curtain plenum via twenty 0.040 inch holes. The second and third chamber each had low (1 percent) porosity screens to reduce velocity gradients in order that the entire curtain perimeter be symmetrically supplied with helium. The curtain nozzle duct was a 15 mm high, 1 cm wide duct which symmetrically surrounded the ORTL nozzle. In fact, one wall of the curtain duct was the ORTL nozzle (refer to Figure 20).

A critical design point was the need for confinement of the central HF flow by the curtain gas. The analysis is based upon the work of Sawyer* on two-dimensional reattaching jet flows. Referring to Figure 21 a jet with uniform velocity profile spreads after leaving the duct. The potential core, represented by the inside triangle, diminishes in thickness as the jet develops until a distance X_o, where the helium curtain layer and HF nozzle layers coalesce. At that point there is no confinement. Sawyer gives the empirical relation for X_o as

$$X_o = (6.97 - 28.9C)t$$

where t is the duct thickness and $C = \sigma/t$ where σ is the boundary layer thickness inside the duct, and

$$\sigma = \left(\frac{\eta \ell}{\rho u}\right)^{1/2}$$

where η is the viscosity in poise, ℓ the duct length in cm, ρ the fluid density in g/cm^3 and u the velocity in cm/sec. X_o for He and SF_6 is shown in Table 6.

For SF_6, X_o is well into the exhaust duct at 16 torr at 700 cm/sec. The same is true for He and SF_6 at 76 torr. For He at 16 torr, the curtain velocity must be increased.

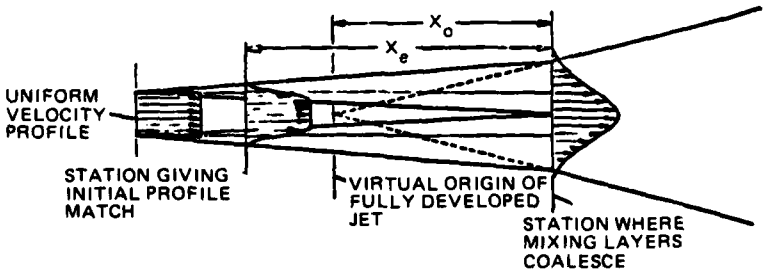

Figure 21. Development of a uniform velocity jet.

*R.A. Sawyer, Fluid Mechanics 17, 481 (1963).

TABLE 6. COALESCENCE DISTANCE, X_o

Pressure (torr)	Velocity (cm/sec)	σ(He) (cm)	$\sigma(SF_6)$ (cm)	X_o(He) (cm)	$X_o(SF_6)$ (cm)
76	700	0.18	0.01	1.7	6.7
16	700	0.40	0.074	0	4.8
16	2100	0.20	-	1.2	-
16	5300	0.13	-	3.3	-

A second important design issue was the turbulent mixing layer that occurs between the ORTL and curtain flows. In this layer, the temperature is reduced. (This will affect the ORTL efficiency.) To minimize the mixing layer, the criterion is to match the momentum rather than the velocity of the two flows.* When helium was used in the curtain and SF_6 was used in the nozzle, the difference in molecular weight implied an order of magnitude increase in the curtain velocity over that in the nozzle.

The degree of mixing turbulence is a complex problem. This analysis of curtain confinement was at best only a design guide. The treatment did not take into account heat addition to the ORTL core. One expected the jet to both expand further in area and to increase in velocity. Because of this, some experimental effort was devoted to empirically assessing the effect of curtain velocity and gas on ORTL performance, and choosing an optimal operating point.

3.1.4.3 Preheated Fixed Bed Heat Exchanger

A heater assembly was implemented to provide temperature control of the ORTL medium. This consisted of a fixed bed heat exchanger, Figure 22, similar to the one used in the extracavity experiments. In order to minimize the heat losses which were observed in the earlier experiments, design improvements were made. These included: gold plating the inner walls of the stainless box, increased heat capacity in the bed, isolation of the bed by a vacuum jacket, separation of the cover and the box, and insulation of the cover by dual metal shrouds. By isolating the bed, heat losses were minimized. The heat exchanger

*A.L. Brown and A. Roshko, J. Fluid Mech. 64, 775 (1974).

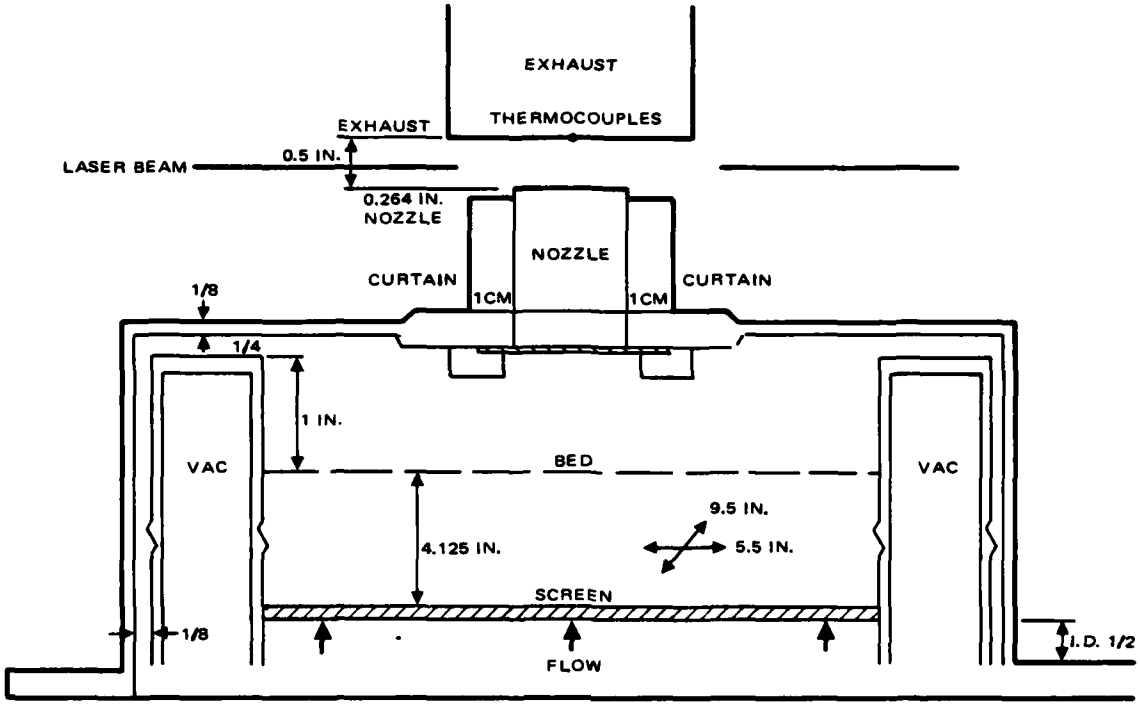

Figure 22. Intracavity ORTL heater assembly.

was preheated by passing hot nitrogen gas through it from three commercial (Hotwatt) gas heaters. During this preheating stage, the gas exited through a port in the heater cover. (This port was sealed when ORTL medium was flowing.) The aluminum bed temperature was monitored by three thermocouples located at various depths inside the bed. Once the temperature of the entire aluminum bed reached the desired value, the ORTL gas was passed through it producing an output gas temperature equal to the temperature of the aluminum pellets. The ORTL medium exited the bed through the nozzle into the interaction region.

After exiting the heater bed, the hot ORTL gas lost heat by three mechanisms: gas mixing from cool and hot regions above the heater bed, conduction by cool nozzle walls, and mixing with cool curtain gas. This is schematically illustrated in Figure 23. The major heat loss mechanism was determined to be gas mixing above the heater bed. In order to prevent hot ORTL gas from contacting the cooler heater box enclosure walls, a dual shroud system was installed inside the heater box. The upper shroud consisted of a top plate, 0.020 inch stainless, which rested on top of the heater box. A lower aluminum plate rested below the stainless shroud and was insulated from it by ceramic

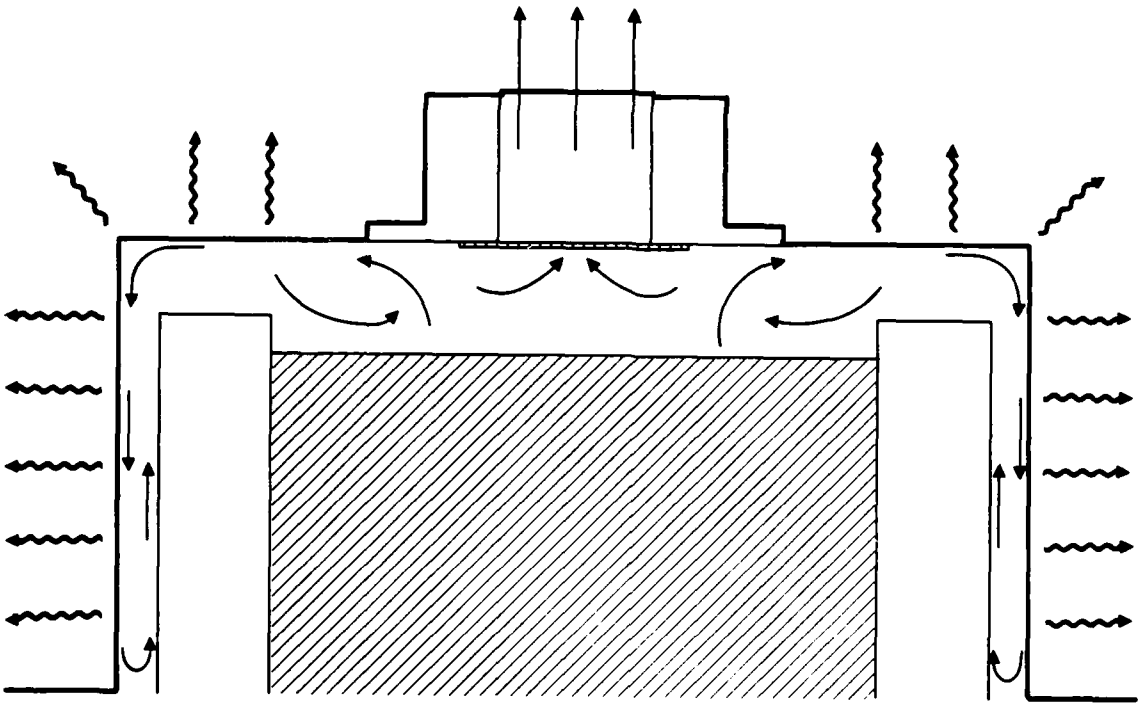

Figure 23. Gas mixing in heater box.

washers. The lower shroud was attached to eight 0.25 inch aluminum rods contacting the heater bed. The rods conducted heat from the bed to the aluminum plate, thereby heating the inner shroud. This lower shroud also included a nozzle-like section which entrained the flow into the ORTL nozzle and prevented contact with the cooler upper stainless shroud.

The heat exchanger was tested with ORTL gas in the absence of a pump laser beam. The heater bed was preheated with hot N_2 at 600°K. The heating capacity of the system, as well as the losses are shown in Figure 24. Temperatures above 470°K could be maintained for the first 25 minutes of run time. This provided adequate run time without recharging the system. A temperature difference of 80°K was observed between the exit bed temperature and the ORTL exit gas temperature. Subsequent heater tests were conducted with N_2 preheated to 800°K. A bed temperature of 700°K and an exit gas temperature of 550°K were attained.

The ten thermocouples downstream of the intersection zone provided a profile of the ORTL gas temperature, as shown in Figure 25. A 90 percent average exit temperature uniformity along the ORTL optical axis was maintained across 80 percent of the ORTL flow.

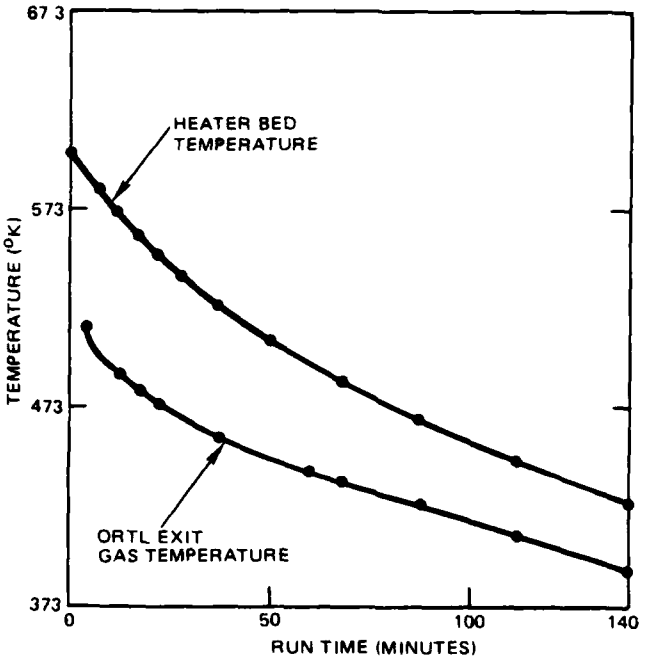

Figure 24. Heater temperature fall off with run time.

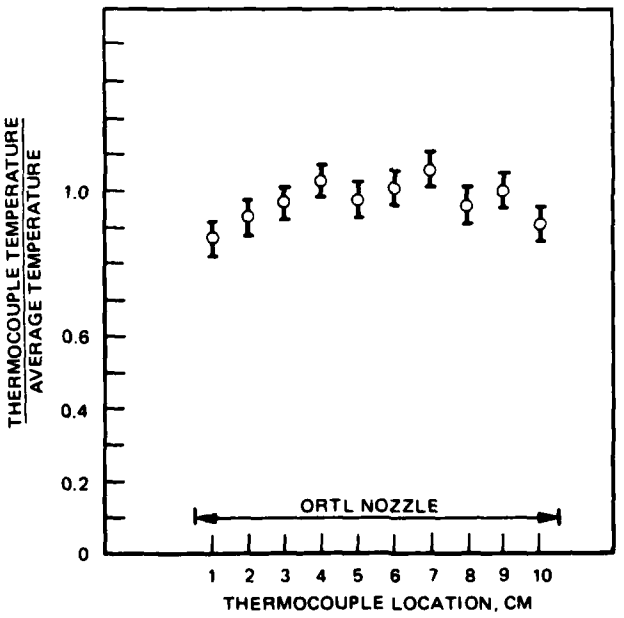

Figure 25. Heated ORTL gas temperature profile (10 cm nozzle).

3.1.5 Chemical Laser Characterization Experiments

Chemical laser characterization experiments were performed with two objectives. The first was to select the operating conditions for the chemical laser. The second was to provide a data base for the intracavity ORTL model. The experiments were conducted using the resonator configuration shown in Figure 26.

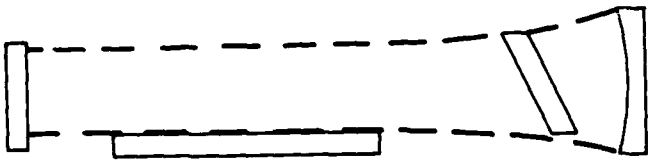

Figure 26. Chemical laser resonator configuration.

The chemical laser performance was characterized with the intent of selecting two operating conditions: a low J spectrum and a high J spectrum. The characterization was done using a nominal 35 percent transmission outcoupler with the flow parameters of the chemical laser varied as indicated in Table 7. The low J spectrum case chosen was that with a total flow rate of 300 millimoles per second and He and NF_3 mole fractions of 0.5 and 0.075, respectively. This produced 525 watts with $1 \rightarrow 0$ lasing on lines 6, 7, 8 and $2 \rightarrow 1$ lasing on lines 5, 6, 7, 8 as shown in Figure 27a. The high J spectrum case chosen was that with a total flow rate of 400 millimoles per second and with He and NF_3 mole fractions of 0.5 and 0.10, respectively. This produced 742 watts with $1 \rightarrow 0$ lasing on lines 6, 7, 8, 9 and $2 \rightarrow 1$ lasing on lines 6, 7, 8 as shown in Figure 27b.

A series of experiments was conducted utilizing outcoupling fractions from 0.04 to 0.68. These were done to help predict the chemical laser small signal gain and cavity loss as well as the spectral changes. The outcouplers consisted of several flat, silicon mirrors with partially reflective coatings. It is important to note in the data shown in Figure 28 that as the overall cavity losses decreased there was a shift toward a higher J distribution.

TABLE 7. PARAMETRIC STUDY OF CHEMICAL LASER POWER VARIATION
(OUTCOUPLING FRACTION = 0.350)

POWER (WATTS)

	He / NF_3	0.3	0.4	0.5	0.6	0.7
$\dot{Z}$ = 200 M MOLES/SEC	0.075	664	380		310	
	0.100		534	461	265	
	0.130		640	494	392	137
	0.160		628	441	196	
$\dot{Z}$ = 300 M MOLES/SEC	0.050			327		
	0.075		602	525		
	0.100				403	142
	0.500		471	414	349	147
Z = 400 M MOLES/SEC	0.075			589	549	216
	0.100			742	663	137

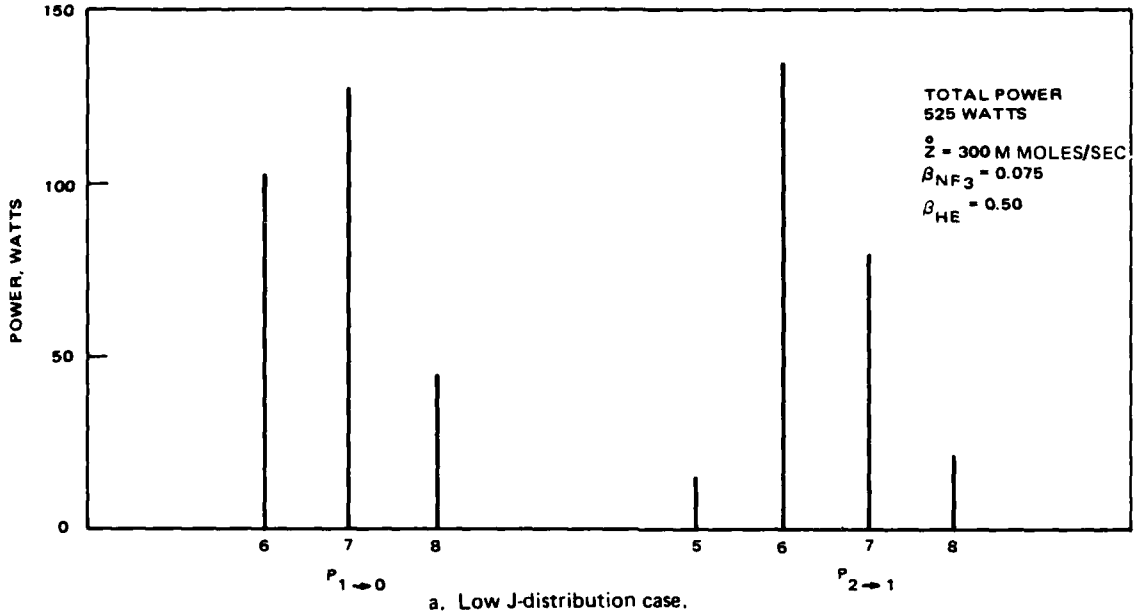

a. Low J-distribution case.

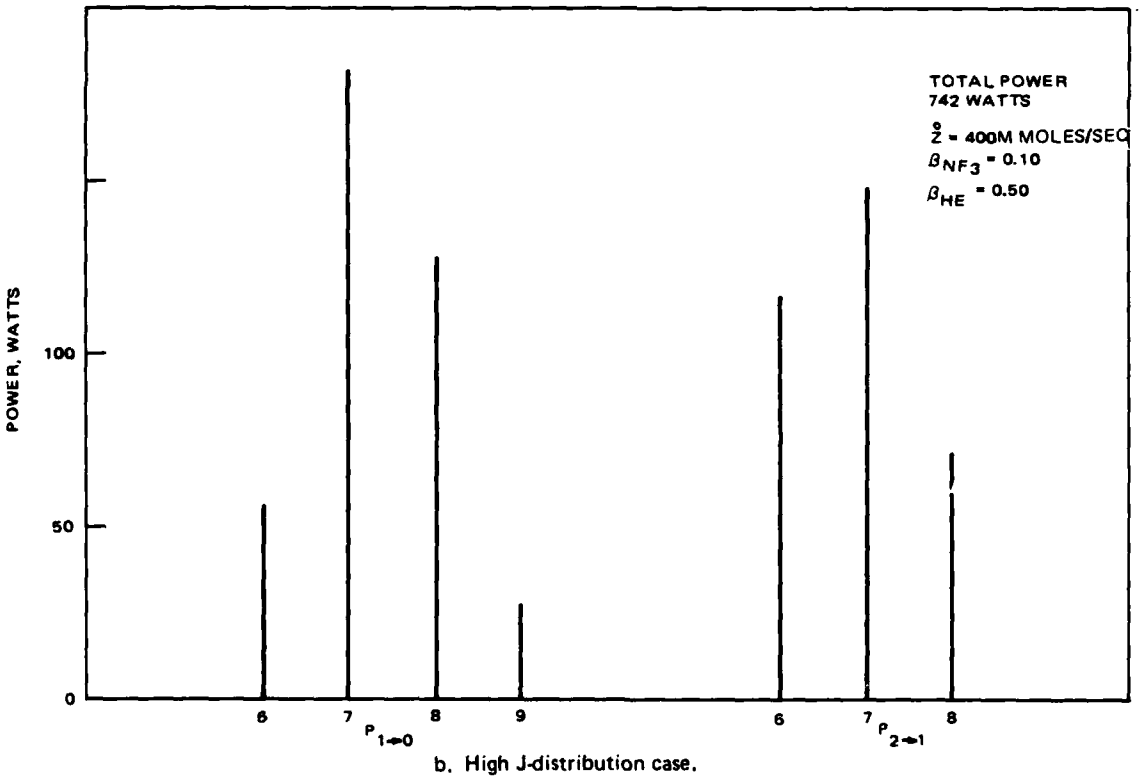

b. High J-distribution case.

Figure 27. Chemical laser spectra for selected operating conditions.

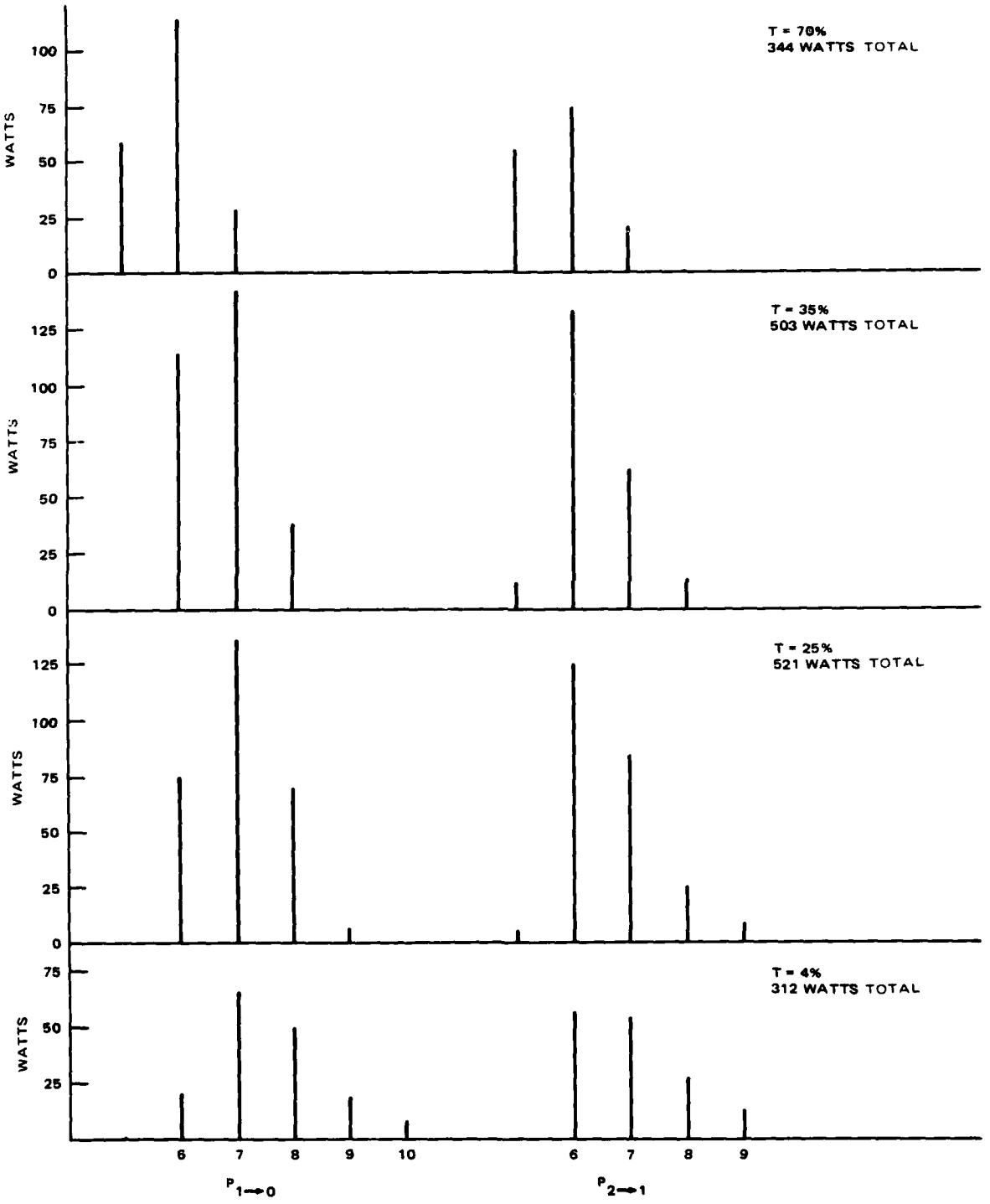

Figure 28. Chemical laser spectrum variation with outcoupling.

It is possible to determine the losses in the system as well as the appropriate small signal gain from the outcoupling data by means of a Rigrod analysis. This is done by curve fitting the formula,

$$P_o = P_S \cdot \frac{T}{2}\left[\frac{2g_o\ell + \ell n(1 - T - L)}{T + L}\right]$$

as shown in Figure 29. In this equation, P_S is the saturation parameter, $2g_o\ell$ is the round trip small signal gain, T is the outcoupling transmission, and L is the round trip cavity loss. By using this method the round trip small signal gain was determined to be 3.0, and P_S to be 510 watts, the round trip cavity loss to be 0.08 to 0.10. This loss is higher than that in a typical chemical laser configuration such as the one that was used in the

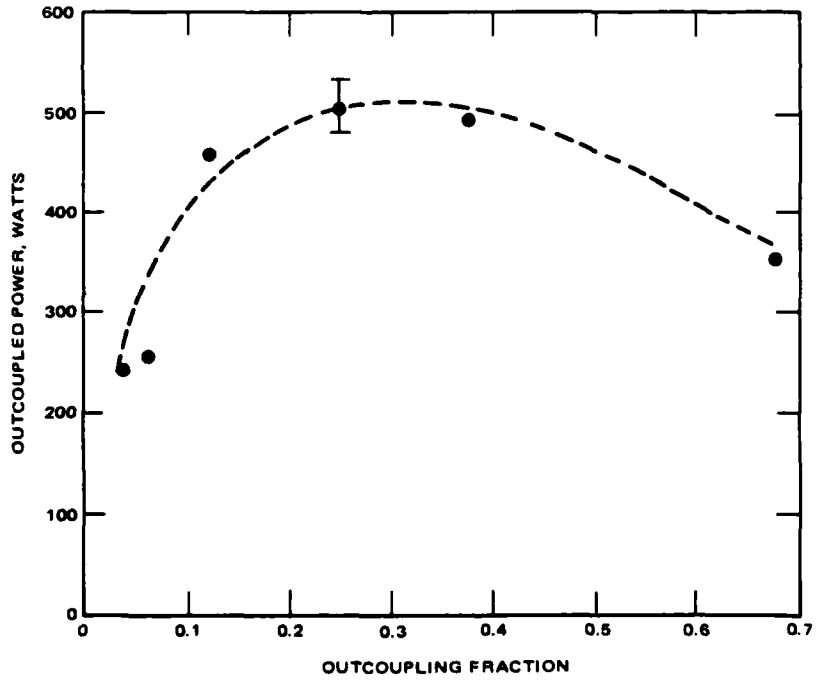

Figure 29. Rigrod curve fit for chemical laser data.

extracavity experiments where the loss was 0.03 to 0.04. The high loss was probably caused by the several apertures which were used to suppress parasitic oscillations in the current longer higher gain resonator.

The chemical laser performance was also characterized with the spectral control mirrors discussed earlier. The effect of these mirrors, as shown in Figure 30 was to prevent oscillation of longer wavelengths. This was accomplished without a decrease in overall power.

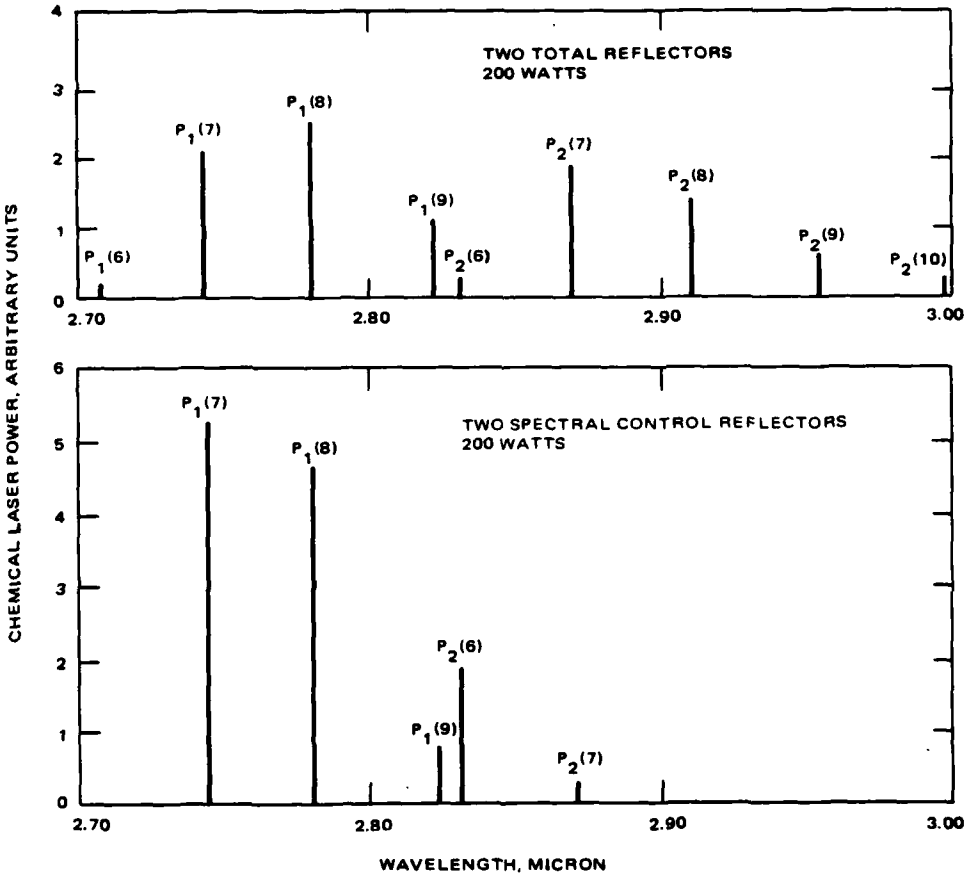

Figure 30. Chemical laser spectral control.

The data base for intracavity modeling is shown in Table 8. The "variable" outcoupling fraction represents the use of a DF mirror providing varying reflectivity and transmittance over the HF spectrum. The OCLI mirrors are the spectral control mirrors. At all conditions, spectra were also measured.

TABLE 8. CHEMICAL LASER PERFORMANCE

RESONATOR		OUTPUT POWER (WATTS)	POWER ABSORBED IN M1 (WATTS)	APERTURES (WATTS)	TOTAL POWER (WATTS)
TOTAL REFLECTOR (M1)	OUTCOUPLING				
5M MOLY	0.675	354	3.3	0.7	360
5M MOLY	0.375	489	12.8	0.7	503
5M MOLY	0.250	502	18.3	5.0	526
5M MOLY	0.120	460	41.2	6.2	508
5M MOLY	0.062	254	67	47	377
5M MOLY	0.060	244	63	25	349
5M OCLI	VARIABLE	500	23	2.8	524
5M OCLI	0.062	249	14.8	12.5	416
5M OCLI	0.375	479	36.7	0.3	516
5M OCLI	0.675	394	3	-	397

3.2 INTRACAVITY EXPERIMENTS

3.2.1 Overview

The parameters varied in the intracavity experiments included the following: HF partial pressure, ORTL flow velocity, curtain velocity, inlet temperature, and diluent. The parametric range investigated is summarized in Table 9.

TABLE 9. INTRACAVITY EXPERIMENTAL PARAMETER RANGES

Parameter	Range
ORTL pressure	16-29 torr
HF partial pressure	0.2 - 3.5 torr
Curtain velocity*	X1 → X8
Velocity	500-1400 cm/sec
ORTL inlet temperature	295^{o} - $550^{o}K$
Diluent	SF_6, He

*The ratio of curtain velocity to ORTL gas velocity is shown.

3.2.2 Chemical Laser Operation in the Intracavity Configuration

A typical chemical laser spectral distribution for a closed cavity resonator with spectral control mirrors, with no ORTL medium present is tabulated in Table 10. The power in each line typically did not vary by more than 15 percent. An example of this is given in Figure 31 for which spectra were recorded at the start, middle, and end of a test series.

The HF pump irradiance (watts/cm^2) in the intracavity configuration is the sum of the ORTL absorption (measured as the sum of the ORTL gas heating and the ORTL output power), the optical component absorption (mirrors and apertures), and other unmeasured diffraction losses. The intracavity irradiance is limited by the non-ORTL losses and decreases as ORTL loading increases. In order to determine the ORTL irradiance in a particular experiment, the loss to each optical component was measured. (Unmeasurable losses exist, but were ignored.) Table 11 lists the powers absorbed by the mirrors and apertures for four runs with HF absent from the ORTL flow. The

TABLE 10. TYPICAL CHEMICAL LASER CLOSED CAVITY SPECTRAL DISTRIBUTION (NO ORTL LOAD)

Transition	Watts	%
P_1 (6)	34	13
P_1 (7)	88	35
P_1 (8)	33	13
P_1 (9)	2.4	1
P_2 (5)	20	8
P_2 (6)	75	29
P_2 (7)	4	1
V = 1 → 0	157	61
V = 2 → 1	98	39
Total	255	100

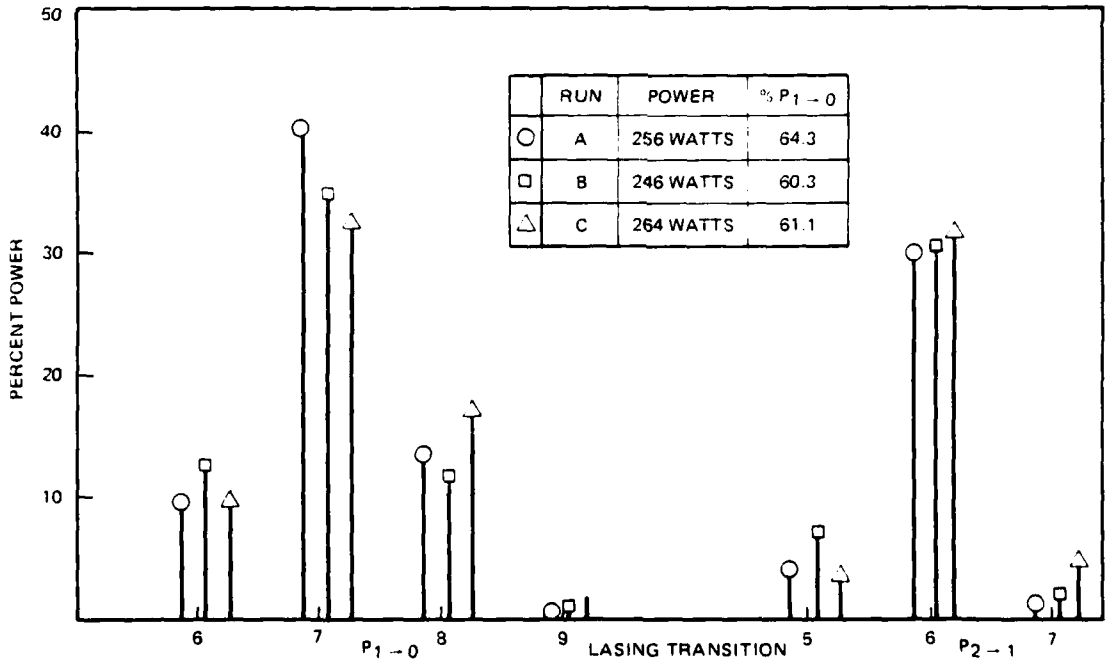

Figure 31. Typical chemical laser spectra.

TABLE 11. CHEMICAL LASER POWER EXTRACTION
(NO ORTL GAS) (POWERS IN WATTS)

	Total Power	Laser Mirrors		Apertures		
		Concave	Flat	Concave	Flat	Aerowindow
Run 1	240	72	85	42	16	25
Run 2	236	78	79	42	18	19
Run 3	241	85	88	33	21	14
Run 4	243	86	79	49	15	14
Average	240	80	83	42	18	18
Loss (percent)	7.7	2.6	2.6	1.3	0.58	0.58

losses are calculated relative to a 2.6 percent average loss for each spectral control mirror. The 2.6 percent average value is derived from the Rigrod analysis of the data discussed previously. The irradiance at the ORTL cell in this configuration would be estimated to be on the order of

$$\flat = \frac{2 \times \text{total laser power}}{\text{total loss} \times \text{area}} \approx \frac{2 \times 240 \text{ Watts}}{0.077 \times 0.8 \text{ cm}^2} = 7.8 \text{ kW/cm}^2$$

The factor of two comes from summing the circulating radiation fields in each direction that can pump the ORTL medium. In the presence of absorbing HF gas in the ORTL, the total extracted power typically increased, but the losses decreased and the average irradiance inside the resonator changed very little. However, the irradiances from each direction of the ORTL cell were then different and were different from that at the other side of the chemical laser gain medium. This analysis is therefore only an approximation of the actual situation.

Typical pump laser spectral distributions in the presence of HF loads are shown in Figure 32. The spectrum with HF absent is at the bottom of the figure. The addition of HF causes the $P_1(6)$, $P_1(7)$ and $P_2(6)$ transitions

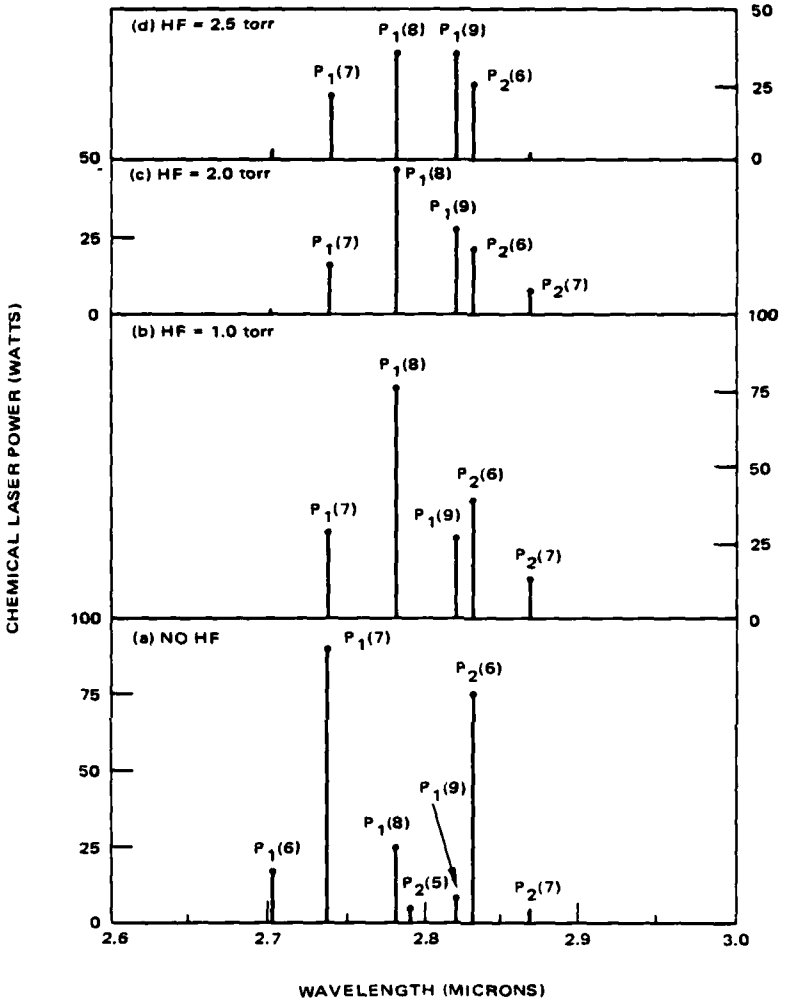

Figure 32. Chemical laser spectra versus ORTL HF pressure (295°K).

to be attenuated, and the $P_1(8)$, $P_1(9)$ and $P_2(7)$ transitions to be amplified. Note that the laser spectrum does not shift to higher J transitions, and that the loss introduced by the two spectral control mirrors is effective in suppressing the $P_1(10)$ and $P_2(8)$ transitions.

3.2.3 ORTL Curtain Velocity

The role of the curtain gas was to confine the ORTL flow when it intersected the pump beam, and to maintain that confinement up into the ORTL exhaust duct. The interaction of the helium curtain jet with the ORTL jet is a complex fluid dynamics problem because of the heat addition in the ORTL core from the absorption of pump laser radiation and because of the mass difference between SF_6 and helium. An empirical approach was utilized to determine the most appropriate curtain flow velocity.

The influence of curtain velocity on ORTL power was investigated at several HF partial pressures. The HF/SF_6 flow rate was 4.45 millimoles/sec corresponding to a velocity of 700 cm/sec. The total pressure was 16 torr and the inlet temperature was 293°K. Helium curtain flow velocities of 3 and 7.4 times 700 cm/sec were used. The higher flow rate is the conductance limit of the ORTL exhaust pump. The results are shown in Figure 33. The two

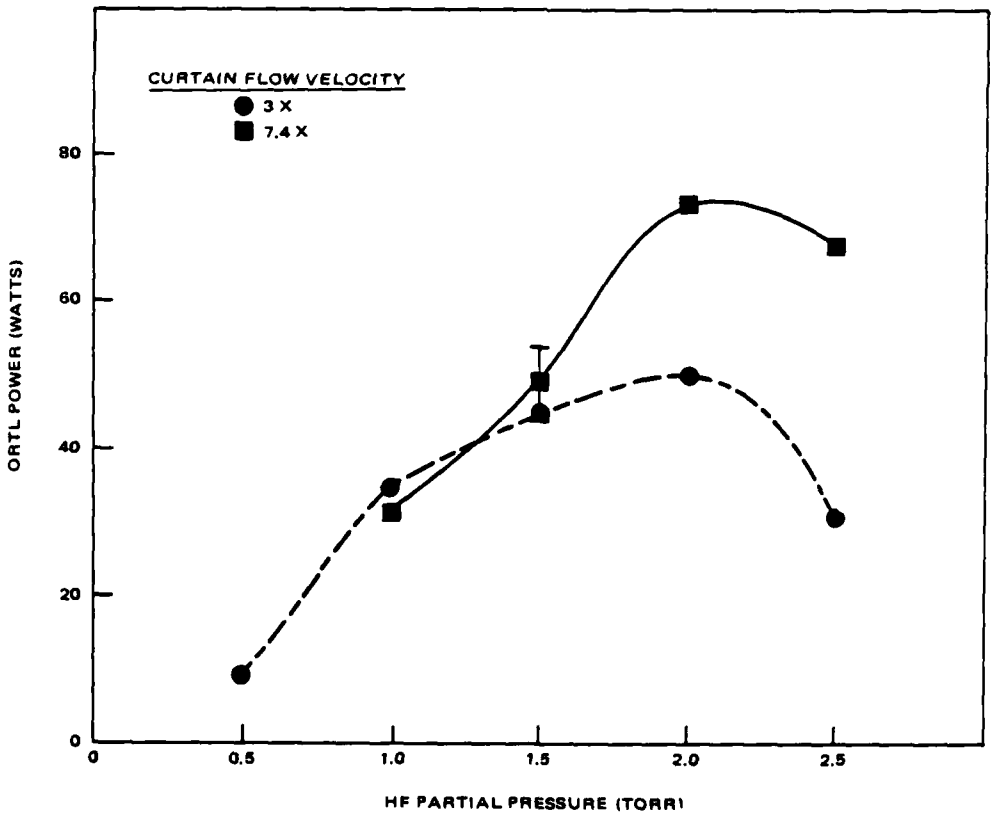

Figure 33. Effect of curtain velocity on ORTL power.

curves deviate at 2 and 2.5 torr HF. The higher curtain velocity 5.2×10^3 cm/sec was therefore selected for most of the experiments.

3.2.4 ORTL Flow Velocity

The ORTL gas velocity defines the interaction time or residence time of HF molecules in the pump radiation field. This in turn influences the average ORTL temperature, and therefore the kinetic processes and the efficiency of the system. Thus, the ORTL power will be velocity dependent. This dependence was investigated by varying the ORTL flow velocity from 500 cm/sec to 1400 cm/sec. For this test series, the curtain velocity was always three times faster. Two HF partial pressures, 1 torr and 2 torr, were examined at a total pressure of 16 torr. The results are shown in Figure 34. The ORTL power changes little between 500 cm/sec and 700 cm/sec, but drops by over a

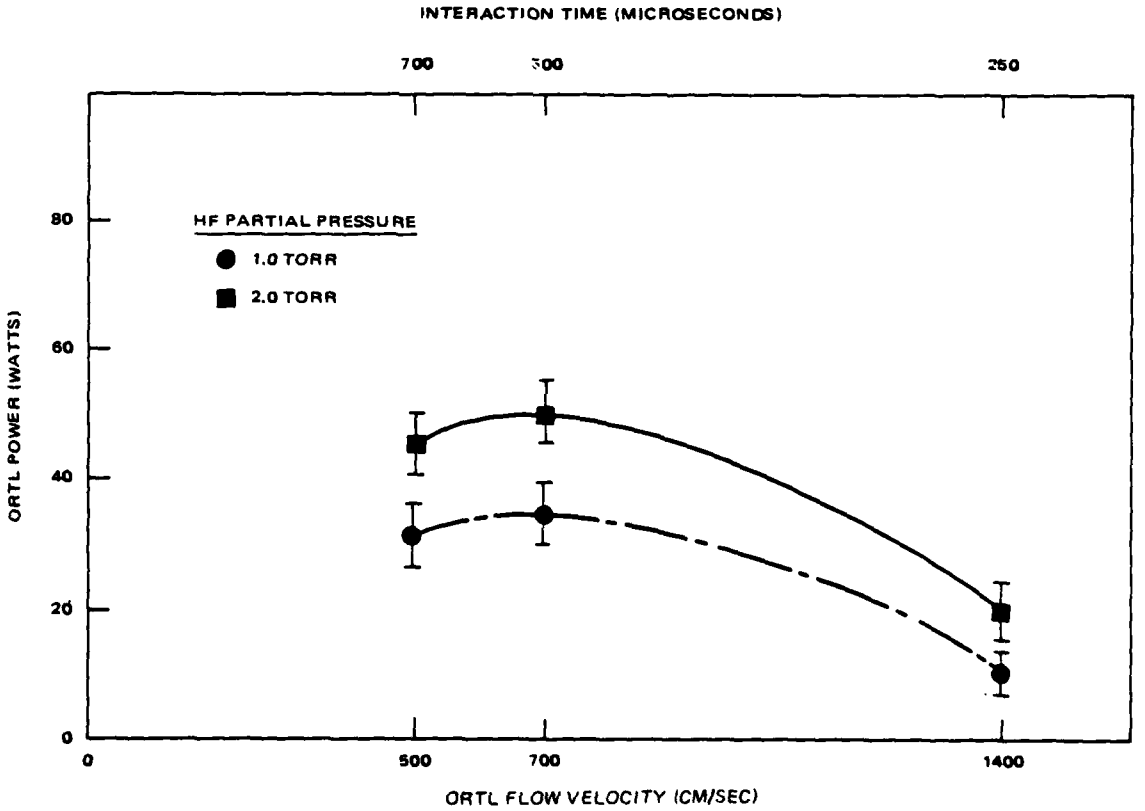

Figure 34. ORTL output power as a function of flow velocity.

factor of two from 700 cm/sec to 1400 cm/sec. The power drop is largely a result of halving the interaction time from 500 μs, thus reducing the exit ORTL gas temperature from 572°K to 420°K. The velocity was fixed at 700 cm/sec in subsequent experiments. Unless specifically denoted, the ORTL flow velocity in the experiments described below was 700 cm/sec.

3.2.5 Performance Characterization (295°K)

These 295°K inlet ORTL gas temperature experiments were performed under the following conditions:

1. Beam cross section is 2.25 x 0.35 cm = 0.8 cm^2. Chemical laser resonator consists of two spectral control mirrors. Chemical laser operated under conditions of Table 11.

2. The ORTL nozzle defines a 10 cm gain length, 3 cm absorption length and a 2.6 cm^3 volume.

3. The ORTL pressure, flow rate, and velocity are: 16 torr, 4.45 mmoles/sec, and 700 cm/sec, respectively. The diluent is SF_6.

4. The ORTL resonator is formed by a nominal 3 percent transmitting silicon flat, and a 99.8 percent total reflector.

5. The HF partial pressure is varied from 0.26 torr to 2.5 torr.

ORTL power as a function of HF partial pressure was investigated in two test series. ORTL power as a function of HF partial pressure is shown in Figure 35. Lower loss conditions produced higher ORTL output power. A maximum of 91 watts was outcoupled at 2 torr HF partial pressure. A near field burn taken in plexiglas defined an ORTL beam cross section of 0.75 cm x 0.35 cm = 0.26 cm^2.

ORTL output spectra at various HF concentrations are given in Figure 36. The lasing lines shift to higher J-transitions with increased HF pressure because of the higher ORTL gas temperature. The fraction of the 1 → 0 band ORTL power increases with increased HF pressure because the resulting higher gas temperature allows better power coupling into the ORTL 1 → 0 band.

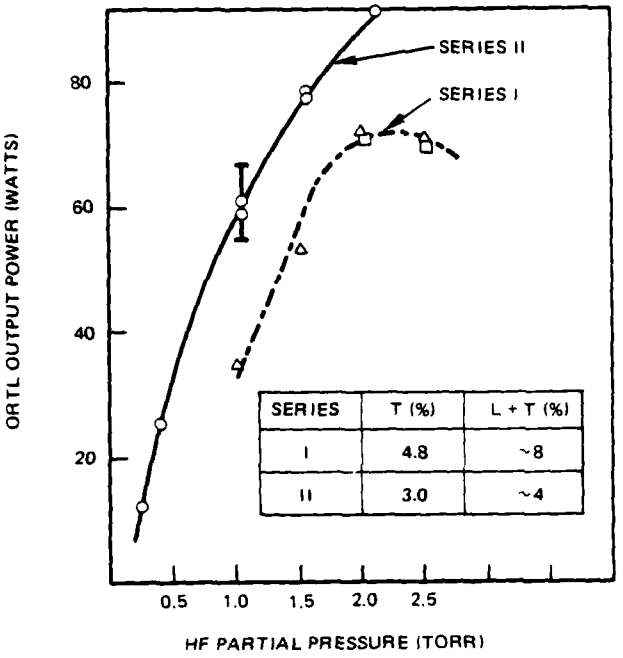

Figure 35. ORTL power (295°K) as a function of HF pressure.

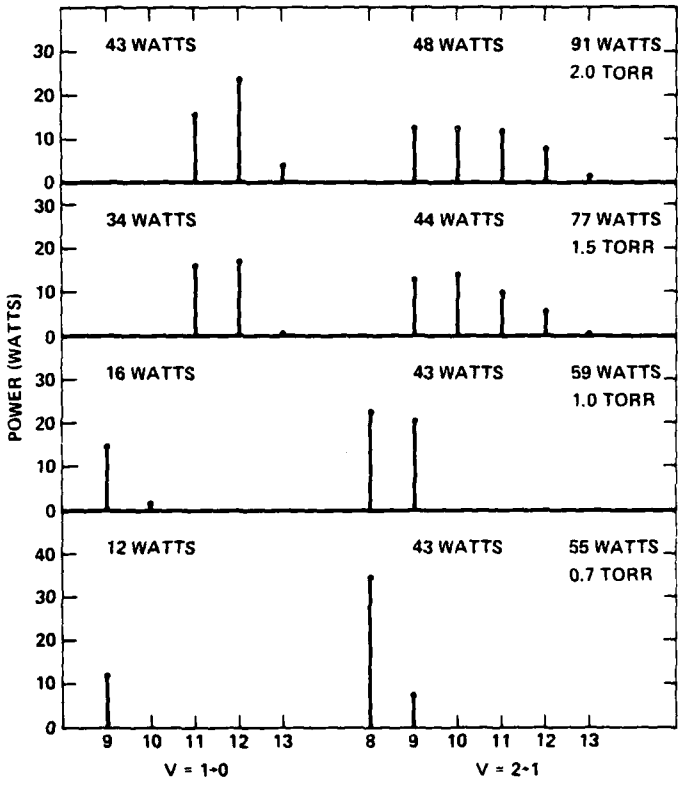

Figure 36. ORTL spectra at different HF partial pressures (295°K).

ORTL performance results for Series II are summarized in Table 12. The ORTL efficiencies were calculated from the data under the power distribution column according to the following definitions:

- η_i = input efficiency = $(P_{GAS} + P_{ORTL})/(P_{GAS} + P_{ORTL} + P_L)$
- η_c = conversion efficiency = $P_{ORTL}/(P_{GAS} + P_{ORTL})$
- η_o = overall efficiency = $P_{ORTL}/)P_{GAS} + P_{ORTL} + P_L)$
- $\eta_o = \eta_i \times \eta_c$

The chemical laser pump power is determined from the sum of the power in the ORTL gas, the ORTL output power, and the chemical laser mirror and aperture powers. The total intracavity chemical laser power (Table 12, column 6) varied with the ORTL loading in the same manner as normal chemical laser power varied with outcoupling fraction (e.g., Figure 29).

Plots of the ORTL efficiencies as functions of HF partial pressure are shown in Figure 37. The input efficiency increased with HF pressure because the increased ORTL load dominated the fixed chemical laser resonator loss. The conversion efficiency decreased slowly with increasing HF pressure. This may be due in part to decreasing intracavity flux as the ORTL loading increased. A peak overall efficiency of 21 percent at 2 torr HF pressure was obtained. The corresponding input and conversion efficiencies were 71 percent and 30 percent, respectively. The peak conversion efficiency of 40 percent occurred at 0.7 torr HF.

3.2.6 Performance Characterization ($T > 295^{o}K$)

Elevated ORTL inlet temperature experiments were performed with the aim of improving the absorption of chemical laser radiation by the ORTL load. The experimental parameters used with elevated inlet temperatures are summarized in Table 13.

In Figure 38 the ORTL power is plotted as a function of HF pressure at inlet temperatures ranging from $295^{o}K$ to $385^{o}K$. The total pressure was 16 torr and the total ORTL resonator loss was approximately 8 percent.

TABLE 12. INTRACAVITY EXPERIMENTS AT 295°K INLET TEMPERATURE

HF Concentration		Power (watts)				Efficiency (%)			ORTL Exit Gas Temperature (°K)										
									Average	Thermocouple Location									
$N \times 10^{16}$ (#/cm^3)	P (Torr)	ORTL Output P_{ORTL}	ORTL Gas P_{GAS}	Chem Laser Optics	Total P_L	η_I	η_C	η_O	Temperature	1	2	3	4	5	6	7	8	9	10
6.92	2.11	90.7	214	122	427	71	30	21	712	295	327	536	959	734	983	838	1013	933	505
5.16	1.58	77	175.5	120	372	68	31	21	636	295	327	503	876	715	822	729	842	791	456
5.16	1.58	78	163.8	121	363	67	32	22	616	295	352	625	871	676	667	709	805	749	411
3.44	1.05	58	119	172	349	51	33	17	528	295	327	433	725	570	672	603	681	643	328
3.46	1.06	60.5	132	172	364	53	32	17	553	295	358	600	720	570	676	623	659	617	411
2.41	0.74	56	97	219	372	41	37	15	488	295	457	587	600	498	554	519	529	503	337
2.42	0.74	55	81	232	368	37	40	15	458	327	404	567	602	483	558	504	542	452	303
1.38	0.42	20	37	256	313	18	35	6	374	295	339	409	425	373	406	401	400	372	323
1.37	0.42	25	44	250	319	22	36	8	389	295	358	410	450	393	423	412	420	390	337
1.38	0.42	20	37	256	313	18	35	6	374	295	339	409	425	373	406	401	400	372	323
0.86	0.26	12	22	208	242	14	35	5	344	295	303	321	369	347	370	369	389	345	327

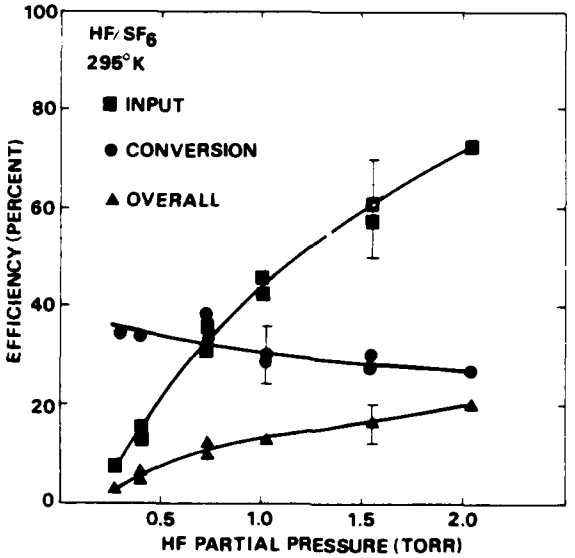

Figure 37. ORTL efficiency versus HF pressure (295°K).

TABLE 13. ORTL CONDITIONS AT ELEVATED INLET TEMPERATURES

Diluent	SF_6
Flow rate	4.45 mmoles/sec
Velocity	700 cm/sec
Inlet temperature	295 - 550°K
HF pressure	0.5 - 3.0 torr
Total pressure	16 - 29 torr

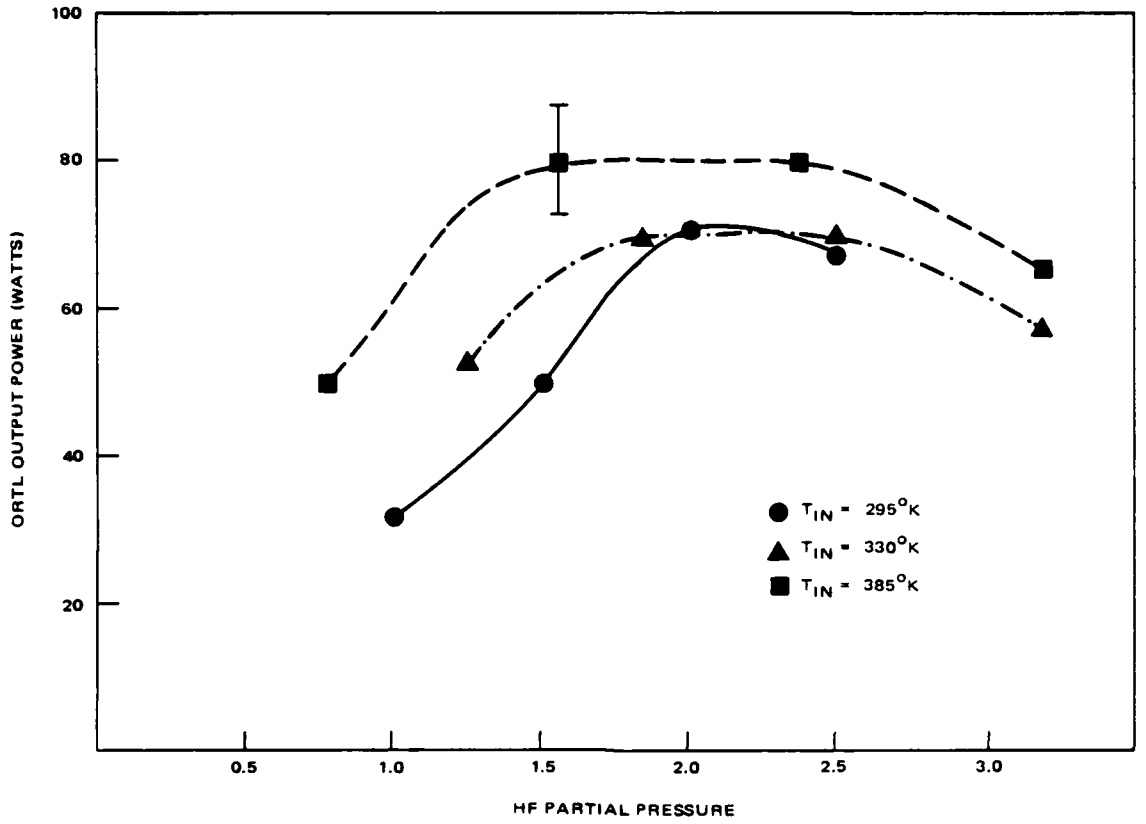

Figure 38. ORTL output variation with HF pressure and temperature (295 - 385°K).

In Figure 39, results from an experimental series using slightly higher (10 percent) loss optics are plotted over the range 400°K - 550°K. Although different resonators with slightly different loss were used, the important observation to note is that the ORTL power peaks at approximately 2 torr HF in all cases. Accordingly, subsequent experiments were done at a fixed HF pressure of 2 torr.

Results with 4 percent loss optics are shown in Figure 40. The ORTL power increased from 91 watts to 152 watts as the inlet temperature increased from 295°K to 525°K, approximately a 67 percent improvement. The residual power in the gas, $\dot{Q}$, decreased from 213 watts to 145 watts and the exit gas temperature was constant although the inlet temperatures increased. The decreased temperature rise can be understood if one realizes that at constant

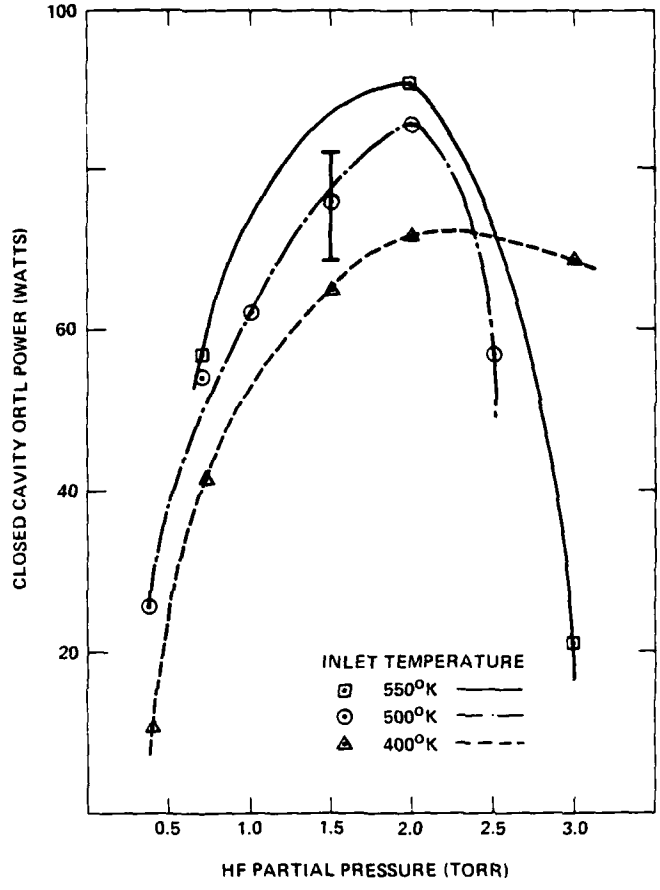

Figure 39. ORTL output variation with HF pressure and temperature (400°K - 550°K).

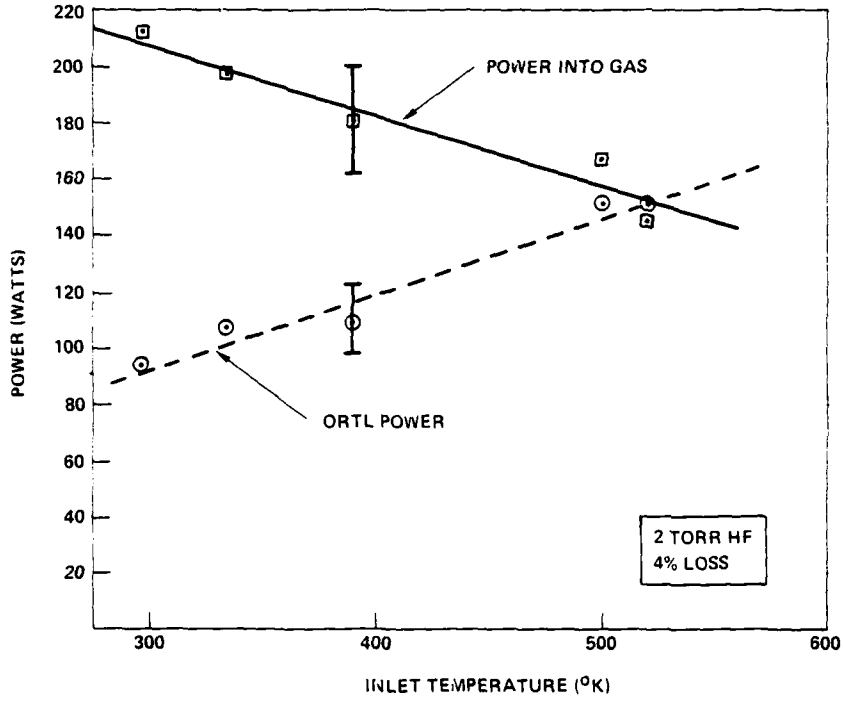

Figure 40. ORTL performance variation with temperature (constant pressure).

HF pressure, the HF number density was nearly halved in going from an inlet temperature of 295°K to 525°K. Note that the total power absorbed (the sum of ORTL output and gas heating) was approximately constant as the inlet temperature was increased, although the HF density was dropping. Thus, the HF molecules are more effective in absorbing and converting the chemical laser radiation.

The ORTL efficiencies at elevated inlet temperature are plotted in Figure 41. They are derived from the power distribution values listed in Table 14. The ORTL input efficiency in Figure 44 is a level 70 to 75 percent. The results in the last row of Table 14 show lower input efficiency because the low number density was not appropriate to the inlet temperature of the ORTL. The conversion efficiency in Figure 41 increased from 30 to 51 percent, as inlet temperature increased. (This result was anticipated from Figure 40.) The overall efficiency, a product of η_o and η_i increased from 21 to 36 percent as inlet temperature increased in Figure 41.

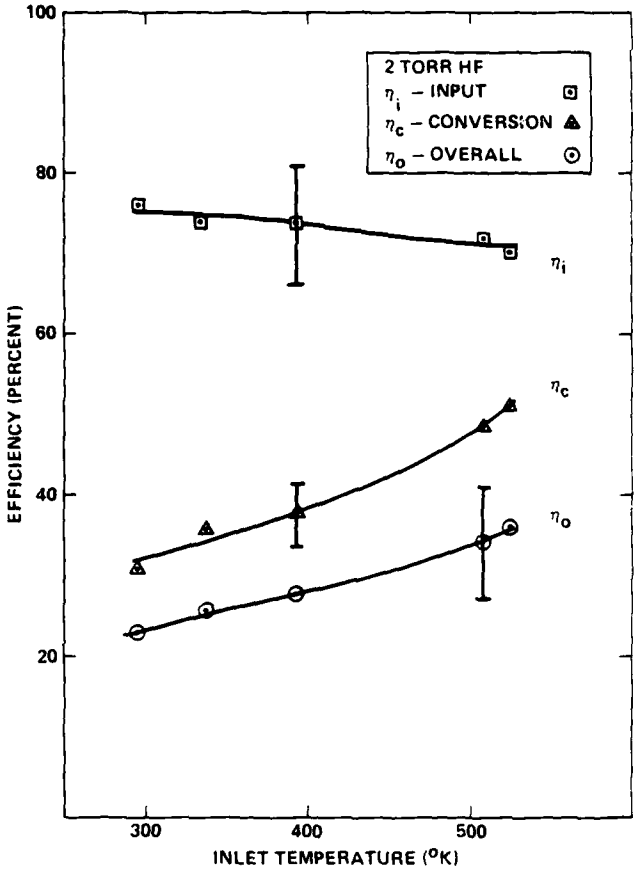

Figure 41. ORTL efficiency as a function of inlet temperature.

TABLE 14. INTRACAVITY EXPERIMENTS AT ELEVATED INLET TEMPERATURE

HF Concentration		Power (watts)				Efficiency (%)			ORTL Exit Gas Temperature (^{o}K)											
									Average Temperature	Thermocouple Location										
N x 10^{16} (#/cm^3)	P (Torr)	ORTL Output P_{ORTL}	ORTL Gas P_{GAS}	Chem Laser Optics	Total P_L	η_I	η_C	η_O		1	2	3	4	5	6	7	8	9	10
3.7	2.0	150	145	127	422	0.70	0.51	0.36	Exit 774	673	780	820	792	824	935	755	780	704	673
									Inlet 520	523	533	537	524	524	524	495	506	515	515
3.9	2.0	122	152	122	441	0.72	0.48	0.34	Exit 793	633	732	850	829	849	959	798	765	717	801
									Inlet 500	508	516	516	507	504	502	479	484	495	491
5.0	2.0	109	181	100	390	0.74	0.38	0.28	Exit 721	444	490	590	822	856	972	945	740	705	654
									Inlet 389	393	399	399	396	387	387	377	377	382	397
5.8	2.0	107	197	107	411	0.74	0.36	0.26	Exit 712	418	457	701	824	834	967	936	713	649	621
									Inlet 334	333	335	341	338	338	333	322	326	323	325
6.6	2.0	94	213	99	406	0.76	0.31	0.23	Exit 715	313	348	498	873	897	1006	861	775	761	703
									Inlet 295	295	295	295	295	295	295	295	295	295	295
1.6	0.7	74	43	249	366	0.32	0.64	0.20	Exit 510	479	535	540	526	532	558	498	481	476	471
									Inlet 431	438	443	446	436	433	432	418	413	420	432

Further observations based on the data of Table 14 can be made. As expected, highest intracavity conversion efficiency, 64 percent, is for 0.7 torr HF, for the lowest concentration. For all 2 torr HF conditions the average exit temperature is between 750 and 800°K. This temperature is still considerably above the achieved maximum inlet temperature of 550°K. Further increases in inlet temperature might be expected to produce higher efficiencies.

3.2.7 ORTL Nozzle Comparisons

The majority of the ORTL experiments were performed with the 10 cm x 0.75 cm ORTL nozzle (Nozzle N-2). Limited experiments with a short, 7 cm x 0.75 cm ORTL nozzle (N-3) were also performed. The motivation for using a shorter gain length ORTL nozzle is illustrated in Figure 42. The upper figure is a typical exit temperature profile across the long nozzle at 295°K inlet temperature with 2 torr HF. Thermocouple positions 1-3, corresponding to 3 cm along the ORTL gain direction are colder than the middle positions. This indicates that the pump beam does not span the full ORTL nozzle. The lower figure data from the short nozzle is clearly more uniform, with less unexcited regions along the ORTL gain direction.

A summary of the results obtained with the small nozzle is given in Table 15. The peak ORTL power of 146 watts at 500°K (comparable to that obtained with the long nozzle, i.e., 152 watts) was obtained with efficiencies of $\eta_i = 0.68$, $\eta_c = 0.56$, and $\eta_o = 0.38$. A comparison of ORTL efficiencies with the two nozzles is given in Figure 43. The input efficiency is the same, within experimental error. The conversion efficiency is comparable at low temperature, but at 500°K is 0.56 for the short nozzle and 0.48 for the long nozzle. The error bars for η_c are $\pm$10 percent. The slight improvement in conversion efficiency occurs because less waste heat Q is produced, 116 watts versus 167 watts, for the same ORTL power. The overall efficiencies 0.38 and 0.36 are comparable.

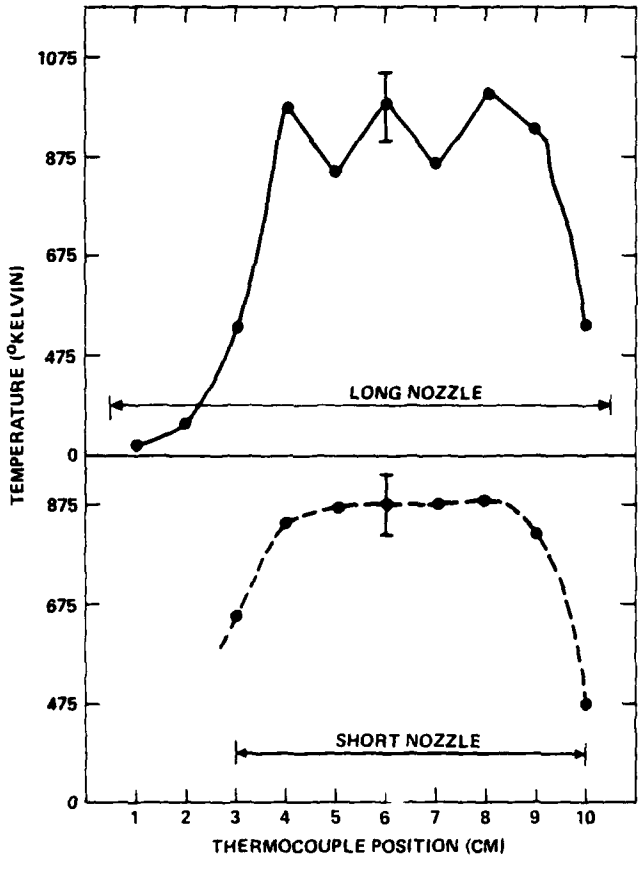

Figure 42. Temperature profiles in long and short nozzle.

TABLE 15. INTRACAVITY EXPERIMENTS AT ELEVATED INLET TEMPERATURE WITH THE SMALL ORTL NOZZLE

HF Concentration		Power (watts)				Efficiency (%)			ORTL Exit Gas Temperature (^{o}K)											
$N \times 10^{16}$ (#/cm^3)	P (Torr)	ORTL Output P_{ORTL}	ORTL Gas P_{GAS}	Chem Laser Optics	Total P_L	η_I	η_C	η_O	Average Temperature		Thermocouple Location									
											1	2	3	4	5	6	7	8	9	10
3.9	2.0	146	116	125	387	0.68	0.56	0.38	Exit	792	684	836	861	863	860	883	807	543		
									Inlet	501	468	514	519	522	516	526	506	442		
5.0	2.0	93	156	100	349	0.71	0.37	0.27	Exit	794	679	853	873	868	866	890	819	506		
									Inlet	388	376	394	394	392	394	399	387	369		
6.6	2.0	83	176	84	343	0.76	0.32	0.24	Exit	764	647	841	866	878	875	888	823	473		
									Inlet	295	295	295	295	295	295	295	295	295		
6.6	2.0	81	196	83	360	0.77	0.29	0.22	Exit	812	686	896	914	926	926	939	878	504		
									Inlet	295	295	295	295	295	295	295	295	295		

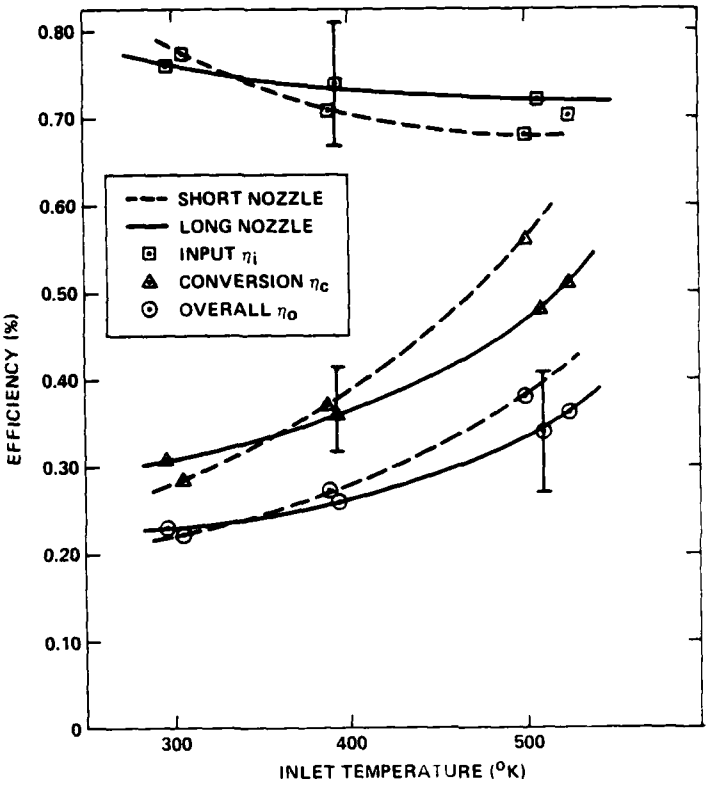

Figure 43. ORTL efficiencies with different nozzles.

3.2.8 ORTL Diluent Comparison

A limited investigation of ORTL performance with helium diluent was performed at 295°K inlet temperature using a single SF_6 reference point. The test matrix is shown in Table 16. The starting point for the test matrix was the condition that for the same HF partial pressure the same temperature rise in the ORTL medium be achieved for both SF_6 and helium. This translated to the conditions listed in the first two rows of Table 16, which compensated for the greater heat capacity of SF_6 compared to helium. However, the observed temperature rise with the helium diluent was not as great as expected, and so the other conditions were investigated. A plot of the ORTL power obtained as a function of velocity is given in Figure 44. ORTL power equivalent to that with SF_6 diluent was achieved with a 1.5 times greater temperature rise with helium diluent. A comparison of ORTL efficiencies for the matching power conditions is given in Table 17. The overall efficiencies were comparable, but the

TABLE 16. He/SF_6 DILUENT COMPARISON: ORTL CONDITIONS

Diluent	HF Pressure (torr)	Total Pressure (torr)	Velocity (cm/sec)	Observed Temperature Rise (°K)
SF_6	1.5	16	700	300
He	1.5	25	2240	240
			1600	320
			1000	400
			700	450

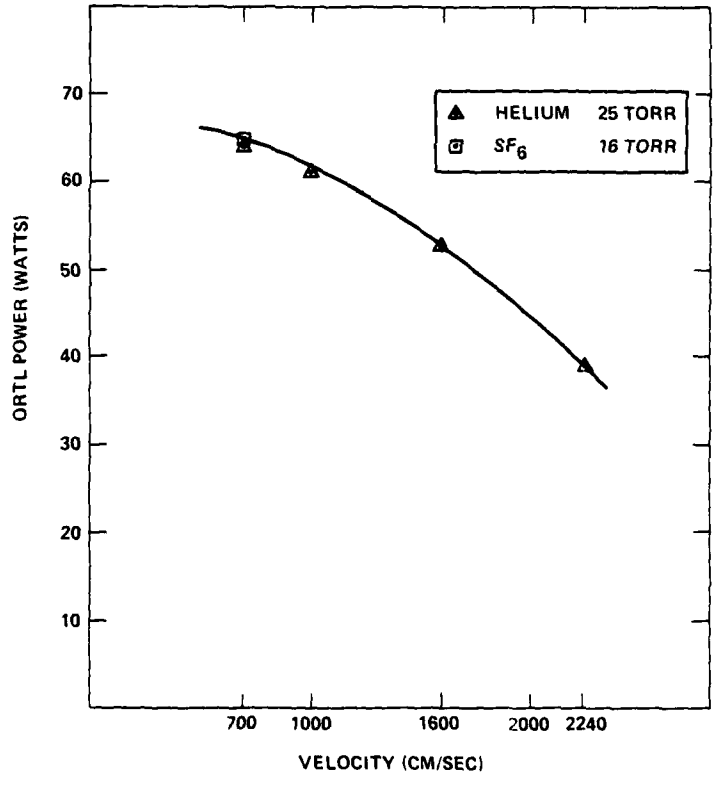

Figure 44. ORTL performance with SF_6 diluent.

TABLE 17. He AND SF_6 DILUENT ORTL PERFORMANCE COMPARISON

Diluent	ORTL Power (watts)	η_i (%)	η_c (%)	η_o (%)
He	65	41	51	21
SF_6	67	62	31	19

conversion efficiency for helium was higher. In conclusion, comparable overall efficiency and ORTL power was demonstrated with helium, but at a higher ORTL medium temperature.

3.2.9 Small Signal Gain Measurements

Small signal gain measurements in a flowing ORTL medium at 295°K inlet temperature were performed using a low power tunable HF probe laser. A detailed discussion of the measurement is presented in Appendix A. The results will be summarized here. The apparatus is shown schematically in Figure 45. A conventional dual beam technique was used to measure reference and amplified power. Gain was measured on $P_1(9)$, $P_1(10)$, $P_2(9)$, and $P_2(10)$ transitions. Absorption was observed below $P_1(9)$, and the probe laser did not oscillate above $P_2(10)$. The small signal gain results are plotted in Figure 46 and given in tabular form in Table 18. The gain length was estimated from the thermocouple temperatures along the ORTL gain direction as described in Appendix A. The single pass gain varied from 9 to 19 percent. The maximum measured small signal gain was (2.76 $\pm$0.26) percent/cm, for $P_2(9)$ at 2 torr HF.

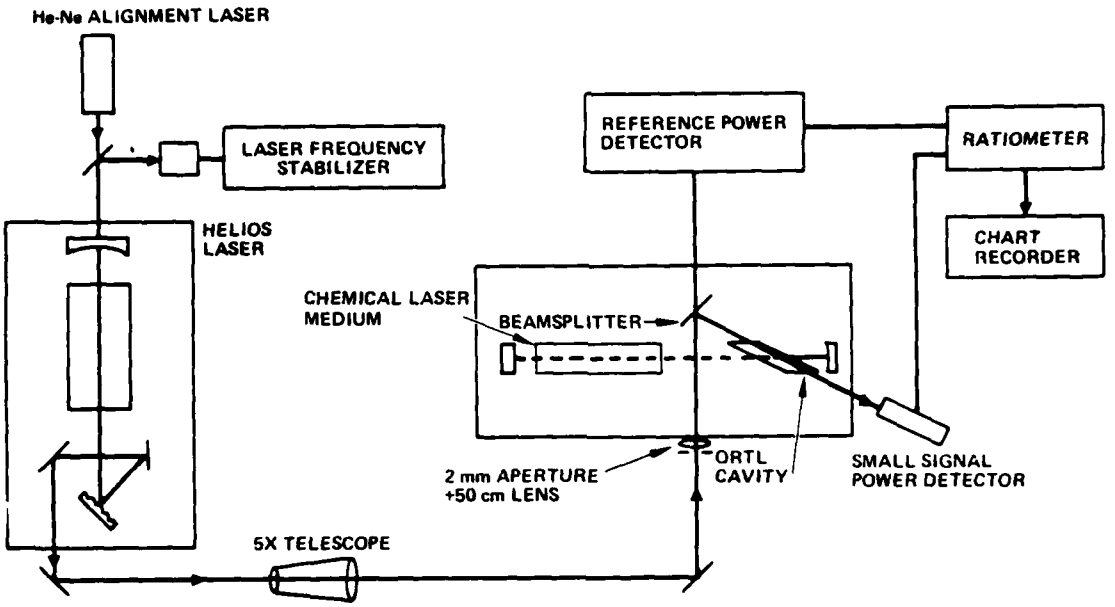

Figure 45. Small signal gain measurement apparatus.

TABLE 18. ORTL SMALL SIGNAL GAIN MEASUREMENTS

ORTL HF Pressure (torr)	Probe Line	Gain (%)	Gain Length (cm)	g_o (%/cm)
2	$P_2(10)$	15.5 ±1	6.5 ±0.2	2.22 ±0.26
1	$P_2(10)$	6.83 ±0.25	6.0 ±0.2	1.10 ±0.11
2	$P_1(10)$	9 ±1	6.3 ±0.2	1.36 ±0.2
1	$P_1(10)$	6 ±1	6.0 ±0.2	0.97 ±0.19
2	$P_1(9)$	11.1 ±0.5	6.3 ±0.2	1.68 ±0.18
1	$P_1(9)$	9 ±1	6.1 ±0.2	1.41 ±0.21
2	$P_2(9)$	19 ±0.5	6.3 ±0.2	2.76 ±0.26
1	$P_2(9)$	10.5 ±0.5	6.0 ±0.2	1.66 ±0.17

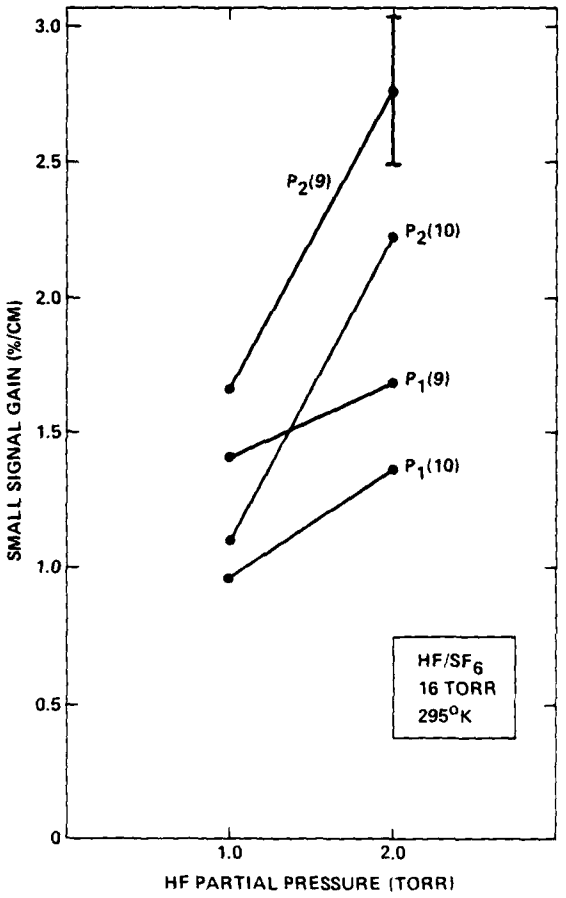

Figure 46. ORTL small signal gain.

3.2.10 Summary

Significant experimental milestones were attained in the intracavity experiments. The highlights of this task were:

- Spectral control coatings performed as designed.
- Intracavity ORTL showed no temporal instabilities.
- Elevated ORTL inlet temperature produced increased efficiency, as expected.
- 38 percent maximum overall efficiency was achieved.
- 152 watts maximum ORTL power was achieved.
- 2.8 percent/cm maximum small signal gain was measured.
- Comparable helium and SF_6 diluent ORTL performance was observed.

4.0 ANALYSIS

4.1 EXTRACAVITY ORTL MODEL

At the outset of this program, a computer model of the extracavity configuration that propagated vibrational (V-) level populations in the ORTL gas flow direction using a rate equation for the population of each V-level had been developed. The code contained resonant optical pumping, vibrational-vibrational (V-V) transfer, and vibrational-translational (V-T) deactivation as driving terms. The populations of five levels were calculated, with each level's manifold of rotational states assumed to be in thermal equilibrium at the gas temperature. After the driving terms had produced an inversion sufficient to initiate lasing, gain was clamped at the threshold value. Each integration step consisted of a time interval during which the populations were pumped out of the threshold values followed by a restoration of them thereto, with each of the transitions required in the restoration process signalling the creation of a photon. The code treated the entire interaction region as a single streamline, calculating populations and gas variables only as a function of downstream coordinate.

During this program, the ORTL code was modified to include effects that were considered likely to become significant. The major changes were:

1. The restriction to five V-levels was removed. At high fluxes, higher V-levels are significantly populated and the old restriction would pile molecules up at V = 4.
2. The assumption of thermal equilibrium within a V-level was replaced by the finite rotational-rotational (R-R) rates measured by Hinchen and Hobbs* as driving terms in rate equations that treat each vibrational-rotational state as a separate species. The former pump-restore-count photons algorithm became unwieldy with all of these (50) populations to track, so a rate equation for photon flux was introduced:

$$\frac{d\phi_{vj}}{dt} = c(g_{vj}-g_{th})(\phi_{vj}+\phi_s)$$

*Hinchen and Hobbs, J. Chem. Phys. 65, 2732 (1976).

where

ϕ_{vj} = flux on line (v,j)

c = speed of light

g_{vj} = gain on line (v,j)

g_{th} = threshold gain

ϕ_s = starter flux

This had had success elsewhere*, and allowed stimulated emission to be added to the rate equations directly. Energy differences between different rotational states are large enough in HF to cause R-R transfer to proceed at rates that are not infinite compared to other processes.

3. Multiple stream tubes or segmentation was introduced. This means that variation in two dimensions in a plane normal to the direction of the ORTL gas flow can be modeled. Such variation might be due to spatial inhomogeneity in the pump laser beam, or to the fact that different portions of the ORTL gas see the pump beam in different states of depletion. Those closest to the pump laser are most strongly pumped. It might be expected that segmentation would be important in conjunction with finite R-R transfer. Such rates will limit ORTL output power at very high pump flux, and this "bottlenecking" could occur in a part of the ORTL cell at lower average pump flux than that required to bottleneck the entire cell.

As a preliminary to the analysis of the extracavity ORTL data, a study of the effects of these new features on model accuracy was performed. Because all of them may be used or suppressed at the option of the user, and all increase the calculation cost per case, it is worthwhile knowing what is needed and what is not needed in analyzing a particular set of data. A case, similar to many in this program, from an earlier experimental study was modeled with the new features. Extending the number of vibrational levels past five produced no discernable change in model result for that case. Figure 47 suggests that calculated ORTL performance is sensitive to the rate of R-R transfer, and, for this sort of case at least, not nearly as sensitive to spatial variation in

*J. Thoens, W.L. Hendricks, S.C. Kurzius, F.C. Wang, Advanced Laser Flow Analysis (ALFA) Theory and User's Guide, AFWL-TR-19 (February 1979).

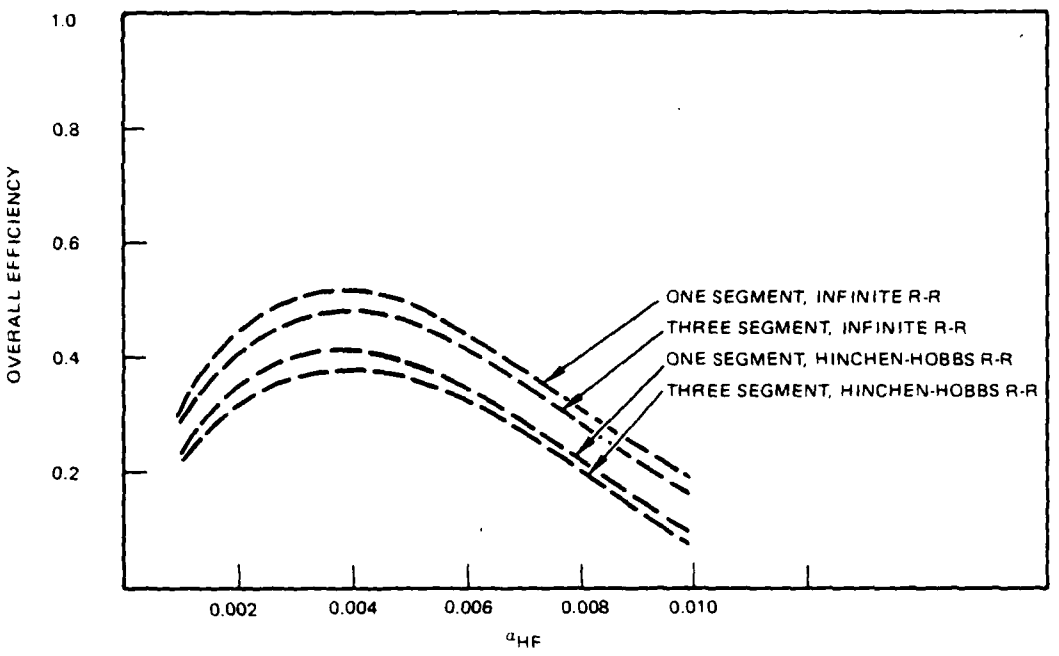

Figure 47. Extracavity model (sample results).

pumping flux. It was deemed essential to include finite R-R rates and, in the interest of economy, it was decided to conduct most of this part of the analysis without segmentation.

In summary, the extracavity ORTL model is quite comprehensive, treating each (v,j)-state as a separate species whose population evolves in time under the influence of: (1) resonant optical pumping; (2) stimulated emission; (3) V-V anharmonic pumping; (4) V-T deactivation; (5) R-R collisional transfer. The code permits subdivision of the ORTL gas flow into multiple stream tubes. This allows assessment of a spatially heterogeneous pump beam and of the variation in pumping produced by beam depletion in a high absorption ORTL cell. The optics of the laser are modeled in less detail. A Fabry-Perot resonator is assumed, so diffraction losses and imperfect filling of the cavity by the resonator mode are not taken into account.

4.2 EXTRACAVITY EXPERIMENTS

This section deals with a comparison between model results and extracavity ORTL laboratory data. Most of the laboratory work was performed with the "low J" pump beam spectrum (see Table 2) and with helium diluent in the ORTL cell. The comparison is confined to these conditions. Model results are presented as regions upon graphs. These regions are bounded by code results obtained using the R-R rates of Hinchen and Hobbs' data and by those obtained using R-R rates one-half as large. The uncertainty in these rates is of at least this order.

Figures 48, 49 and 50 present, respectively, input, conversion and overall efficiencies as functions of HF mole fraction for the gas parameters shown thereon. In these and succeeding calculated results, it is assumed that diffractive and scattering losses in the ORTL cell were insignificant compared to the approximately 2.4 percent cavity loss presented by the resonator mirrors. Should that not have been the case in the laboratory, then calculated conversion efficiencies would be expected to be higher than those observed. The matter was not pursued sufficiently to allow quantitative assessment of this issue. Calculated and measured input efficiencies agree well enough to provide confidence in the rates used in the model. Generally, computed conversion and therefore overall efficiencies exceed their measured counterparts.

Because an increase in ORTL gas inlet temperature increases the absorption coefficient but also increases the deactivation rates, it is expected that there is some optimum value for this parameter. Figure 51 shows that the model selects 375°K as the optimum while laboratory values were still increasing, albeit ever so slowly, at 450°K. The apparent conclusion is that preheating the gas in the extracavity ORTL cell has some effect but not a very large one for a low J pump laser.

In Figure 52 one sees calculation and experiment indicating similar trends as pumping flux is increased. Neither shows the decline in efficiency that would be seen if the R-R rates began to significantly "bottleneck" the excitation transfer. Calculations showed no such effect even at twice the highest flux level available in the laboratory.

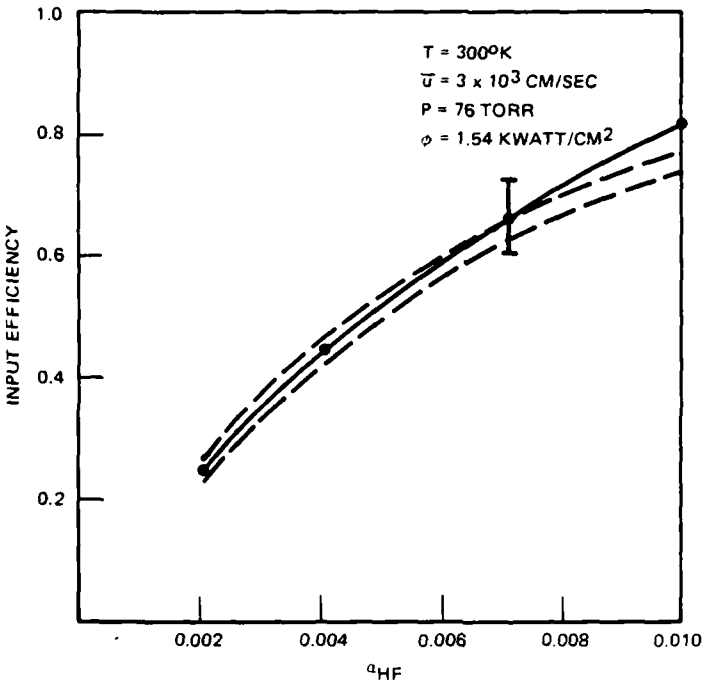

Figure 48. Extracavity ORTL input efficiency.

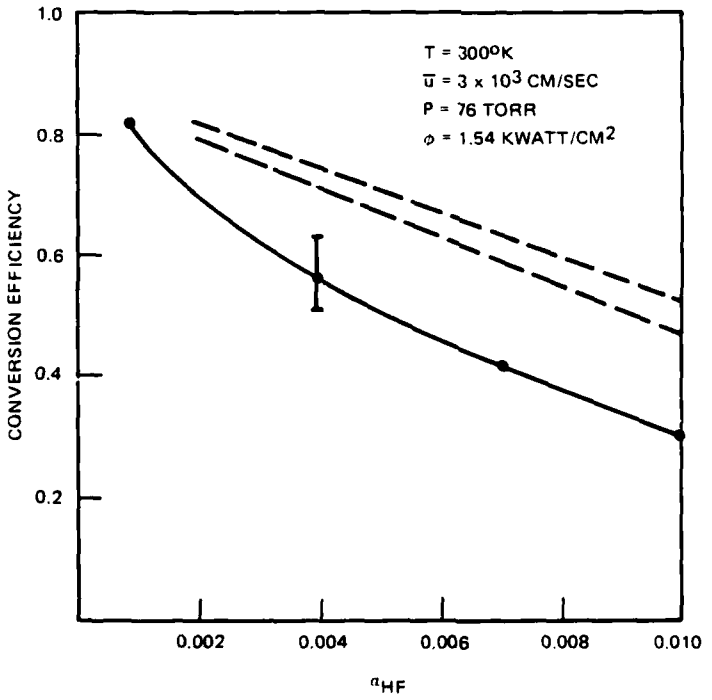

Figure 49. Extracavity ORTL conversion efficiency.

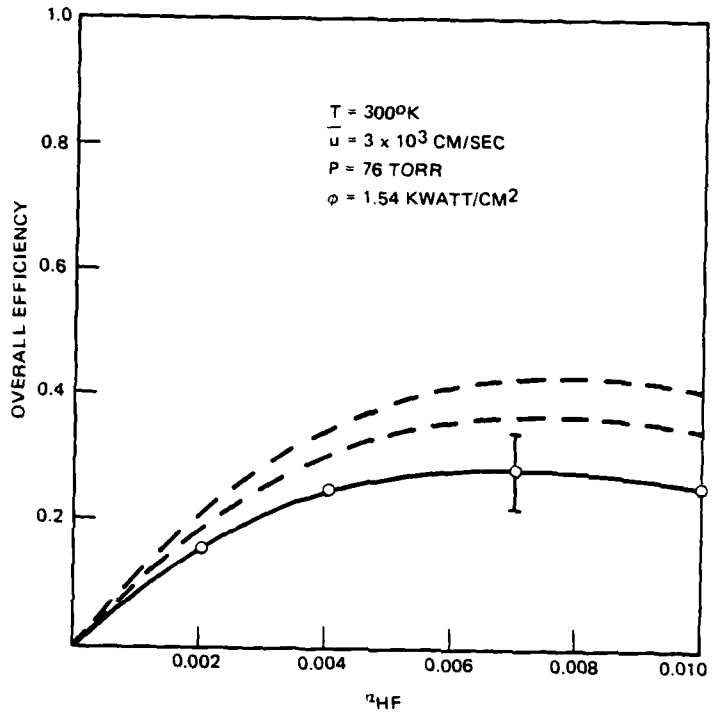

Figure 50. Extracavity ORTL overall efficiency.

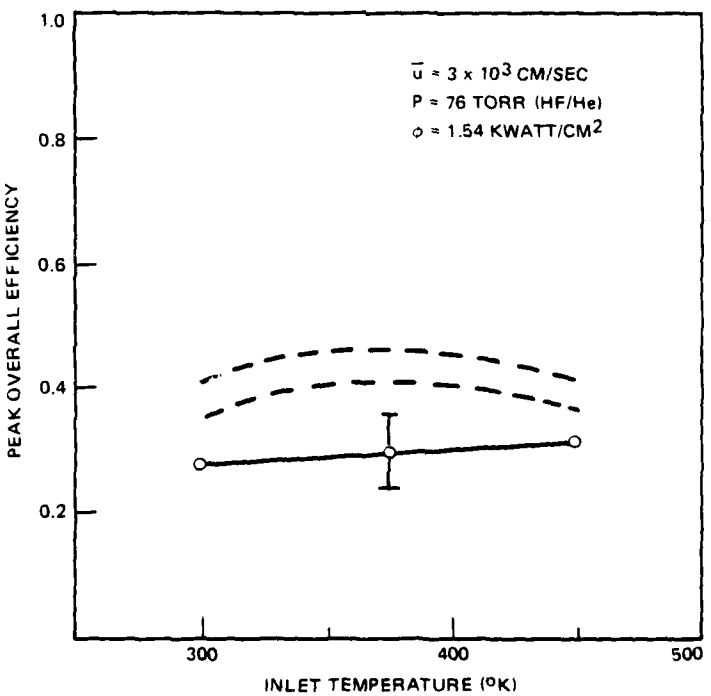

Figure 51. Peak Extracavity overall efficiency versus inlet temperature.

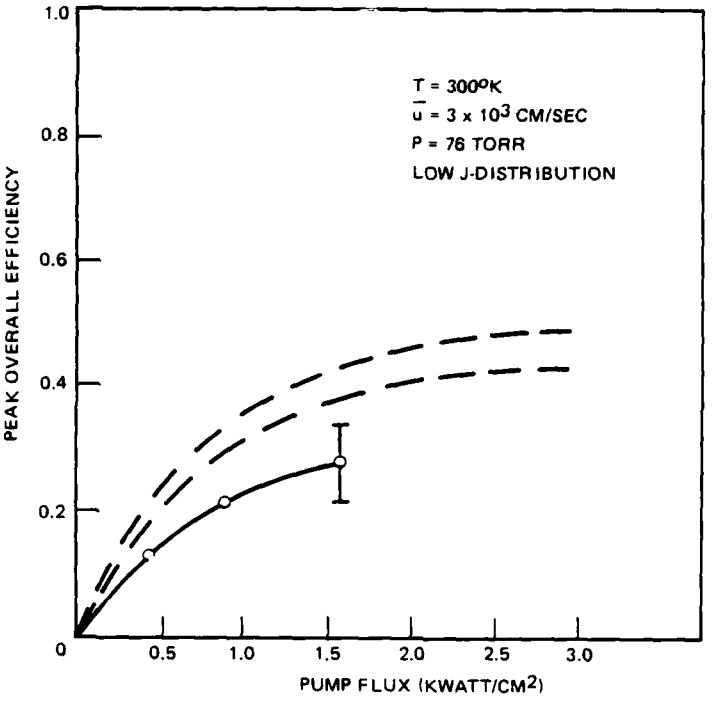

Figure 52. Peak extracavity overall efficiency versus pump flux.

4.3 INTRACAVITY ORTL MODEL

In principle, the difference between the extracavity and intracavity ORTL configurations is that the former is presented with a pump beam that is constant in time, while the latter, through the load the ORTL absorption presents, affects the power spectrum of the pump beam. This section describes the features incorporated into the ORTL model to extend it to the intracavity case.

4.3.1 Chemical Laser Simulation

The pump laser model must be economical enough to allow it to be interrogated at each integration step in an ORTL run without breaking the bank, so to speak. Therefore, a descriptive model has been developed that is curve fitted to measured outcoupled power spectra while retaining sufficient kinetic features to allow excitation to be transferred among various (V,J) states as ORTL loading varies. The data used in the fitting were obtained with the

pump laser operating at a fixed set of conditions, with only the resonator mirrors changing from run to run. Therefore, the model needs to simulate the behavior of the chemical laser at a particular operating point but with various threshold gains.

The data provided for this purpose consisted of:

1. Power spectra obtained through each of four outcouplers (T = 0.04, 0.25, 0.35, and 0.675). The totally reflecting resonator mirror for these cases had a reflectivity, R, of 0.99 throughout the wavelength region of interest.
2. An additional power spectrum of limited use with the same totally reflecting mirror and a T = 0.12 outcoupler. The most prominent lines were off scale but ratios of strengths of other lines were useful in defining the dependence of outcoupled power on outcoupling fraction when the power on a line peaked near T = 0.12.
3. Power spectra obtained through three of the outcouplers mentioned in 1 above (T = 0.04, 0.35, and 0.675) with the totally reflecting mirror replaced by a spectral control mirror. Figure 53 presents $R(\lambda)$ curves for this element. They will be discussed further below.
4. Power spectra measured using each of the two non-transmitting mirrors described above with output flux transmitted through a mirror designed to have constant transmittance in the DF spectrum. Its outcoupling fraction therefore increased as wavelength decreased in the HF region of the spectrum (see Figure 54).

The kinetics of the chemical laser simulation (CLS) is similar to a simplified version of the ORTL kinetics. Vibrational level populations are propagated using rate equations that contain V-T and V-V deactivation terms, stimulated emission, and a driving term that represents the net rate at which all chemical reactions in the gain region produce HF molecules in excited states. Stimulated emission rates are obtained as already described in the extracavity ORTL model discussion. For V>0, then, the rate equations are of the form:

$$\frac{dN(V)}{dt} = D(V,t) + \chi(V + 1) - \chi(V) + U(V)$$

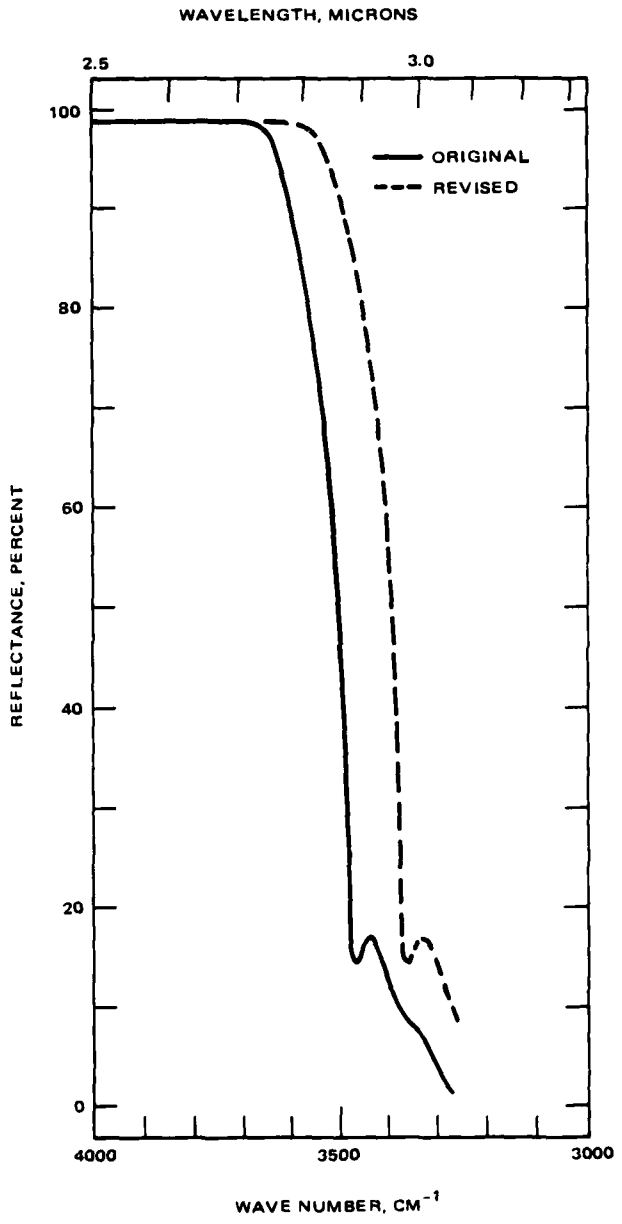

Figure 53. Spectral control mirror reflectance.

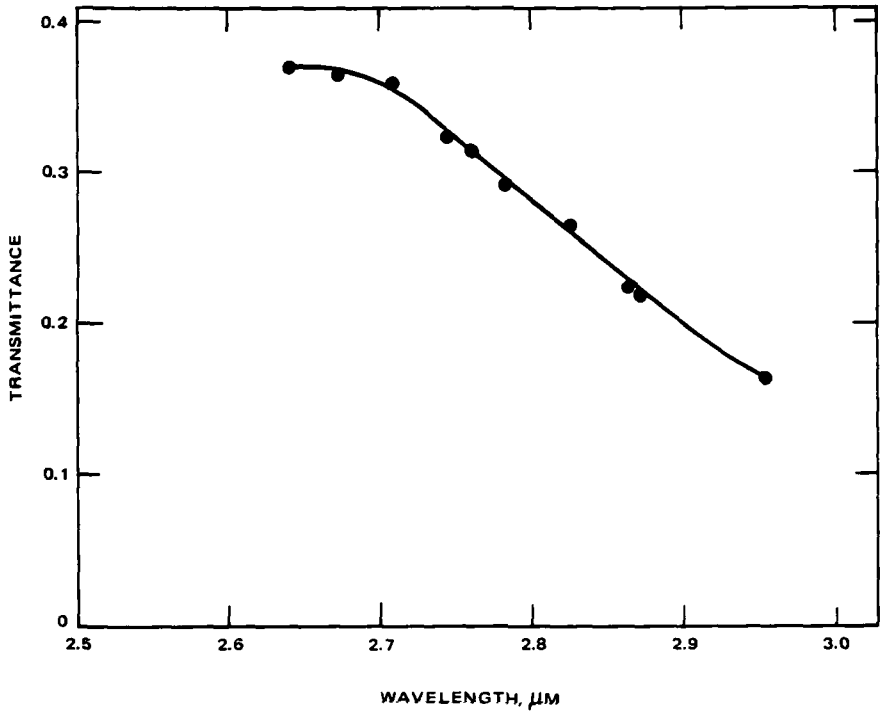

Figure 54. Transmittance of DF outcoupler in the HF spectral region.

where

$N(V)$ = population density of level V

$D(V,t)$ = phenomenological driving term

$\chi(V) = \sum_J g(V,J)\phi(V,J)$

$g(V,J)$ = gain on transition $(V,J-1) \rightarrow (V-1,J)$

$\phi(V,J)$ = flux on transition $(V,J-1) \rightarrow (V-1,J)$

$U(V)$ = net increase in $N(V)$ due to V-V, V-T terms

The explicit time dependence in $D(V,t)$ models the decay of excitation production downstream in the chemical laser. The form of the driving term is:

$$D(V,t) = P(V)e^{-t/\theta}$$

in which P(V) and the characteristic decay time θ are regarded as adjustable parameters in the fitting.

By themselves, vibrational level populations cannot provide gains on laser transitions and, due to the rather large value of B_e for HF, the readily calculated Boltzmann equilibrium rotational state populations are not directly relevant here. An equation derived by Hough* from the assumption that each (V,J) population relaxes to its Boltzmann value with a characteristic time constant $\tau(V,J)$ is used to generate gains. For a two level or single band system, Hough obtained

$$g(V,J) = \frac{g_e(V,J)}{1 + K(V,J) \cdot \tau(V,J) \cdot [4J/(2J - 1)] \cdot \phi(V,J)}$$

in which

$g(V,J)$ = gain on transition $(V,J-1) \rightarrow (V-1,J)$

$g_e(V,J)$ = Boltzmann gain on transition $(V,J-1) \rightarrow (V-1,J)$

$\phi(V,J)$ = flux on transition $(V,J-1) \rightarrow (V-1,J)$

$\tau(V,J)$ = relaxation time of states $(V,J-1)$ and $(V-1,J)$

and $K(V,J)$ is defined by

$$g(V,J) = K(V,J) \cdot \left[\frac{2J + 1}{2J - 1} N(V,J-1) - N(V-1,J)\right]$$

For a three level system additional terms due to cascading effects arise which clutter up the gain equation considerably. In the interest of notational simplicity, the resulting equations for non-equilibrium gain in a two-band lasing system are presented below with the (V,J)-dependence suppressed, and

*J.J. Hough, Efficient Model for HF Lasers with Rotational Nonequilibrium, SAMSO-TR-78-79, 1978.

with subscripts 10 and 21 referring to the 1->0 and 2->1 transitions respectively. For two transitions that form a cascade then:

$2,J-2 \rightarrow 1,J-1$

$$g_{21} = \frac{g_{21e}[1+\phi_{10}K_{10}\tau_{10}(1+d_0/d_1)]+g_{10e}\phi_{21}K_{10}\tau_{21}}{[1+\phi_{21}K_{21}\tau_{21}(1+d_i/d_2)][1+\phi_{10}K_{10}\tau_{10}(1+d_0/d_1)]-\phi_{21}K_{21}\phi_{10}K_{10}\tau_{21}\tau_{10}}$$

$1,J-1 \rightarrow 0,J$

$$g_{10} = \frac{g_{10e}[1+\phi_{21}K_{21}\tau_{21}(1+d_1/d_2)]+g_{21e}\phi_{10}K_{21}\tau_{10}(d_0/d_1)}{[1+\phi_{21}K_{21}\tau_{21}(1+d_1/d_2)][1+\phi_{10}K_{10}\tau_{10}(1+d_0/d_1)]-\phi_{21}K_{21}\phi_{10}K_{10}\tau_{21}\tau_{10}}$$

In these equations, d_i is the degeneracy of the state in V-level i that is involved in the cascade. The τ were regarded as adjustable fitting parameters.

Another parameter that was regarded as adjustable to some degree was the unmodeled cavity loss L. When the power absorbed by all monitored losses from the chemical laser was totaled, the curve of power versus loss did not continue to climb with decreasing total loss. An elementary analysis suggested that this unmodeled loss was about 6 to 10 percent, and it was regarded as adjustable within that range in the curve fitting.

The values of the key parameters found to best fit the outcoupling data with the constant reflectivity mirror are:

$$P(1) = 1.6 \times 10^{20} \text{ molecules/cm}^3 \cdot \text{sec}$$

$$P(2) = 4.0 \times 10^{20} \text{ molecules/cm}^3 \cdot \text{sec}$$

$$\theta = 10 \text{ } \mu\text{sec}$$

$$\tau(V,J) = 1.0 - 2.5 \text{ } \mu\text{sec}$$

$$L = 0.06$$

Figure 55 displays the fit obtained using these values.

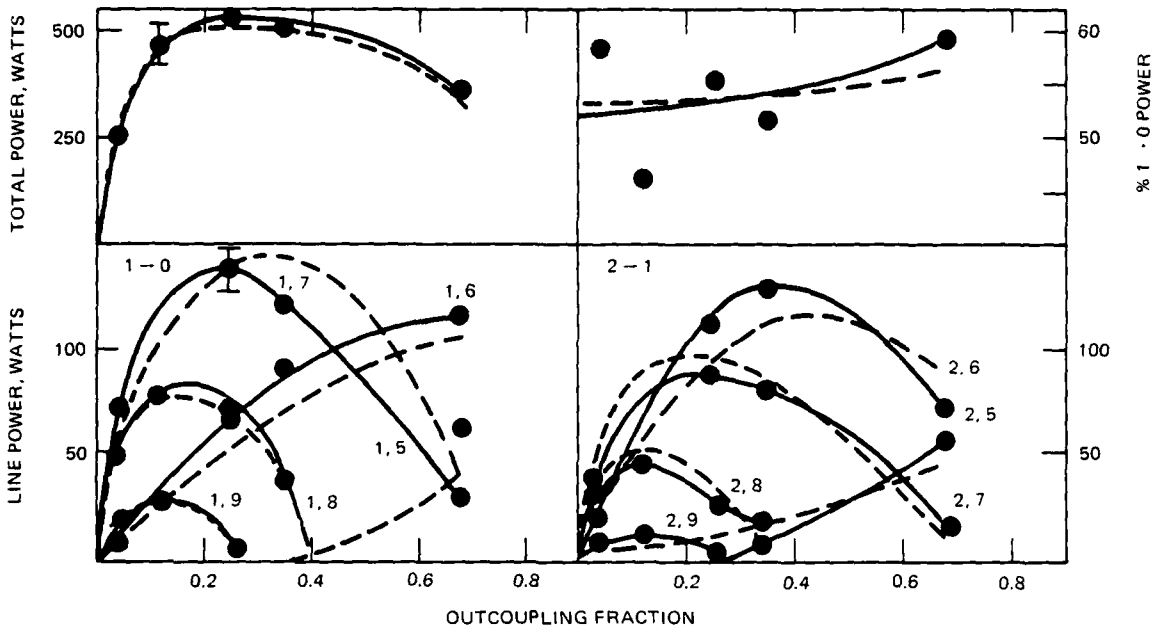

Figure 55. CLS curve fit to data taken with totally reflecting mirror (R = 0.99).

Examination of the data obtained using the spectral control mirror revealed that the reflectivity curve provided by the manufacturer was not appropriate to the laboratory situation. Spectral control mirror power absorption calculated from the curve and observed outcoupled power spectra produced values far larger than the measurement values. If it is assumed that the shape of the reflectivity curve is more or less correct but is shifted to longer wavelength (Figure 53) better agreement is obtained. Table 19 compares the spectral control mirror power absorption calculations with the measured values. Note that the revised spectral properties result in a better model calculation. Accurate assessment of the reflectivity of the spectral control mirrors experienced during intracavity experiments proved difficult because measurements could not be performed during actual ORTL runs. The operational temperature of the front surface of each mirror was not known, so it could not be duplicated for reflectivity measurements. The manufacturer estimates that a 75°K rise in mirror temperature would produce over half of the "red shift" posited in Figure 53.

TABLE 19. SPECTRAL CONTROL MIRROR ABSORPTION
(WATTS)

Outcoupling Percentage	Measured*	Calculated	
		Original $R(\lambda)$	Revised $R(\lambda)$
4	148	1900	173
35	36.7	290	29
67.5	3.0	30	4.5

*Uncertainty ±10 percent.

When the shifted reflectivity of the spectral control mirror replaces the constant reflectivity of the other mirror in the CLS input data, and all other parameters are the same as those used in fitting the data for the R = 0.99 mirror, the performance of the model is quite gratifying. Figure 56 shows the agreement between model and experiment resulting from the curve fit of Figure 55.

It would be possible to have the ORTL code call the CLS directly during an ORTL model run but, even though the CLS requires less than 1 CPU second, a typical run might call it 10,000 times and the resulting cost was adjudged to be undesirably high. Therefore, it was decided to run the CLS to provide a matrix of stored results. The ORTL code calls a routine that performs interpolation among these numbers. Obviously, it is not possible to have the ORTL provide, say, 12 absorption coefficients and then have a prerun databank of 5 or 6 raised to the 12th power of cases searched in 12 dimensional space for the result. The absorption coefficient spectrum must be characterized by a smaller set of parameters. Satisfactory results were obtained using a 5-member set, namely:

1. N(2)/N(1) denoted by C_1
2. N(1)/N(0) denoted by C_o
3. ORTL HF partial pressure denoted by P_{HF}

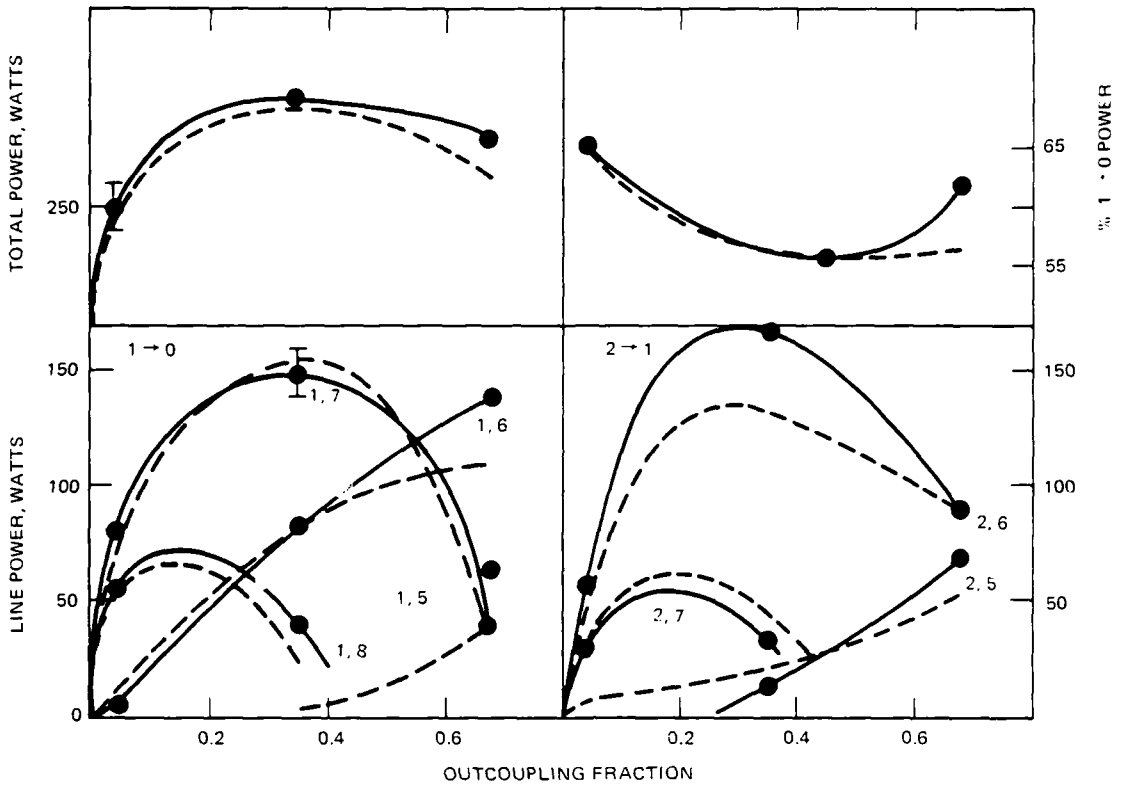

Figure 56. CLS comparison to data taken with spectral control mirror.

4. ORTL gas temperature denoted by T
5. ORTL threshold gain denoted by g_{th}

where N(V) is the population density in vibrational level V.

The numbers actually stored in the databank are those values of the CLS output power spectrum appropriate to ORTL loss coefficients that are derived from Boltzmann distributions at the ORTL values of C_o, C_1, P_{HF}, T, with the provision that any calculated negative ORTL absorption, i.e., gain, that exceeds in absolute magnitude the ORTL threshold gain is set instead to the threshold value. Although Boltzmann values of a sort are used, these are not the values that would result from assuming actual rotational thermal equilibrium in the ORTL, because C_1 and C_o are somewhat higher than they would be in a true equilibrium situation. Table 20 attempts to clarify the situation. The set of absorption coefficients in column III of Table 20 constitutes a

TABLE 20. EXAMPLE OF STORED ORTL ABSORPTION COEFFICIENTS

P_{HF} = 1 torr, C_0 = 0.340, C_1 = 0.371, T = 510°K, g_{th} = 0.00137						
J	I Boltzmann Absorption Coefficient for These Parameters		II Absorption Coefficients ORTL Code, Non-Boltzmann Calculations		III Stored Absorption Coefficient	
	1→0	2→1	1→0	2→1	1→0	2→1
4	0.381	0.239	0.372	0.233	0.381	0.239
5	0.239	0.149	0.232	0.143	0.239	0.149
6	0.117	0.0718	0.114	0.0609	0.117	0.0718
7	0.0418	0.0234	0.0411	0.0227	0.0418	0.0234
8	0.00700	0.00142	0.00685	0.00002	0.00700	0.00142
9	-0.00354	-0.00461	-0.00137	-0.00137	-0.00137	-0.00137
10	-0.00411	-0.00412	-0.00137	-0.00137	-0.00137	-0.00137
11	-0.00241	-0.00234	-0.00137	-0.00137	-0.00137	-0.00137
12	-0.00105	-0.00104	-0.00132	-0.00098	-0.00105	-0.00104

reasonable approximation to the set in column II if the spectral distribution and magnitude of the power absorbed by the ORTL cell from the chemical laser that are calculated when the former is used are sufficiently close to the spectral distribution and magnitude of the power absorbed by the ORTL that are calculated when the latter set is employed. That is, differences between those two sets are significant only insofar as they result in different calculated values of ORTL cell pumping. Table 21 presents the spectrum of power absorbed by the ORTL cell computed with each of the two sets of absorption coefficients. Based upon this and numerous similar results, it was concluded that the approximation of replacement of true ORTL absorption coefficients by those in the right hand column does not significantly degrade the model. The virtue of

TABLE 21. POWER SPECTRUM ABSORBED BY ORTL
(watts)

Line	With Stored Absorption Coefficients	With Non-Boltzmann ORTL Code Coefficients
$P_1(7)$	104.6	110.9
$P_1(8)$	83.9	80.6
$P_1(9)$	-1.0	-1.0
$P_2(6)$	66.3	76.6
$P_2(7)$	72.9	67.6
Total	326.7	334.8

this procedure is that it reduces the number of stored values in the data bank by more than four orders of magnitude.

The ORTL code running in the intracavity mode then simply replaces references to the input spectrum with calls to a subroutine that locates the four parameter set within the data bank matrix, performs linear interpolation, and returns a new pump spectrum.

4.4 INTRACAVITY EXPERIMENTS

The goal of the modeling task was to produce a calculational tool that could be applied to regions of parameter space unavailable in the laboratory, such as high temperature, high pressure, large size, etc. The complexity of the intracavity ORTL system is such that this goal can be reached only with considerable input of phenomenological information. Comparison of calculated results with a sufficient variety of laboratory data can indicate the degree to which model results may be relied upon. In this section comparisons are made for variation with HF partial pressure at a constant 295°K inlet temperature of the following quantities:

1. ORTL outcoupled power
2. Chemical laser mirror absorption

3. ORTL gas heating
4. Total chemical laser power
5. ORTL small signal gain
6. ORTL input efficiency
7. ORTL conversion efficiency

and for variation with inlet gas temperature at a constant 2.0 torr HF partial pressure of:

8. ORTL conversion efficiency
9. ORTL output power

The data used in this section were all obtained using an ORTL cell (N-2) that measures 10 cm along its optical axis. For modeling purposes, it was inferred from data of the sort presented in Figure 42 that only 7 cm of the cell was actually illuminated by the pump beam.

Figure 57 shows the model/experiment comparison for outcoupled ORTL power. Unfortunately, the experiments were completed before the intracavity model was operational. While more data points would have allowed more careful comparison of model and experiment, it is probable that the predicted optimal HF pressure is slightly lower than that which was observed. The good fit displayed in Figure 58 for the chemical laser mirror absorption tends to confirm the reflectivity versus wavelength curve adopted for the spectral control mirrors.

The calculated ORTL medium heating curve in Figure 59 has the same trend as the laboratory results, but is somewhat low, suggesting that conversion efficiency is somewhat high in the model. Time did not permit a detailed examination of the kinetic rates used in the computer code that might have shed some light on this area.

The fit shown in Figure 60 for total chemical laser power is probably better than that in Figures 57 and 59, again hinting that a moderate improvement in the model kinetic rates, specifically R-R and V-T rates, might be possible.

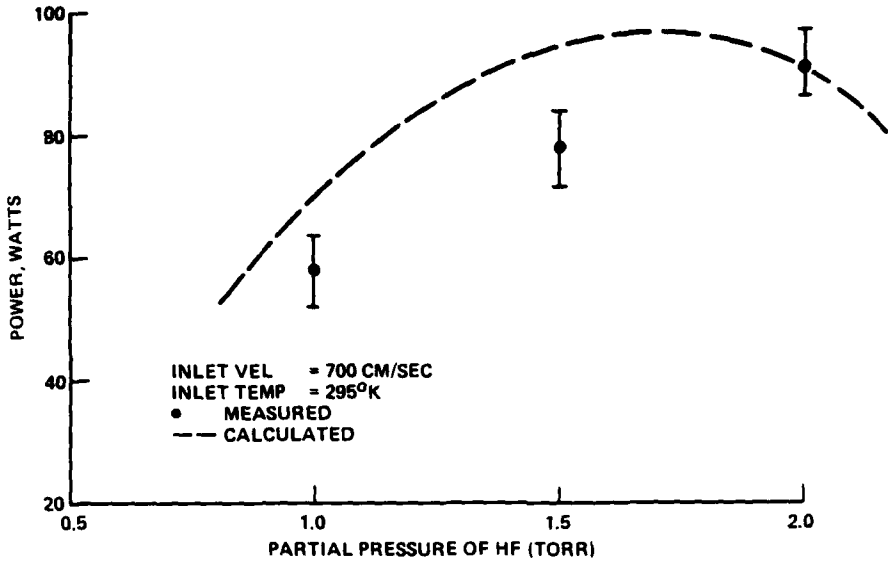

Figure 57. ORTL power versus HF pressure.

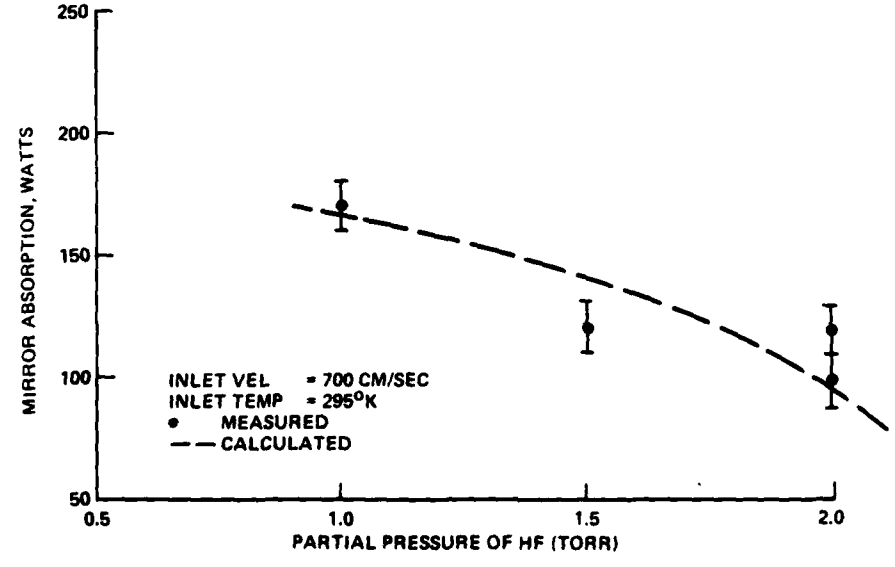

Figure 58. Chemical laser mirror absorption versus HF pressure.

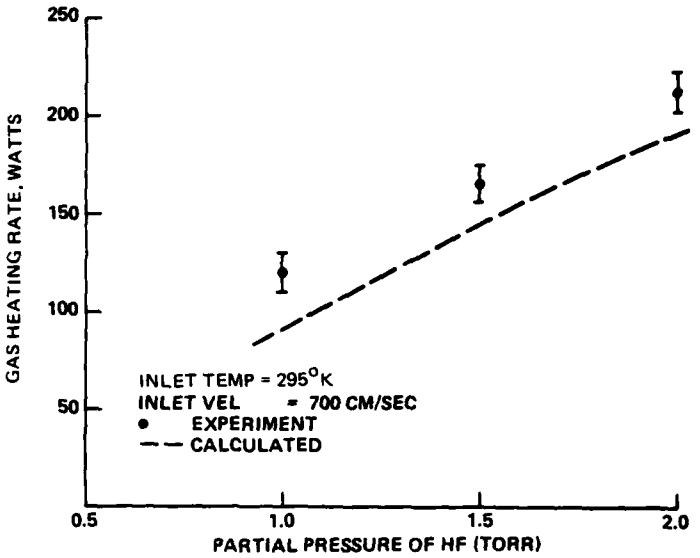

Figure 59. ORTL gas heating versus HF pressure.

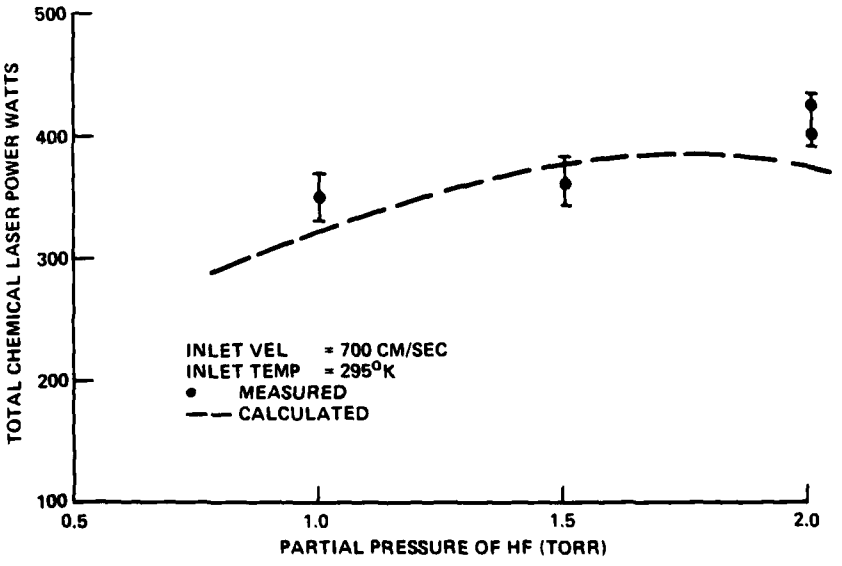

Figure 60. Total chemical laser power versus HF pressure.

The small signal gain data were not available until late in the program, so they could not be used in the curve-fitting phase of code development. Figure 61 shows the intriguing result that the 2 → 1 band small signal gain was nevertheless well-fit by the model, but that the 1 → 0 band data was not.

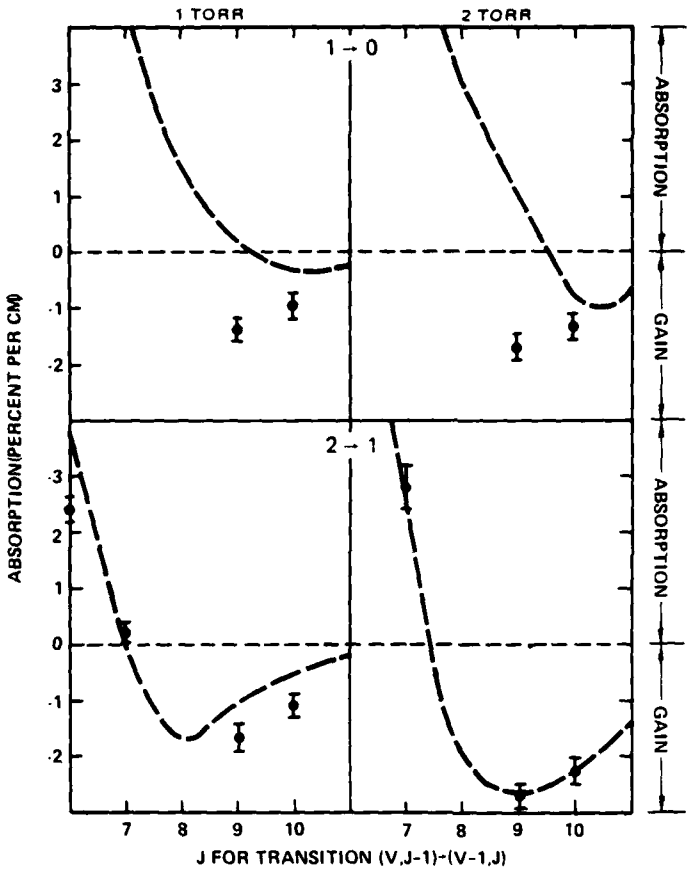

Figure 61. ORTL small signal gain.

The absorption coefficient modeling scheme described earlier receives strong support from the input efficiency curve of Figure 62. The conversion efficiency curve agrees fairly well with experiment. The above remarks about kinetic rates have the same applicability to the conversion efficiency.

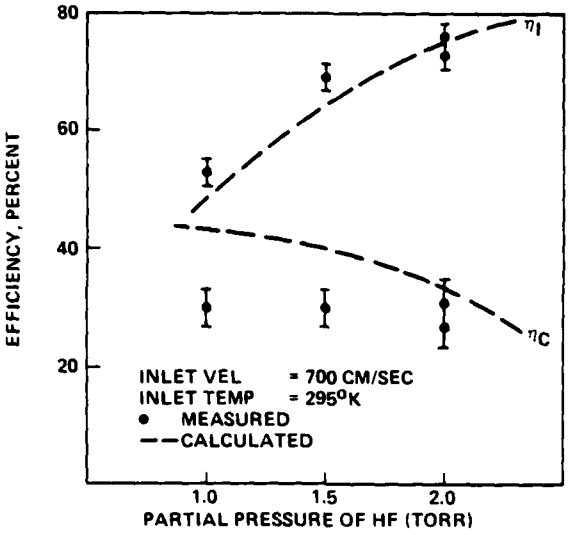

Figure 62. ORTL inlet and conversion efficiencies versus HF pressure.

Operating the ORTL cell at higher inlet temperature has many potential advantages. R-R transfer rates increase with temperature in any physically reasonable model, and published measurements of HF self-deactivation indicate a decrease with temperature up to 800-900°K. These two facts suggest higher conversion efficiency at elevated temperature. The agreement between calculation and experiment shown in Figure 63 engenders confidence that the model may be used to assess further gains in ORTL performance available through further increases in inlet gas temperature.

Higher ORTL gas temperature also means that ORTL gas absorption coefficients will change. At inlet, the gas is prepared to absorb strongly on higher J-lines than it would at room temperature. The increased load on the chemical laser will affect its performance in a way that is not easy to anticipate. With proper matching of HF pressure to the chemical laser, increases in ORTL output power even greater than would be expected from conversion efficiency increases alone were achieved. From Figure 64, one sees that model and measurement are in excellent agreement on the effect upon ORTL output power of increased ORTL gas inlet temperature. Model assessment of the effect of inlet gas temperatures higher than those achievable in the laboratory device is included in the next section of this report.

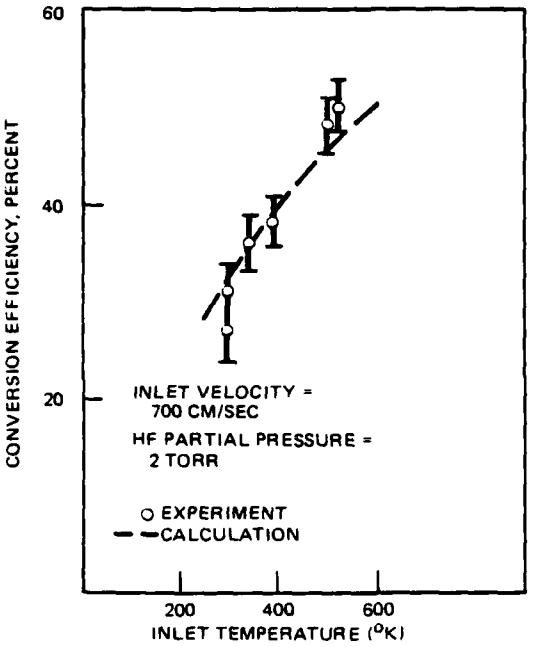

Figure 63. Conversion efficiency versus inlet temperature.

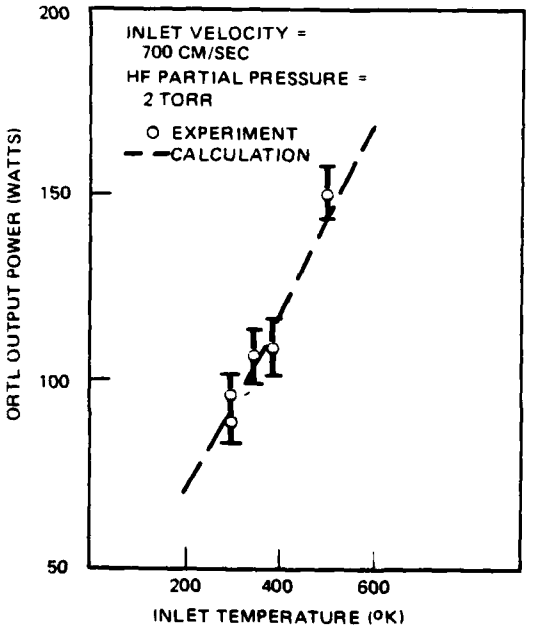

Figure 64. ORTL output power versus inlet temperature.

The computer code has shown fair to excellent agreement with experiment in the preceding comparison. The weakest link undoubtedly is the small signal gain fit on the $1 \rightarrow 0$ band, but this has evidently not had an impact upon the quality of model predictions in outcoupling cases. It would be interesting to pursue this matter, but it appears reasonable to conclude that, at present, this result is not a serious detriment to use of the code. The tendency of the code to be a bit too optimistic about conversion efficiency at lower HF partial pressure and to select a lower optimum operating value of partial pressure place assessable uncertainties in extensions of the model to other regions that require any design based upon its predictions to incorporate commensurate flexibility. In simpler words, model predictions have error bars.

The major trend in the comparison is that the model agrees well with laboratory results, especially so in the temperature dependence that has such a pronounced influence on performance. Any optimized system would pay particular attention to ORTL inlet temperature and here the model appears firmly anchored in the data. It is reasonable to impute quantitative significance to code calculations for scaled-up ORTL systems.

4.5 SCALING

In order to predict the performance of high energy ORTL systems, a brief extrapolation study using the experimentally validated intracavity model was performed. This effort consisted of first predicting the ideal conditions and optimum performance for a device the size of the one utilized in this program and then of further idealizing the calculation to represent a high energy system.

The overall efficiency (η_o) of the ORTL system may be approximately represented as*:

$$\eta_o = \frac{g_{oc} - g_{thc}}{g_{oc}} \times \frac{\alpha h/l_c}{g_{thc}} \times \frac{g_{oo} - g_{tho}}{g_{oo}} \times \frac{-\frac{1}{2l_o}\ln(1 - T)}{g_{thc}} \times \eta_c$$

*A.Y. Yariv, Quantum Electronics, 1975 (John Wiley & Sons, New York).

where:

g_{oc} = chemical laser small signal gain.

g_{thc} = chemical laser threshold gain.

α = ORTL absorption coefficient.

h = ORTL absorption length.

l_c = chemical laser gain length.

g_{oo} = ORTL small signal gain.

g_{tho} = ORTL threshold gain.

l_o = ORTL gain length.

T = ORTL outcoupling fraction.

η_c = ORTL conversion efficiency.

This form, derived from consideration of a single-line laser, is used here as a guide to the physical considerations in our compound multiline system. Further expanding on some of these terms:

$$g_{thc} \simeq -\frac{1}{2l_c} \ln R_1 R_2 - \frac{1}{2l_c} \ln L_c + \frac{\alpha h}{l_c}$$

$$g_{tho} \simeq -\frac{1}{2l_o} \ln (1 - T) - \frac{1}{2l_o} \ln L_o$$

$$\eta_c \equiv \frac{\text{ORTL outcoupled power}}{\text{ORTL outcoupled power + ORTL resonator loss + ORTL gas heating}}$$

in which:

R_1, R_2 = wavelength dependent reflectivities of chemical laser mirrors.

L_c = chemical laser diffraction and scattering losses.

L_o = ORTL losses other than outcoupling.

Conversion efficiency cannot be simply expressed because it is a result of the complex interplay of pumping rates and kinetic rates of several sorts.

From the efficiency point of view, then, one seeks to have: the chemical laser small signal gain far above the threshold gain, with the latter determined entirely by the ORTL absorption; the ORTL small signal gain far above

its threshold gain, with the latter determined almost entirely by outcoupling; and very favorable kinetics so that η_c is near unity.

Some ground rules for the laboratory size performance optimization adopted ab initio were:

- ORTL inlet velocity was not altered from the laboratory value of 700 cm/sec. The main effect of such variation would have been to alter the average gas temperature in the ORTL; this effect can be controlled by varying the inlet gas temperature.
- The apparent 6 percent diffraction/scattering loss in the chemical laser was not changed. The view was taken that some loss is inherent in any laser ans this value might as well be carried through the computer studies.
- The overall efficiency was taken to be the ORTL output divided by the maximum outcoupled chemical laser power, namely 515 watts. ORTL output power is presented as the figure of merit for intercase comparison.

The first parameter to be optimized is suggested by Figures 63 and 64. The highest achievable ORTL gas inlet temperature was apparently too low for optimum performance. The gas temperature determines the value of the kinetic rates, which in turn determine η_c, and are major determinants of the absorption coefficients, α. Therefore, the optimum product of η_c and α was, in effect, sought. Figure 65 displays the model results for 2.0 torr HF partial pressure. 800°K was selected for the remainder of the optimization study. Figure 66 shows that lower HF gas pressure is preferred at this temperature than at room temperature.

The chemical laser threshold gain varies with wavelength as discussed above. The spectral control mirrors actually employed in the experiments might be improved upon. To investigate this, several other filter mirror characteristics were devised in an effort to minimize the effective threshold gain in the driver laser resonator. Mirror reflectivities are shown in Figure 67, as are the calculated ORTL output powers at 1.0 torr HF for each of them, including the laboratory filter, here designated as filter #1. It was recognized that, in a larger intracavity ORTL system, the spectral control mirrors would provide a lower loss per centimeter than that encountered in the laboratory. For example, if the chemical laser had ten times as much gain

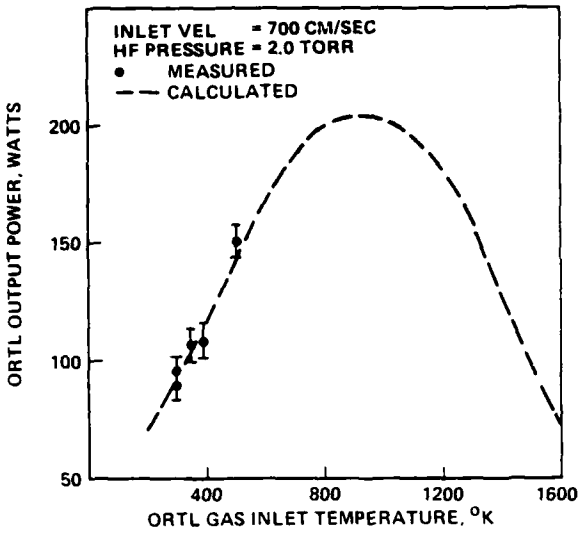

Figure 65. Predicted ORTL output power versus inlet gas temperature.

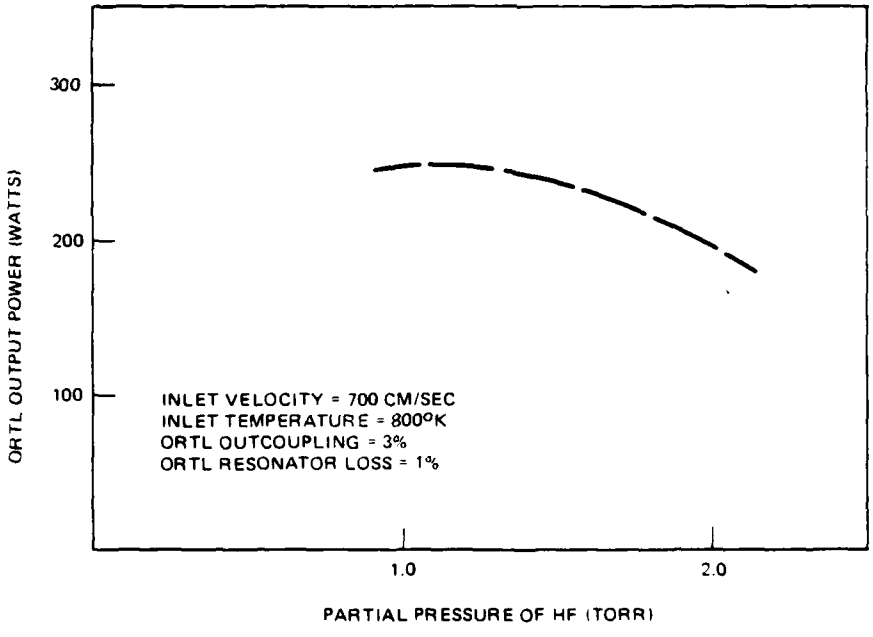

Figure 66. Predicted ORTL output power versus HF partial pressure.

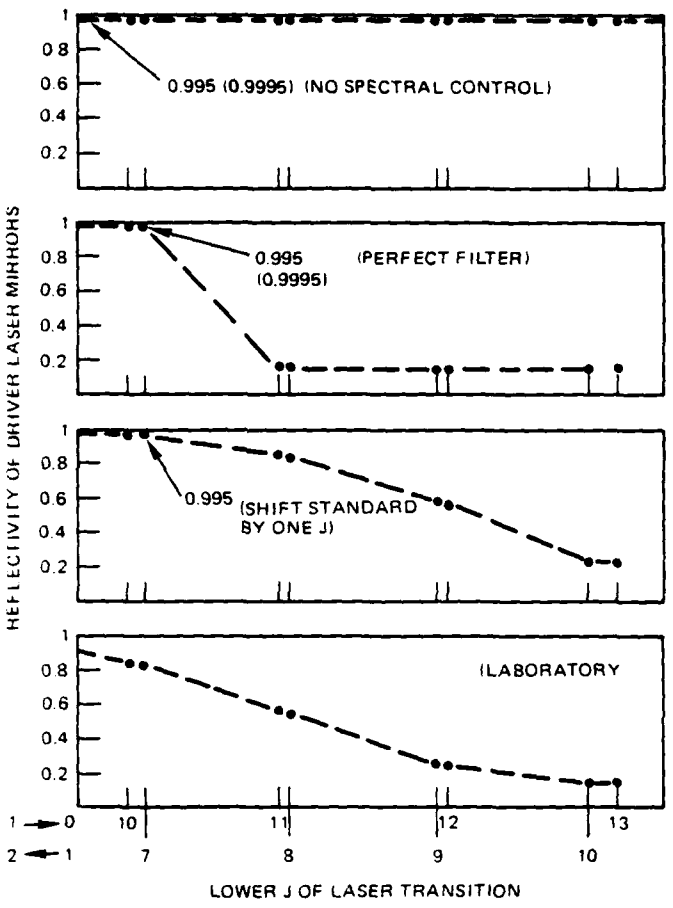

FILTER NO.	ORTL OUTPUT (WATTS)
4 (4')	374 (389)
3 (3')	408 (429)
2	379
1	354

INLET VELOCITY = 700 CM/SEC
INLET TEMPERATURE = 800°K
HF PARTIAL PRESSURE = 1.0 TORR
1% ORTL OUTCOUPLING
0% ORTL SCATTERING/DIFFRACTION LOSS

Figure 67. Predicted ORTL performance for various spectral control costing characteristics.

length, the mirror loss per centimeter would be about one-tenth as great on the lasing lines enjoying peak reflectivity. To assess the likely effect of this in a scaled-up system, an investigation of laboratory-scale model performance with spectral control mirrors with 99.95 percent peak reflectivity instead of the 99.5 percent maximum actually available was undertaken. Calculated performance for the intracavity ORTL using mirrors with this ultra high reflectivity (denoted by a prime) are included in Figure 67. An interesting preliminary observation is that, at this elevated temperature, the model hints that a spectral control filter may not be required. This is a result of the

low gain in the chemical laser at high J values. The high temperature ORTL gas absorbs at the normal chemical laser oscillation J values. Above the J value for which the ORTL absorption becomes gain, the chemical laser gain is below threshold. The validity of this prediction must be assessed carefully, in light of the fact that there is no data base for the CLS in this region.

The kinetic rates that dictate η_c are influenced by diluent concentration although the mathematical forms provided by the literature* suggest that this effect is not as significant as that of temperature. Figure 68 is the result of a brief investigation into what was anticipated to be a relatively minor effect upon η_c. The SF_6 partial pressure that had been selected initially to provide the same molar flow as that used in the laboratory, namely 42.4 torr, was found to be near enough to optimal to be retained for the rest of this study.

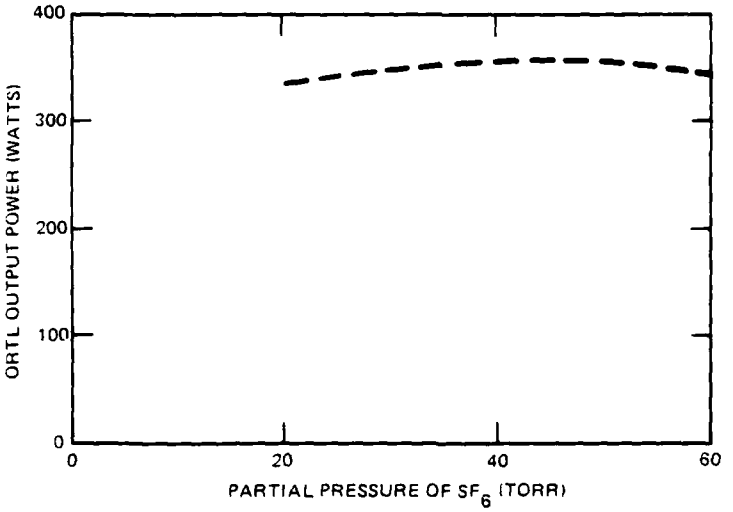

Figure 68. Predicted ORTL performance versus diluent partial pressure.

The ORTL cell in the laboratory device suffered efficiency penalties from diffraction and scattering and from insufficient small signal gain. The former effect was estimated at 1 percent roundtrip with an outcoupling of 3 percent. In a large device, it is anticipated that small signal gain would swamp outcoupling loss which in turn would overpower diffraction and scattering.

*N. Cohen and J.F. Bott, A Review of Rate Coefficients in the H_2-F_2 Chemical Laser System, SAMSO-TR-76-82, April, 1976 and Supplement, SAMSO-TR-78-41, June 1978.

To simulate this, resonator loss was set to zero and outcoupling to 1 percent. Figure 69 displays the result of first removing resonator loss and then reducing outcoupling to 1 percent. For the range of interest, idealizing the resonator in this way improves ORTL performance by about 45 percent.

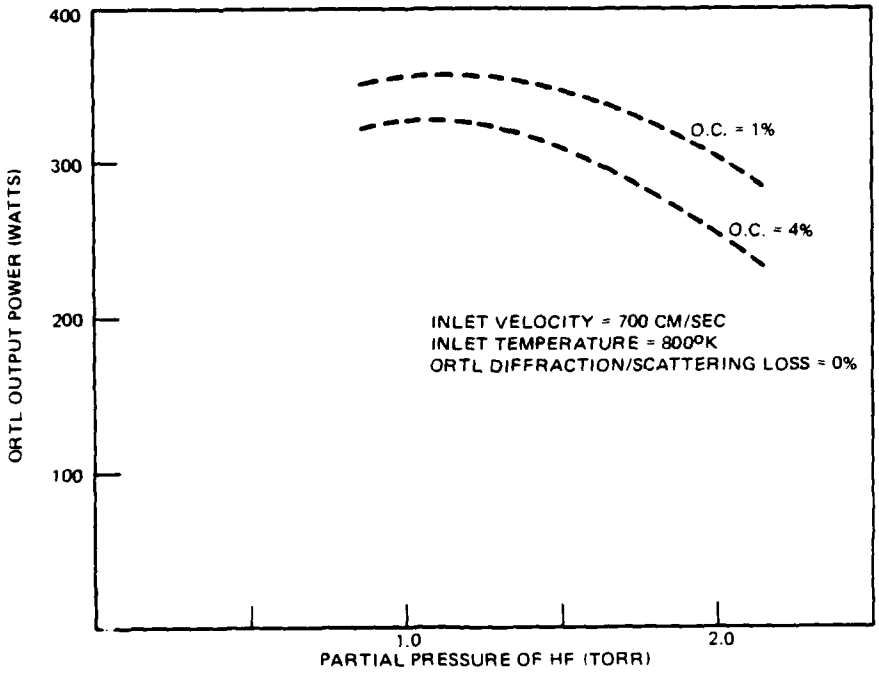

Figure 69. Idealized ORTL performance.

The chemical laser small signal gain has been regarded thus far as fixed in this parametric study. One might ask whether a larger gain region together with, perhaps, more HF in the ORTL, might result in a more efficient system. This question was tackled with the model, putting 1.5 and then 2.0 times longer gain regions into the chemical laser. This is equivalent to 1.5 and 2.0 times higher flux. The curves presented in Figure 70 suggest that some improvement is available from this. The reader should note that these calculations were done using filter No. 2 (see Figure 67) and an ORTL resonator free of loss except for 1 percent outcoupling, so direct comparison with results presented in some of the previous figures is not available.

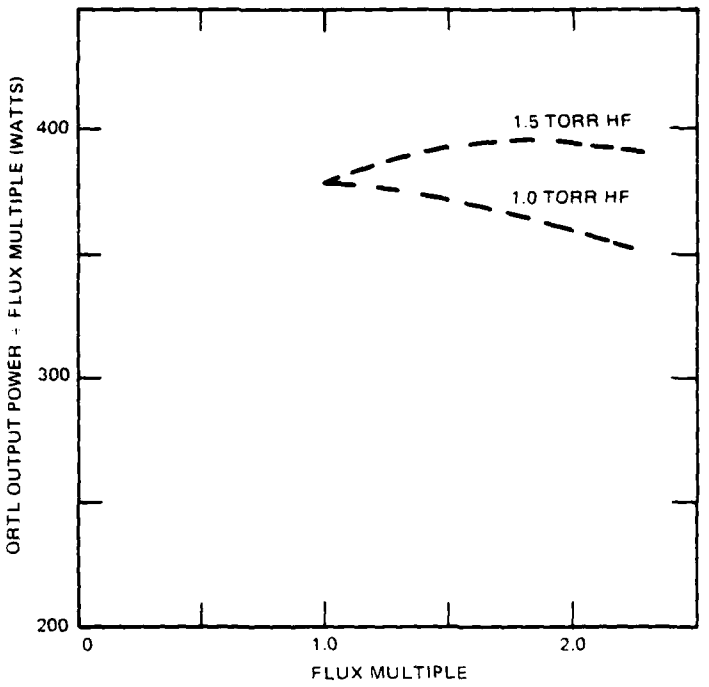

Figure 70. ORR output power versus pumping flux.

As a finale, some of the best cases were run with various filters and 1 percent total loss with the results shown in Table 22. Efficiencies are simply ORTL output power divided by 515 watts times the flux multiple (i.e., either 1.0, 1.5, or 2.0). The highlighted cases indicate the highest efficiencies with and without spectral control. These results suggest that overall efficiency greater than 85 percent may be achieved, in a properly designed large scale device.

In summary, the model optimization study indicates that:

- The laboratory device could produce about twice as much ORTL power as was actually realized, with the use of higher inlet gas temperature (800°K) and redesign of the chemical laser spectral control mirrors.
- With the elevated ORTL gas inlet temperature, spectral control mirrors may be unnecessary and excellent performance could be obtained without them if the pump flux were higher.
- A properly designed scaled-up system could achieve 85 percent or greater efficiency.

TABLE 22. SUMMARY OF BEST MODEL CONFIGURATIONS

Filter	HF Partial Pressure (torr)	Flux Multiple	Efficiency (%)*
2	1.0	1.0	73.6
2	1.5	1.0	73.6
2	1.5	1.5	76.3
2	1.5	2.0	76.3
2	2.0	2.0	75.3
3	1.0	1.0	79.2
3	1.0	1.5	77.9
3'	1.0	1.0	83.3
3'	1.0	1.5	85.8
3'	1.5	1.5	86.2
4	1.5	1.0	74.8
4	1.5	1.5	76.5
4'	1.0	1.0	75.5
4'	1.5	1.5	82.9

*Efficiency $\equiv \frac{\text{ORTL Output Power}}{515 * \text{Flux Multiple}}$

5.0 CONCLUSIONS

This experimental program addressed several fundamental physics issues critical to intracavity ORTL operation. These critical issues were: optimization of ORTL parameters (inlet gas temperature, HF partial pressure, total pressure, flow velocity, and diluent) for a given pump laser power and spectrum; possible efficiency limitations resulting from a rotational-rotational transfer bottleneck under high pumping flux; and control of the coupling between the pump laser and the ORTL load by means of spectral control coatings in the chemical laser resonator and temperature regulation of the ORTL medium. Simultaneously, the ORTL model was extended to include the finite rotational-rotational transfer kinetics, and an intracavity model was developed utilizing a chemical laser simulation (CLS) code. The experimental data were used to validate the intracavity model so that efficiency projections and designs for high energy systems could be made.

The program has successfully addressed the fundamental intracavity ORTL physics. The experiments qualitatively verified theoretical expectations. At the pump fluxes utilized no rotational bottleneck was observed; high efficiency, high energy systems can be configured at similar flux levels. The intracavity ORTL model agrees quantitatively with the data in most cases. In the remaining areas, the disagreement is small enough that further variation of kinetic rate values (within their experimental uncertainties) will probably provide agreement. Efficiency projections for large systems have been made. As a result of this program, there is an experimentally validated intracavity ORTL model that can be used for high energy system designs.

The ORTL overall efficiency is a product of the input efficiency and the conversion efficiency. The input efficiency depends on the pump laser spectrum and the ORTL operating conditions, primarily the HF partial pressure, the absorption length, and the medium temperature. The conversion efficiency depends upon the molecular kinetics, primarily the relative value of the rotational-rotational transfer rate to the total HF deactivational rate. Since these rates are temperature dependent, the conversion efficiency is also dependent upon the operating temperature. For a given pump laser

spectral distribution, the input efficiency increases as the HF partial pressure increases; on the other hand, the conversion efficiency decreases due to an increase in HF-HF deactivation, and in the energy required to achieve inversion. By elevating the ORTL inlet temperature, the power coupled into the ORTL medium and hence the input efficiency increases. Furthermore, the conversion efficiency increases due to an increase in the r-r transfer rate and a decrease in the HF deactivation rate. These trends are evidenced in the experimental data. The model predicts that further heating would improve performance until inlet temperatures of 800 - 1000^{o}K are reached. Above that the efficiency decreases as the small signal gain drops.

Three diluents, helium, SF_6, and CF_4 were experimentally investigated. CF_4 has a large HF deactivation rate and therefore did not perform well. Helium and SF_6 yielded comparable overall efficiency in both the extra- and intracavity configurations. However, at room temperature, the conversion efficiency was better with helium diluent, probably because helium has a smaller deactivation cross-section than SF_6. Because of its larger specific heat, less SF_6 is required for a fixed HF concentration. Thus, SF_6 diluent offers the advantage of lower ORTL operating pressure so that the pressure drop between the chemical laser and ORTL media is lower and the aerowindow requires a lower mass flow. On the other hand, the larger index of refraction of SF_6 will contribute a larger index of refraction change for a fixed temperature variation in the ORTL medium. A system study, taking into account gas storage, would select the optimum diluent for a particular application.

A rotational bottleneck was not observed with pump fluxes up to 20 kwatt/cm^2. This is in agreement with the ORTL model. High energy system designs at this level yield compact ORTL designs which efficiently use the HF mass flow in the ORTL.

The spectral control coating was successfully developed and tested in the ORTL experiments. The resonator mirrors with this coating sustained pump fluxes of 5-10 kwatt/cm^2 without any obvious deterioration. Temporally stable intracavity ORTL operation with overall efficiencies up to 38 percent were achieved using a spectrally controlled resonator. Better performance is predicted if the cut-off wavelength is optimized and the short wavelength

reflectivity is improved. The intracavity ORTL model also indicates that it may be possible to achieve good overall efficiency with a chemical laser resonator without a spectral controlled coating, coupled with very high ORTL medium inlet temperatures. While this result, if true, would allow significant simplification in intracavity ORTL implementation, care must be exercised in making such an extrapolation.

The ORTL efficiency has been shown to critically depend on the inlet temperature in both the extracavity and intracavity configurations. High average temperature can be achieved by adjusting the gas composition, the gas velocity and the inlet temperature. These three parameters are interdependent. The ideal situation would be to raise the inlet temperatures for efficient power coupling and to adjust the flow velocity so the temperature rise during the ORTL interaction is small. For a pump laser with J = 6, 7, 8, and 9, the optimum inlet temperature predicted by the model is 800-1000^{o}K. In the 300-500^{o}K range achieved in the laboratory, the higher the inlet temperature, the higher the ORTL efficiency. Obviously, the maximum 550^{o}K is not high enough to achieve high input and conversion efficiencies. Thus, the achieved overall efficiency (38 percent) is not as high as one can project with proper inlet temperature.

A complete intracavity ORTL model has been developed. Results of this code have been verified by comparison with the experimental parameters. The parameters compared include: ORTL outcoupled power, ORTL gas heating, and the ORTL efficiencies derived from this measured data. This model/experiment comparison indicates that the results from the model agreed very well with the experimental data and that this model can be used in designing ORTL systems. Based upon this verified ORTL code, large-scale ORTL devices can probably achieve overall efficiencies of 85 percent or greater.

There are some areas in which further work could profitably be done. These include: further exploration of kinetic rate optimization in the model, experimental implementation of higher inlet temperatures, more detailed ORTL small signal gain measurement and comparison with the model, more careful investigation of the roles of helium and SF_6 in the ORTL process, and investigation of operation with no spectral control filters. While there is some

additional understanding to be derived from further work at the present power levels, it would be very profitable to scale the experiments to higher levels where meaningful ORTL medium homogeneity and beam quality measurements could be made. Further work might also include utilization of the model for conceptual designs of systems of interest to chemical laser users.

APPENDIX A

SMALL SIGNAL GAIN MEASUREMENTS

The purpose of these experiments was to measure the small signal gain of the intracavity ORTL under several operating conditions, in order to aid in the study and optimization of ORTL systems. This Appendix will describe the techniques and apparatus used in the experiments. The data results will then be presented and the important conclusions briefly discussed. An error analysis and suggestions for future work will conclude this Appendix.

The small signal gain of a laser medium is the amplification of a laser signal propagating through the excited gain region. The gain g is described by the exponential function

$$I = I_o \cdot \exp(g.L)$$

where I_o is the input laser intensity and I the laser intensity after passing through the excited gain region of length L. Directions transverse to the direction of propagation are neglected in this simplification by using plane waves for I and I_o, and assuming spatially homogeneous gain. In these experiments, a probe laser beam from a completely separate and independent laser was passed through the fixed length gain region, so that the gain g is found as

$$g = \frac{\ln(I/I_o)}{L},$$

and only L and (I/I_o) needs to be measured for each experiment. The mirrors defining the ORTL optical cavity were removed during the course of the experiments, so that only the unloaded, or non-lasing gain was measured.

The intensity of the probe laser beam was kept low in order to measure the true small signal gain. All gain measurements were performed with I in the W/cm^2 regime in order to eliminate saturation effects.

The absorption due to HF molecules in the gain path is calculated in an exactly analogous manner. The transmission T of a laser beam through a medium of length L whose absorption constant is α is

$$T = \exp(-\alpha L)$$

so that

$$\alpha = \frac{\ln T}{-L}$$

The absorption constant is a linear function of absolute pressure P, so α can be reduced to $\alpha = \alpha_o P$. This α_o varies with both wavelength and temperature. This Appendix will tabulate g and α_o under several operating conditions.

The small signal gain measurement was done with a dual beam technique in order to obtain reliable data. The system consisted of a Helios probe laser, some beam control optics and power measurement and recording devices, along with essentially the entire chemical laser and ORTL systems. This Appendix describes only the modifications and additional apparatus required for the gain measurements, referring the reader to the detailed description of the chemical laser and ORTL in the body of the report.

A diagram of the experimental arrangement is shown in Figure A-1. The probe laser was a Helios model CLI HF laser. The most important properties are its single-line output tunability, unlimited continuous operation, and good beam quality. It was operated with the output horizontally polarized. The output was then reflected twice at right angles by aluminized mirrors. These reflections rotated the polarization and directed the beam toward the ORTL at a slightly increased elevation. The beam was then expanded and focussed by a Janos Optical Corporation calcium fluoride 5X telescope to an adjustable pinhole and lens about 4m away, after two more reflections from aluminized mirrors near the ORTL which returned the beam to the original horizontal polarization.

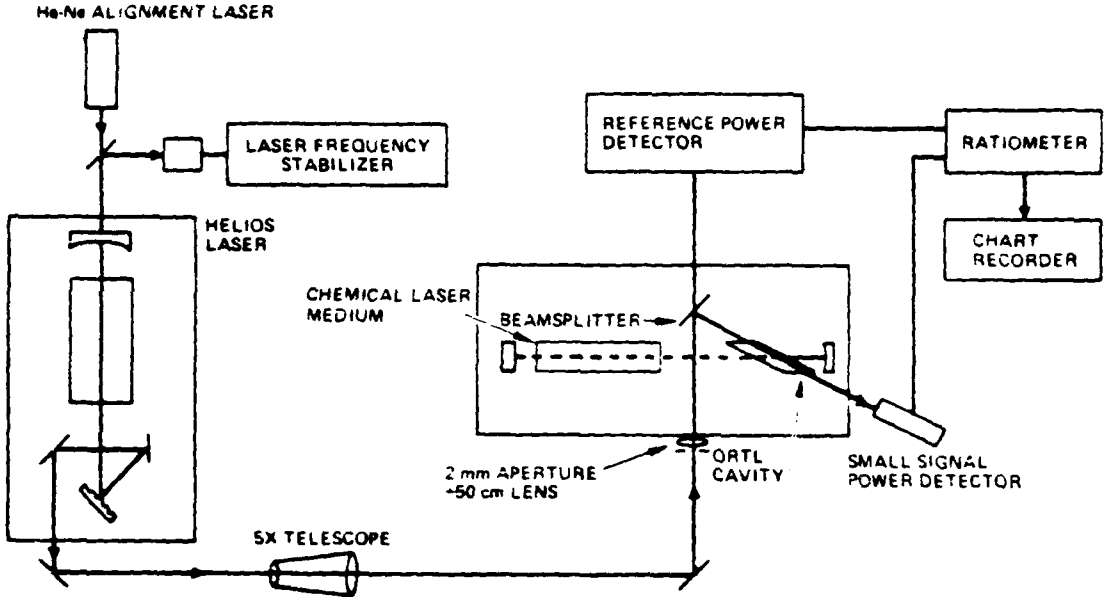

Figure A-1. Small signal gain experimental apparatus.

The pinhole and lens combination were carefully chosen to provide a beam of minimum diameter in the ORTL gain medium. Diffraction by a 2 mm diameter pinhole at the 3 μm wavelengths used would have caused a much larger beam at the ORTL nozzle 50 cm away, and mechanical complexities did require the adjustable pinhole outside the main ORTL box. By adding a 50 cm lens, the plane wave section transmitted through the pinhole would be focussed to an Airy pattern of calculable dimensions. A pinhole was chosen, in fact, such that its diameter was identical with the diameter of the Airy disc, the focussing of the lens compensating diffraction effects. The beam was nearly uniform in diameter over a long distance, and for a 3 μm wavelength, turned out to be 1.91 mm. An aluminum aperture of 0.077 inch (1.96 mm) was chosen.

The beamsplitter inside the ORTL cell was a 1 mm thick flat disc of MgF_2 coated on one side with a coating which experimentally reflected about 50 percent of the incident light at 45 degree angle of incidence. Since the beam splitter was used near Brewster's angle, negligible power was reflected from the uncoated surface, and the probe beam stayed circular in cross section. The 1:1 beam splitting ratio was chosen to allow the two power meters to operate on the same scale.

Laser Precision models RK-5100 and RK-3240 radiometers were used with type RKP-545 pyroelectric detector heads to measure the I and I_o signals. These heads feature internal choppers operating at 32 Hz, but the direct outputs of the power meters were filtered to change the response to a 1 second time constant. This decreased the noise in the radiometer to a level consistent with the other sources of error in the experiment. The output from the two radiometers was then formed into a ratio by an Intech model A733 programmable multifunction module to get I/I_o, which was recorded during the experiment on a Honeywell chart recorder. In addition, I, I_o and $(I/I_o)-1$ were also recorded, the latter on a scale 4 times more sensitive than I/I_o.

This dual beam method could correct for variations in signal intensity by recording the ratio of the power in the two paths. The radiometer detector heads were not moved during the experiments, so false intensity variations were eliminated. The data was still taken in several steps, how3ver. The chemical laser could be operated for only 45 $\pm$15 seconds, after which a cooling time of 5 to 15 minutes was required. During this longer interval, the data could be briefly reviewed, and the laser controls adjusted or reset accordingly. The gain experiments were performed in the following manner. With the probe laser on but the ORTL and chemical laser off, the initial ratio I/I_o was recorded. The HF gas was then introduced into the ORTL, and a new I/I_o value was recorded, any changes being due to the absorption by HF. The chemical laser was then turned on, and its mirror alignment quickly adjusted for maximizing the I/I_o gain. The chemical laser beam was then shuttered twice for about 10-second periods. The ratio I/I_o when the laser was shuttered should have been identical with the value recorded before the chemical laser was turned on, but the increased value when the chemical laser was operating indicated the gain in the ORTL. The difference between the two ratios was directly read from the chart recordings.

Additional measurements, both when the chemical laser was on or off, were done in similar manners. The ORTL HF operating pressures could be easily cycled from 2 Torr to zero several times during a data run, which gave accurate values for the HF absorption at the operating wavelength of the probe laser.

The probe laser wavelength was easily changed during the chemical laser cooling time between data runs. The intensity in the probe beam was most easily varied during a single run by using partially reflecting mirrors to attenuate the beam. Several filters were placed in one holder, and were switched in and out during the chemical laser run to measure the saturation intensity I_s. In order to measure the gain in different positions in the 7.5 mm by 3.0 mm ORTL cavity, the pinhole was translated both horizontally and vertically during a chemical laser run. The Helios laser output was first defocussed to a spot about 9 mm in diameter at the pinhole while the power was increased to get a reasonable signal through the 2 mm pinhole.

At room temperature the HF gas in the ORTL laser absorbs certain lines of the probe laser. This absorption depends on the gas pressure, and in fact can be used to calibrate the relative flow rate. The absolute pressure calibration depends on the absolute absorption coefficient and interaction length. Since neither of these was known precisely, the data was normalized to a 2 Torr condition which was calibrated separately with another non-optical technique. At 2 Torr HF, the transmission through about 10 cm of the $P_1(6)$ line was (0±1)% indicating an absorption coefficient α_o greater than 30%/Torr-cm. At the $P_1(7)$ line, (12±1)% transmission was observed, giving an α_o of (10.6±0.4)%/Torr-cm. The $P_1(8)$ line gave a value a little easier to measure, so at this wavelength, several pressures were measured, as shown in Table A-1. The fourth column is the measured transmission. These values are converted into an absorption coefficient α_o in the next column, based on the flow controller pressure. This number should be constant, so its variance shows the uncertainty in the actual pressure in the cell. A statistically weighted average is α_o = (2.89 ±0.45)%/Torr-cm. Since the absorption constant did not vary, this average value was used to determine the actual HF pressures listed in the last column. The errors assigned to the points include the larger systematic error of ±16 percent from the α_o average. If the data is analyzed differently, for example, each day's data normalized separately to its own 2 Torr value, much smaller relative errors could result. The larger uncertainty, however, would remain when comparing runs of different days.

TABLE A-1. ORTL ABSORPTION (295°K INLET)

Date	ORTL Set Pressure	Probe Line	Trans-mission (%)	α_o (%/Torr-cm)	Measured ORTL Pressure (Torr)
2/26/82	2 Torr	$P_1(6)$	0 ±1	≥30	2.50 ±0.4
2/26/82	2	$P_1(7)$	12 ±1	10.6 ±0.4	2.50 ±0.4
2/26/82	2	$P_1(8)$	48.6 ±0.8	3.61 ±0.08	2.50 ±0.4
2/26/82	1.5	$P_1(8)$	57.0 ± 0.6	3.75 ±0.08	1.95 ±0.3
2/26/82	0.75	$P_1(8)$	78.4 ±0.8	3.24 ±0.13	0.84 ±0.1
2/26/82	2.5	$P_1(8)$	53.6 ±0.6	2.49 ±0.04	2.15 ±0.3
3/2/82	0.5	$P_1(8)$	85.9 ±0.8	3.04 ±0.18	0.53 ±0.1
3/2/82	1.0	$P_1(8)$	73.8 ±0.7	3.04 ±0.09	1.05 ±0.2
3/2/82	2.0	$P_1(8)$	58.5 ±0.6	2.68 ±0.05	1.85 ±0.3
3/2/82	2.5	$P_1(8)$	53.9 ±0.5	2.47 ±0.04	2.14 ±0.3

The small signal gain measurements on four different probe lines at two different pressures are summarized in Table A-2. The measurements were all taken on one day, so they can be compared with each other directly without too much concern for drift. The pressure listed is from the flow rate setting, and has an estimated error of ±8 percent from run to run. The ORTL gas temperature here, as in the following charts, is the temperature of the ORTL thermocouple at position #9. As seen from the temperature profile in Figure A-2, this seems to be close to an average temperature. Each temperature, as well as the average profile, has an estimated error of ±10°C. The interaction length was also measured from this profile, and assigned with a ±0.2 cm uncertainty. Due to the large uncertainties in the data, a more careful integration of gain versus temperature profile was not warranted. The final column in Table A-2 is the calculated gain coefficient g_o using the tabulated

TABLE A-2. SMALL SIGNAL GAIN MEASUREMENTS

Run	ORTL HF Pressure	Probe Line	Gain (%)	ORTL Temp (°C)	Interaction Length (cm)	g_o (%/cm)
1	2 Torr	$P_2(10)$	15.5 ±1	680°C	6.5 ±0.2 cm	2.22 ±0.26
2	1	$P_2(10)$	6.83 ±0.25	360	6.0 ±0.2	1.10 ±0.11
3	2	$P_1(10)$	9 ±1	640	6.3 ±0.2	1.36 ±0.20
4	1	$P_1(10)$	6 ±1	360	6.0 ±0.2	0.97 ±0.19
5	2	$P_1(9)$	11.1 ±0.5	670	6.3 ±0.2	1.68 ±0.18
6	1	$P_1(9)$	9 ±1	350	6.1 ±0.2	1.41 ±0.21
7	2	$P_2(9)$	19 ±0.5	680	6.3 ±0.2	2.76 ±0.26
8	1	$P_2(9)$	10.5 ±0.5	350	6.0 ±0.2	1.66 ±0.17

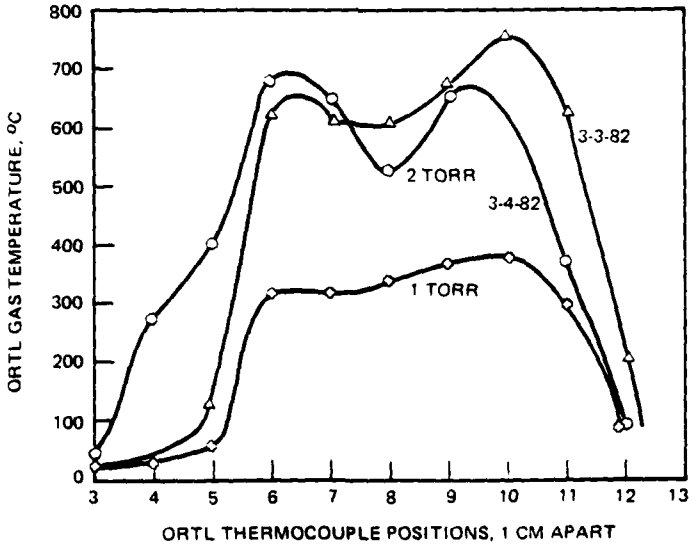

Figure A-2. ORTL gas temperature profile. (Data at 1 and 2 Torr taken on 3/3/82 was reproduced from run to run, but the following day, all profiles were similar to the one labeled at 2 Torr.)

gain, interaction length, and pressure and with their combined uncertainties. While the lower pressures have a slightly higher gain coefficient per Torr, operation at the higher pressures always leads to higher gains.

Most of the absorption measurements were made on the following day, and are listed in Table A-3. The absolute pressure may be different than that used the preceding day, and the chemical laser alignment is certainly different, as indicated in Figure A-2. The average ORTL temperature was also a little lower for some of the runs. These data were taken with the chemical laser on, and although incomplete, should be compared to the room temperature absorption measurements in Table A-1. No absorption at room temperature was expected for the $P_2(6)$, or $P_2(7)$ lines. The anomalous temperature for Run 3 was a result of gross chemical laser misalignment. Even though the chemical laser was operating at low power, the $P_1(7)$ line still had more transmission than recorded at room temperature. The 42 percent transmission figure was taken before the chemical laser was too far misaligned.

TABLE A-3. ORTL ABSORPTION (HEATED MEDIUM)

Date	Run	ORTL HF Pressure (Torr)	Probe Line	Trans-mission (%)	ORTL Temp. (°C)	Interaction Length (cm)	α_o (%/Torr-cm)
3/3/82	1	2	$P_1(6)$	0 ±1	680°C	6.3 ±0.2	≥30
3/3/82	2	"	$P_1(6)$	0 ±1	340	6.0 ±0.2	≥60
3/4/82	3	2	$P_1(7)$	>42	~50	7	≤ 6
3/4/82	4	2	$P_2(6)$	56 ±2	570	7.5 ±0.2	3.9 ±0.4
3/4/82	5	1	$P_2(6)$	83.4 ±1	260	7.5 ±0.2	2.4 ±0.2
3/4/82	6	2	$P_2(7)$	84 ±1	510	6.4 ±0.2	1.4 ±0.2
3/4/82	7	1	$P_2(7)$	98.5 ±0.2	260	7.2 ±0.2	0.21 ±0.04

The dependence of the gain on probe position in the ORTL gain region was measured to show relative gain differences. Both horizontal and vertical translations were measured. Because the background ratio I/I_o varied with an uncertainty of ± 2 percent, the uncertainty in the gain change is also that large. The $P_2(9)$ line was used in order to allow the smallest change to be measured. As the probe beam was translated horizontally over a 0.225 inch (5.7 mm) range roughly centered on the ORTL lasing axis, the gain was not seen to change with an uncertainty of ± 2 percent gain, or ± 13 percent relative gain. The vertical variation did show a slight drop in gain away from the ORTL axis. A (2.5 ± 1) percent decrease in gain was seen, or (17 ± 7) percent relative gain, at an 0.025 inch displacement in both directions. The probe beam never left the ORTL gain region, so these small variations in gain are reasonable.

Uncertainties in the data just described arise from a number of different sources. Three of these: the absorption calibration factor, electronic noise, and the laser line frequency stability, give relative errors less than 1 percent from the true value, while the drift in the data due to uncertainties in the chemical laser operation gives relative errors from 2 to 20 percent.

The transmission of a cleaned piece of CaF_2 or BaF_2 was used to calibrate the I/I_o measurements. Assuming a scattering loss of (0.1 ± 0.05)% per surface, and negligible absorption in samples less than 4 mm thick, the total loss for a CaF_2 window is (5.99 ± 0.07)% and for a BaF_2 sample, is (6.98 ± 0.07)%. The measured deflection of $(I/I_o)-1$ on the chart recorder for CaF_2 was (1.24 ± 0.02) inches, and for BaF_2, (1.40 ± 0.02) inches. The calibration factors are thus (4.83 ± 0.1)%/inch and (4.98 ± 0.1)%/inch, and since two CaF_2 samples were measured, a weighted average gives (4.88 ± 0.06)%/inch. The theoretical value, from the chart recorder calibration of 10%/(2.04 ± 0.02)" gives (4.90 ± 0.05)%/inch. This agreement is better than expected, and the calibration factor used is (4.88 ± 0.06)%/inch, for a systematic eror of ± 1.2 percent.

The uncertainty in the electronics and recording apparatus is of a similar magnitude to the calibration error. The pyroelectric power meters were somewhat influenced by external noise, but a one-second integration time reduced fluctuations to about a 1 percent value. The ratiometer is linear to better than 0.5 percent, and the chart recorders have similar values. These values are negligible compared to the chart recorder reading error.

There are two sources of error in reading the chart recorder. The smaller error is simply the uncertainty of the distance measured between two lines, estimated as ± 0.02 inch. The relative error of this contribution, thus varies from 1 percent to 10 percent, depending on the actual distance. This error is, however, contained in the uncertainty in specifying the two lines whose distance is being measured. The I/I_o and $(I/I_o)-1$ traces drifted over substantial areas of the paper. Drifts up to 10 percent have been included as uncertainty in the data in Section IV. Because the ratiometer is expected to cancel all variations (to within less than 1 percent) in their absolute values, the variations must be a real effect of the chemical laser/ORTL system. The laser gas flow rates, chemical laser alignment and irreproducibility, and ORTL gas temperature rise all contributes to slow fluctuations in the data. In addition, the experiments were run in such a way as to prevent attainment of equilibrium, so some estimate of the asymptotic limit was sometimes required.

Combining these errors, a 1.2 percent systematic error and the usually much larger random errors, leads to the numbers assigned to the analyzed data. The interpretation of the data must include, however, several more contributions.

The probe laser does not naturally operate on the center of a laser transition, but with the Lansing stabilizer the Helios is locked to near line center. The cavity length is actually slightly modulated at a 520 Hz frequency, so operation is confined to a small frequency interval about the line center. The absorption and gain measurements are thus confined to a narrow frequency interval such that the peak value is actually measured. The estimated error in peak gain due to this frequency shift is assumed to be negligible compared to the other errors in this experiment.

A much larger error in deriving a gain coefficient α_o is the uncertainty in both the gain length and gas pressure. While the nozzle length in the ORTL is nominally 10 cm, the thermocouples placed at the exit of the gain region provide a better estimate of the interaction length. Ideally, the temperature profile would have sharp edges at each end, and be flat over the entire region, indicating uniform heating with no external influences. The profile is not so unambiguous, so an average temperature is assigned to each run, with an error of ±10C° and the nominal length with an error of ±0.2 cm. These errors are loosely based on the variations seen in the laser runs. Similarly, the HF gas flow rate in the ORTL is not perfectly known or easily calibrated under actual operating conditions. Absorptions were measured at several pressures in order to determine the gas density. If the differences from a linear fit were totally due to variances in the gas flow rate, the error would be equivalent to about $\pm$8 percent, at pressures below 2 Torr HF. At higher pressures, the value is even more uncertain, up to $\pm$20 percent. The combination of these two factors significantly increases the uncertainty in the calculated gain coefficient. These values were also included in the data analysis.